

This material has been copied
under licence from CANCOPY.
Resale or further copying of this material is
strictly prohibited.

COMMERCIAL

Le présent document a été reproduit AEEW-R82
avec l'autorisation de CANCOPY.
La revente ou la reproduction ultérieure
en sont strictement interdites.

SECOND REPORT ON THE S.G.H.W. EXPERIMENT IN DIMPLE

by

D. Dallaston^{*}
J. W. Hilborn[‡]
R. G. Jarvis[‡]
P. G. F. Moore

D. H. Day
A. J. M. Hitchcock
E. D. Jones
S. K. Pattenden
G. W. Watson

W. N. Fox
H. R. McK. Hyder
C. J. Kenward
R. Trebilcock

ABSTRACT

The S.G.H.W. experiments in DIMPLE, carried out between June and November, 1960, are described and the results reported.

Five cores have been examined, containing successively air, D₂O, H₂O and two H₂O/D₂O mixtures as coolant simulant. Macroscopic flux distributions have been obtained for each core and radial and axial bucklings deduced. Fine structure variations in the activation of gold, manganese, lutecium and rhodium foils have been measured and these data, together with other flux measurements, have been used to characterize the neutron spectra in the core.

The techniques adopted to handle H₂O/D₂O mixtures are described and the measures used to combat abnormal aluminium corrosion are reported.

The S.G.H.W. fine structure experiment on LIDO is described and the measurements of neutron temperature dependence on coolant temperature reported.

^{*}On attachment from D & E Group, Windscale Works.

[‡]On attachment from A.E.C.L., Chalk River.

A.E.E.,
Winfrith.

May, 1961.

W.3750

CONTENTS

	<u>Page No.</u>
1. Introduction	1
2. Experimental Programme	1
3. Critical Approaches and Measurements of Safety Data.	2
(i) Critical height	3
(ii) Worth of safety rods	3
(iii) Variation of reactivity with moderator height	6
4. Measurements of Flux Distribution by Foil Activation	6
(i) Manganese monitors	6
(ii) Foil positions	8
(iii) Manganese reaction rate distributions	11
(iv) Material buckling and reactivity	14
(v) Gold-manganese ratio	17
(vi) Lutecium-manganese ratio	17
(vii) Rhodium reaction rate distributions	20
5. Spectrum Characterization by Integral Measurements	21
(i) Interpretation of gold-manganese ratio	24
(ii) Interpretation of lutecium-manganese ratio	25
(iii) Manganese cadmium ratio	26
(iv) Gold cadmium ratio	26
(v) Vanadium cadmium ratio	27
(vi) Indium cadmium ratio	28
(vii) Fission chamber measurements	29
(viii) Boron chamber measurements	30
(ix) Summary	31
6. Perturbation Measurements	32
(i) Cadmium absorber effectiveness	32
(ii) Void coefficient in moderator	32
7. Engineering and Operational Features	32
(i) Fine control rod	32
(ii) Flux scanning device	35
(iii) D ₂ O handling	35
8. Aluminium Corrosion	38
9. The Fine Structure Stack	40
(i) Introduction	40
(ii) Calandria tank and fuel channels	40

	<u>Page No.</u>
(iii) Irradiating the stack	41
(iv) The coolant circulation system	41
(v) Measurement of temperature	41
(vi) Operation	42
(vii) Difficulties in operation	43
(viii) Flux measurements	44
(ix) Results	46
10. Acknowledgements	56
11. References	57
Appendix I Calendar of experiments	59
II Foil encapsulator	60
III Least squares fitting programme	61
VI Determination of the resonance self shielding factors in gold and manganese	62
V The foil irradiation scheme	64

TABLES

1. Critical heights, safety rod worths, etc. in cores 1 - 5	4
2. Delayed and photo-neutron yields and half-lives	5
3. Statistical accuracies of the manganese flux monitors	8
4. Co-ordinates of foil positions in the lattice cell	10
5. Macroscopic flux distribution parameters in cores 1 - 5	12
6. Fine structure factors for manganese activation	13
7. Gold/manganese ratio fine structure factors	18 & 19
8. Cadmium ratios and activation ratios in cores 1 - 5	22 & 23
9. Perturbations due to the fine control rod	34
10. Coolant temperatures in the fine structure stack	47
11. Comparison of gold/manganese and lutecium/manganese ratios in the fine structure stack and DIMPLE	50
12. Lutecium/manganese ratios in the fine structure stack at different temperatures	51
13. Effective neutron temperatures at different coolant temperatures in the fine structure stack	53

FIGURES

1. Plan of reactor core
2. Measured and calculated flux decay curves
3. Foil positions in lattice cell
4. Macroscopic radial distribution of gold/manganese ratio
5. Macroscopic axial distribution of gold/manganese ratio
6. Comparison of measured and calculated values of k_{∞}
7. Radial fine structure of manganese activation in core 1 - 5
8. Axial fine structure of manganese activation in cores 1 - 5
9. Radial fine structure of manganese activation at different heights in cell
10. Axial fine structure of manganese activation at different radii in cell
11. Radial hyperfine structure of manganese activation in core 3
12. Ratio of radial hyperfine to fine structure in core 3
13. Radial fine structure of gold/manganese ratio in cores 1 - 5
14. Axial fine structure of gold/manganese ratio in cores 1 - 5
15. Radial fine structure of lutecium/manganese ratio in cores 1 - 5
16. Radial fine structure of rhodium activation in cores 1 - 5
17. Spectrum parameters in the fuel in cores 1 - 5
18. Spectrum parameters in the moderator in cores 1 - 5
19. Reactivity worth of cadmium absorber at different radii
20. Reactivity worth of an air void at different radii
21. Fine structure stack and lifting gear
22. Fine structure stack showing top header
23. Foil positions in fine structure stack
24. Umbrella foil holder
25. Lutecium/manganese ratios in fine structure stack
26. Variation of neutron temperature with coolant temperature in fine structure stack

27. Foil encapsulator

28. Self shielding factors for the gold and manganese resonances

1. Introduction

This report describes the experimental programme carried out at A.E.R.E., Harwell in the DIMPLE reactor and with the fine structure stack on LIDO from June 1960 to November 1960. The experimental results obtained in that period are presented and the analysis of the flux measurements to yield values of material bucklings is described. Interpretation of the experimental results and their correlation with a recommended method of lattice calculation is deferred to a subsequent report.

The design, construction and commissioning of the S.G.H.W. experiment in DIMPLE is described in a previous memorandum (1). The design of a S.G.H.W. power reactor core and that of the DIMPLE experiment were compared in an earlier memorandum (2); the proposed programme of experiments was described in a further note (3).

2. Experimental Programme

The experiments in DIMPLE were designed to confirm the calculated core reactivity of the S.G.H.W.R. and hence the initial enrichment required. Another objective was to show how reactivity varies with coolant density, since it is assumed that for the power reactor to be stable reactivity must fall as steam voidage increases. Knowledge of the flux fine structure was also required to improve calculated values of power rating.

The core infinite multiplication constant may be deduced from the experimental results by two different methods:

- (i) analysis of macroscopic flux distributions to yield material buckling, and hence if M^2 is known, k_{∞} .
- (ii) measurements of various reaction rate distributions from which the separate lattice parameters can be calculated.

The measurements required for both these methods of analysis were made simultaneously during the course of a series of irradiations carried out in DIMPLE under well defined conditions.

In order to simulate the effect of changing the coolant density in the S.G.H.W.R. core, measurements were made on five different core arrangements in DIMPLE. These cores differed only in the composition of the liquid coolant surrounding the fuel rods.

Originally measurements on six cores were planned (see Table 2 of ref. 2). Each core was estimated to require one week for assembly, criticality and safety measurements, and three weeks for foil irradiations. Measurements on core 1 (air in coolant channels) began on 9th May, 1960 and ended on 19th June, 1960. The D₂O coolant for core 2 was loaded on 20th June, 1960. On 22nd June the pressure tubes in zone 2 of the core (the outer driver ring) were opened to reduce the U²³⁵ spike loading, and the aluminium of the pressure tubes was observed to be corroding abnormally (see § 8). Substantial amounts of deuterium gas had been evolved and, after venting the tubes, the experimental programme continued until 1st July when corrosion was observed in the pressure tubes of zone 1.

It was then decided to unload all fuel and coolant from the reactor and to pickle and reclean all the aluminium components which had corroded. As reported earlier, the manufacturer of the aluminium core components had been unable to carry out the acid-alkali cleaning procedure specified by the A.E.A. and it was thought that the corrosion might have resulted from this omission.

Cleaning and reloading was completed by 19th July and measurements with core 2 were then recommenced. Because of the delay caused by the aluminium corrosion, and because it did not appear possible to reduce the time required for experiments on each core to less than one month, it was decided to examine only five cores. The experiments with H₂O/D₂O mixtures were left till last so as to allow time to devise methods of combating the corrosion before introducing H₂O/D₂O mixtures into the reactor, thus minimizing the risk of having to make additional batches of mixture. The actual experimental programme is given in Appendix I.

With minor exceptions the experimental procedure remained unchanged from core to core and the experiments are grouped as follows:

- (i) Approach to critical and determination of safety parameters.
- (ii) Measurement of macroscopic flux distributions and thermal and fast neutron fine structure.
- (iii) Spectrum characterization.
- (iv) Perturbation measurements.

In addition to the measurements reported here, the U²³⁵ and U²³⁸ reaction rates (bare and under cadmium) were measured in the five rings of fuel rods in the clusters. These measurements, which lead to values of the resonance escape probability and fast fission factor, are reported separately (4). It was not possible to measure U²³⁸ reaction rates in core 1b because these irradiations required a high neutron flux which involved recalibrating the reactor instruments and improving the shielding. To avoid delay these modifications were carried out at the end of the programme on core 1b. It proved possible subsequently to carry out measurements in an air core between cores 4 and 5.

At the end of the planned programme an attempt was made to examine the effect of an axial variation in coolant density by measuring the vertical flux distribution in a core with only the bottom four fuel clusters immersed in coolant. This will be reported subsequently.

The fine structure stack on LIDO was commissioned in September and eight runs were carried out in which neutron temperatures were measured with the H₂O coolant at five temperatures between 20°C and 85°C; with only four channels heated; and with air in the fuel channels. These experiments were completed in December 1960.

3. Critical Approaches and Measurements of Safety Data

The Standing Orders for the S.G.H.W. experiment in DIMPLE (5) required that when a new core was loaded the reactor had to be operated under "unconfirmed" conditions (i.e. with additional supervisors and with restrictions on the mode of

operation) until the safety criteria on the lattice certificate has been confirmed. The measurements described in this section were made primarily to confirm the safety of the core.

(i) Critical height

The critical height was determined by an approach to critical procedure specified in detail in the Standing Orders. On completion of the fuel and coolant loading, empty search tubes were inserted in positions 12, 19 and 22 (see fig. 1) and type 12EB40 BF₃ proportional counters were inserted in each of these tubes. The subsequent measurements of extrapolated height H and neutron counting rate N are described in § 12 (c) of ref. (1).

It was hoped to find a best value of extrapolation distance Δh by plotting $(h\hat{c}/ + \Delta h)^2$ against $\frac{(h\hat{c}/ + \Delta h)^2}{N}$ for different values of Δh (where $h\hat{c}/$ is the height of core immersed in moderator), and fitting the plotted curves to a straight line by the method of least squares. However the fit was too insensitive to variation in Δh , and a constant extrapolation distance of 50 cm was arbitrarily chosen for all the cores examined. Using this value, critical height could be predicted from the approach curve to within the experimental accuracy of ± 1 cm.

Values of the top and bottom extrapolation distances for Zone 1 were subsequently obtained from the flux fitting programme. These values as well as the critical heights of the various cores are listed in Table 1.

(ii) Worth of Safety Rods

Two different methods were used to measure the reactivity controlled by the safety rods. The first method was to perform an approach to critical experiment with a bank of rods inserted (keeping the reactor at least 1% subcritical) and to compare the predicted critical height with the critical height of the normal reactor. The reactivity controlled may then be deduced from the change in critical height (see ref. 1, p. 33-35). The method breaks down if the worth of the bank of rods is greater than the reactivity controlled by axial leakage and it becomes inaccurate when the rod worth greatly exceeds the reactivity change over the permissible range of moderator height. The method relies on the dubious assumption that inserting the bank of rods does not change the radial leakage. The later S.G.H.W. cores in DIMPLe, which contained significant amounts of H₂O, showed small changes of reactivity with height and therefore yielded imprecise estimates of rod worth. In these cores it was decided to use a kinetic rod-drop method to check rod worth.

The short period neutron decay following rod drop was observed by means of a pulsed BF₃ counter, a scaler, and a high speed strip chart recorder. With a tape speed of 3 inches per second, it was possible to record counting rates from the scaler up to 20 regular pulses per second. A timing pulse was recorded at the instant of absorber release, and during the next 150 seconds each thousandth pulse from the BF₃ counter was recorded. The initial counting rate was approximately 15,000 per second, and in every case the reactor had been operating for at least 15 minutes so that the delayed neutrons

TABLE I

Critical heights, safety rod worths, etc. in cores 1 - 5

CORE	1a	1b	1c	2b	4	5	3
ZONE 1 "COOLANT"	Air	Air	Air	D ₂ O	20% H ₂ O, 80% D ₂ O	40% H ₂ O, 60% D ₂ O	H ₂ O
ZONE 2 "COOLANT"	Air	D ₂ O	D ₂ O	D ₂ O	D ₂ O	D ₂ O	D ₂ O
No. of Spikes	17	12	12	11	10	10	12
Critical Height (cm)	227.50 ± .08	220.31 ± .06	219.70 ± .02	219.44 ± .03	228.57 ± .02	224.98 ± .02	236.68 ± .02
$\frac{\Delta\rho}{\rho_H}$ (%/cm)	0.0590 ± .006	0.0598 ± .002	0.0606 ± .003	0.0488 ± .0015	0.0406 ± .002	0.0393 ± .002	0.0308 ± .001
1/2/k _∞ (cm. ²)	567 ± 47	424 ± 19	-	330 ± 19	279 ± 15	250 ± 16	216 ± 10
Safety rod bank worth (%) (Approach method)	3.2 ± .5	3.1 ± .5	-	2.9 ± .4	2.3 ± .4	2.1 ± .4	1.4 ± .5
Safety rod bank worth (%) (Flux decay method)	-	-	3.6 ± .5	-	2.7 ± .4	2.5 ± .4	2.1 ± .3

and photo-neutrons were in equilibrium.

The reactivity worth of the safety rods was found by comparing the observed neutron decay with a theoretical decay curve calculated for a value of rod worth close to the actual value. For this purpose observations were limited to the first 15 seconds after rod drop in order to reduce the relative significance of the long-lived delayed and photo-neutrons. The flux decay extending to 150 seconds was used to find the best value of the photo-neutron fraction, again by comparison with theoretical decay curves. It was found that the initial reactivity change could be approximated by a ramp function beginning 0.4 seconds after rod drop and lasting a further 0.7 seconds. (The calculated curves were provided by T.A.S. Division using the PACE analogue computer (6).

The best value of the photo-neutron fraction was found to be $7\% \pm 1\%$. The figure is incorporated into Table 2 which gives the yields and decay constants of all groups of delayed neutrons and photo-neutrons (7), (8). Figure 2 gives a typical comparison of theory with experiment over the first 15 seconds of flux decay following rod drop.

Table 2

Delayed and photo-neutron yields and half lives

Total delayed neutrons from U-235 (97%) and U-238 (3%)		Photo neutrons = 7% of delayed neutrons	
Fraction β_i	Decay constant λ_i (sec ⁻¹)	Fraction β_i	Decay constant λ_i (sec ⁻¹)
.00024	.0127	.000304	.278
.00140	.0317	.000095	.0169
.00125	.115	.000033	.00490
.00273	.311	.000016	.00152
.00090	1.40	.0000096	.000427
.00020	3.87	.0000110	.000116
		.0000015	.0000441
		.00000047	.00000365
TOTAL = .00672		TOTAL = .00047	

Therefore the total delayed and photo neutron fraction $\beta = .00719$

The errors in reactivity worth from the "prompt drop" method arise mainly from the error in estimating flux distortion, and the error in fitting a theoretical decay curve to the observations. The overall uncertainty is of the order of $\pm 15\%$. However the relative worths of the safety rods in the various cores is known to about $\pm 5\%$.

(iii) Variation of reactivity with moderator height

The variation of reactivity with moderator height was measured in each core by pumping the moderator a predetermined amount above the critical height and measuring the resulting steady doubling time. The accuracy of the method was limited at short doubling times by possible non-linearity in the response of the ion chamber recorder and also by the low speed of the fine control pump. This reduced the range of power over which the water height was constant and transients negligible to such an extent that it was not possible to make measurements of doubling times less than ~30 secs., particularly in cases where the photo-neutron sources were intense. At long doubling times the accuracy was limited by the measurement of small differences in moderator height; the Herriott height probes were capable of measuring small differences in height to an accuracy of 0.05 mm.

Using the constants in Table 2, the inhour equation can be calculated, relating doubling time and excess reactivity. Then it is possible to derive the value of reactivity change with moderator height for all cores. These values of dp/dH have an accuracy of about 5%, and are listed in Table 1.

If dp/dH and H are known, the ratio M^2/k_{∞} for the initial 2-zone core may be found using the one group analysis of ref. (1). The calculated values, listed in Table 1, were used to deduce the safety rod worths from the approach measurements.

Values of safety rod worth from both methods are included in Table 1. The kinetic rod-drop method is probably the more reliable for the reasons discussed in (ii) above, and appears to give rod worths approximately 20% greater than those given by the approach method. The disagreement is rather worse in core 3, probably because it had the least dp/dH and the greatest critical height.

4. Measurements of Flux Distribution by Foil Activation

The measurements of macroscopic and fine structure flux distributions, and of relative reaction rates and integral spectrum parameters, were carried out in a series of foil irradiations under standard conditions (see Appendix V). About 20 irradiations were required for each core, the number being determined by the capacity of counting equipment, the availability of foils and "trombones", and convenience in loading and counting. Between 30 and 60 foils were irradiated at a time.

To ensure that the results of successive irradiations were strictly comparable a reliable and accurate monitoring technique was required: this is described below.

(1) Manganese monitors (Fig. 1)

In order to avoid dependence on the reactor instrumentation for an estimate of the total integrated flux, six manganese foils were activated during each one hour irradiation. Three foils were placed in a search tube at a radius of two lattice pitches from the centre, and another three were placed in a search tube at a radius of three lattice pitches (except in core 1 - see ref. 1, page 51).

Since the six activations were all within about 10% of the average, the simple average was adopted as the weighting factor. A statistical analysis of the activations was undertaken to ensure that the error introduced by using the weighting factor was not greater than the true variation in average flux from irradiation to irradiation. The successive irradiations at a pre-determined nominal flux level were supposedly equal as measured by the installed ion chambers. However according to the manganese monitor weighting factors, the RMS deviation of a single irradiation in a group of similar irradiations was between 1% and 2%

The error in the weighting factor itself was found in the following manner. Each of the six activations from a single irradiation was divided by the average, that is by the weighting factor. These ratios were calculated for all irradiations and arranged in six columns; one for each foil position. The deviations of the ratios from the column averages were taken as a measure of the reproducibility of foil activations. These errors should be independent of average flux level. In core 5 for example the RMS or standard deviations of ratios in the six columns were:

1.06%, 1.23%, 1.00%, 0.78%, 0.75%, 0.85%

Each column in this case contained 26 ratios. The average of the six RMS deviations from the mean is 0.95%, and the standard deviation of the mean

is then $\frac{\sigma}{\sqrt{n-1}} = \frac{0.95\%}{\sqrt{5}} = 0.42\%$. The standard deviation of a single

manganese activation is greater than the standard deviation from the mean of six in the ratio $\sqrt{\frac{6}{5}}$ and is therefore equal, in core 5, to 1.04%. Hence in core 5

the statistical error of each weighting factor (0.42%) is significantly less than the observed deviation of the weighting factor from irradiation to irradiation (1-2%). Therefore it may be concluded that the weighting factor is a valid correction which should be applied to all foil activations in a single irradiation.

Table 3 below gives the essential statistics for the manganese monitor activations in each of the five cores.

TABLE 3
Statistical accuracies of the manganese flux monitors

Coolant Composition	Air Core 1	D2O Core 2	H ₂ O Core 3	80% D2O Core 4	60% D2O Core 5
Observed RMS deviation of weighting factors in the group of irradiations with an instrument reading of 2.4×10^7 n/cm ² -sec.	2.0%	2.26%	1.47%	1.92%	1.39%
Total number of monitor activations	126	204	96	108	156
Statistical error of single monitor foil activation	0.88%	1.26%	1.16%	1.20%	1.04%
Statistical error of weighting factor	0.36%	0.51%	0.47%	0.49%	0.42%

Note: The number of foils actually used in calculating the weighting factors and errors was slightly less than the number irradiated. Approximately 3% were lost or damaged and 2 $\frac{1}{2}$ % rejected for other reasons.

If we assume that the error of the manganese activation from the gold-manganese alloy foils is approximately equal to the error of an individual monitor activation it is possible to estimate the theoretical RMS error of a manganese activation (i.e. from alloy foils) after it has been corrected by the irradiation weighting factor. For example in core 1 the estimated RMS error is $.88^2 + .36^2 = 0.95\%$. Similar calculations for the other cores are as follows:

Core 2 = 1.36%
Core 3 = 1.25%
Core 4 = 1.30%
Core 5 = 1.12%

The average of all 5 cores is $1.20\% \pm .07\%$. This figure will be compared with the observed RMS deviation of the gold-manganese foil activations from a theoretical flux distribution. (See section 4 (iii)).

(ii) Foil Positions (Fig. 3)

As explained in ref. 1, gold-manganese, lutecium-manganese, and rhodium foils were distributed throughout the various cores in order to measure the macroscopic and fine structure variations in neutron flux, distinguishing if

possible the thermal, epithermal, and fast components of the neutron spectrum. Figure 3 shows the distribution and designation of foil positions within a single rectangular cell, 8.375 inches (21.272 cm) square and 14 inches (35.58 cm) high. (The radius of an equivalent cylindrical cell would be 4.72" or 12.00 cm).

Table 4 below gives the heights and radial distances of all foil positions in the cell. Heights are measured above and below the mid-plane or "d" position, and radii are measured from the central axis of the stainless steel tie rod. When two small letters or numbers appear together, such as "ce" or "1/4", the two heights or radii are equivalent within the cell because of symmetry. Positions designated "W1", "W1 $\frac{1}{2}$ " etc. correspond to wires on the flux scanning device. They are equally spaced along the cell boundary. Measuring along the cell side from the corner of the cell ("W2 $\frac{1}{2}$ "), which is also the position of the search tube, the distances of the other wires are as follows:-

W1	10.636 cms.
W1 $\frac{1}{2}$	7.091
W2	3.545
W2 $\frac{1}{2}$ /ST	0
W3	-3.545
W3 $\frac{1}{2}$	-7.091
W4	-10.636

TABLE 4

Co-ordinates of foil positions in the lattice cell

Designation	Height (cm)	Radius (cm)
d0	0	0
d1	0	1.852
d2	0	3.020
d3	0	4.188
d4	0	5.382
d5	0	6.551
d6	0	7.010
ce1	± 10.795	1.852
ce2	"	3.020
ce3	"	4.188
ce4	"	5.382
ce5	"	6.551
ce6	"	7.010
bf1	± 13.335	1.852
bf2	"	3.020
bf3	"	4.188
bf4	"	5.382
bf5	"	6.551
bf6	"	7.010
ag1	± 15.875	1.852
ag2	"	3.020
ag3	"	4.188
ag4	"	5.382
ag5	"	6.551
ag6	"	7.010
d W $\frac{1}{4}$	0	10.636
d W $\frac{1\frac{1}{2}}{3\frac{1}{2}}$	0	11.211
d W $\frac{2}{3}$	0	12.783
d W $\frac{2\frac{1}{2}}{3}$ /ST	0	15.042
ce W $\frac{1}{4}$	± 10.795	10.636
ce W $\frac{2\frac{1}{2}}{3}$ /ST	"	15.042
bf W $\frac{1}{4}$	± 13.335	10.636
bf W $\frac{2\frac{1}{2}}{3}$ /ST	"	15.042
ag W $\frac{1}{4}$	± 15.875	10.636
ag W $\frac{2}{3}$	"	12.783
ag W $\frac{2\frac{1}{2}}{3}$ /ST	"	15.042
h W $\frac{1}{4}$	- 17.78	10.636
h W $\frac{2\frac{1}{2}}{3}$ /ST	"	15.042

(iii) Manganese Reaction Rate Distributions

The manganese flux distributions through the inner zone (Zone 1) were determined from the manganese activations of gold-manganese alloy foils; the fine structure was determined from these data and the gold-manganese ratios; the extent of the region of equilibrium spectrum, to which a one-group theory applies, was defined by the gold-manganese ratios.

In a region of equilibrium spectrum the gold-manganese ratio has a constant value at equivalent cell positions and a change in the ratio is a sensitive indication of departure from equilibrium. Preliminary radial and axial plots of gold-manganese ratios (see figures 4 and 5) were therefore used to determine the region of equilibrium. The subsequent analysis was then applied to all the foils irradiated within these regions, whose dimensions are listed in table 5.

The saturation manganese activities were found by the method of ref. 1, § 13. Each activity was then divided by the irradiation weighting factor (see § 4(1)) and the resulting ratios assumed to be independent of irradiation time or reactor power.

In a cylindrical region of equilibrium spectrum the macroscopic flux distribution is $I_0(Kr)\cos(\alpha z + \beta)$, if there is radial in-leakage, and $J_0(Kr)\cos(\alpha z + \beta)$, if there is radial out-leakage. Superimposed on the macroscopic variation is a fine structure distribution, which is assumed to be separable from it. (This assumption breaks down if the gradients are large). A fine structure amplitude factor A_i was assigned to each of the 37 cell positions listed in table 4 and the flux at any point could then be written

$$\phi_i(r, z) = A_i \frac{I_0}{J_0} (Kr) \cos(\alpha z + \beta)$$

The flux in the equilibrium region was then completely specified by values of K , α and β and the 37 A_i . Outside the equilibrium region the flux cannot be represented by this simple function, hence the requirement to specify the extent of the region.

The foil activities from the equilibrium region were fitted to functions $A_i \frac{I_0}{J_0} (Kr) \cos(\alpha z + \beta)$ by a least-squares fitting programme using Mercury (see Appendix III). The results are presented in tables 5 (macroscopic parameters) and 6 (fine structure factors). Points deviating by more than $3\sigma_D$ were rejected, where σ_D , the relative standard error of the distribution, is:-

$$\sigma_D = \left[\frac{\sum \left(\frac{A_i I_0 (Kr) \cos(\alpha z + \beta) - \phi_{\text{observed}}}{A_i I_0 (Kr) \cos(\alpha z + \beta)} \right)^2}{\text{Number of Degrees of Freedom}} \right]^{\frac{1}{2}}$$

and summation is over all experimental points. The number of degrees of freedom is the difference between the number of experimental points and the

TABLE 5

Macroscopic flux distribution parameters in cores 1 - 5

CORE COOLANT	1b AIR	2b D ₂ O	4 ¹ 20% D ₂ O, 80% D ₂ O	5 ² 40% D ₂ O, 60% D ₂ O	3 H ₂ O
$K(m^{-1})$ (Cores 1b, 2b, 4, 3 to (Kr)) (Core 5 Jo (Kr))	1.058 ± .049	0.976 ± .032	0.458 ± .040	0.04 ± .17	1.229 ± .016
α radians/m.	1.342 ± .010	1.383 ± .006	1.355 ± .004	1.387 ± .004	1.347 ± .005
β radians	-1.561 ± .018	-1.612 ± .010	-1.677 ± .006	-1.714 ± .007	-1.756 ± .008
Buckling $[\alpha^2 \pm \frac{K^2_r}{K^2_z}] m^{-2}$	0.985 ± .082	1.025 ± .061	1.640 ± .036	1.922 ± .04	0.405 ± .04
* Asymmetry = K^2_r/K^2_z	0.73	0.933	0.933	0.933	0.933
σ_D	1.95%	1.91%	1.16%	1.32%	1.78%
Upper extrapolation distance cms.	13.05	10.69	11.12	11.86	10.30
Lower extrapolation distance cms.	34.43	30.72	25.88	23.39	19.95
Equilibrium zone: radius height cms.	52 129	53 129	53 129	53 129	73 129

* K^2_r and K^2_z are obtained from two-group calculations (see § 4 (1v))

TABLE 6

Fine structure factors for manganese activation

	Core 1b		Core 2b		Core 4		Core 5		Core 3		
	A	σ_A	A	σ_A	A	σ_A	A	σ_A	A	σ_A	
d0	0.958		0.858	0.017	0.852		0.821		0.806		d0
d1d	0.975						0.900				d1d
1	1.000	0.0076	1.000	0.0058	1.000	0.0038	1.000	0.0043	1.000	0.0048	1
2	1.025	0.0074	1.067	0.0053	1.066	0.0036	1.061	0.0045	1.075	0.0048	2
3	1.080	0.0075	1.147	0.0058	1.164	0.0042	1.169	0.0051	1.178	0.0054	3
4	1.171	0.0091	1.292	0.0072	1.312	0.0049	1.306	0.0063	1.323	0.0063	4
5			1.496	0.0077	1.546	0.0055	1.553	0.0066	1.581	0.0075	5
6	1.389	0.0095	1.576	0.010	1.637	0.0086	1.674	0.0091	1.751	0.0111	6
ce 1	1.039	0.0079	1.036	0.0053	1.031	0.0036	1.020	0.0038	1.008	0.0048	ce 1
2	1.050	0.0091	1.111	0.0058	1.106	0.0035	1.086	0.0038	1.096	0.0052	2
3	1.129	0.0086	1.176	0.0060	1.190	0.0040	1.184	0.0045	1.189	0.0057	3
4	1.209	0.0095	1.323	0.0070	1.341	0.0046	1.328	0.0050	1.333	0.0067	4
5			1.516	0.0080	1.573	0.0051	1.578	0.0060	1.591	0.0076	5
6	1.377	0.020	1.600	0.015	1.670	0.010	1.684	0.011	1.713	0.015	6
bf 1	1.077	0.011	1.096	0.015	1.082	0.0089	1.084	0.010	1.073	0.011	bf 1
2	1.097	0.013	1.125	0.013	1.148	0.0078	1.131	0.0076	1.141	0.011	2
3	1.142	0.011	1.214	0.014	1.250	0.010	1.233	0.0083	1.193	0.011	3
4	1.236	0.011	1.347	0.013	1.365	0.011	1.377	0.011	1.346	0.024	4
5			1.523	0.017	1.578	0.011	1.604	0.011	1.608	0.013	5
6	1.442	0.020									6
ag 1	1.154	0.023	1.188	0.013	1.201	0.010	1.190	0.0079	1.216	0.0099	ag 1
2	1.157	0.016	1.263	0.014	1.270	0.0075	1.237	0.0083	1.258	0.0094	2
3	1.223	0.014	1.328	0.015	1.338	0.0091	1.341	0.010	1.338	0.017	3
4	1.282	0.026	1.414	0.016	1.451	0.0099	1.434	0.011	1.472	0.019	4
5			1.571	0.018	1.650	0.011	1.632	0.013	1.642	0.015	5
6	1.456	0.017									6
d W1/4	1.591	0.013	1.783	0.012	1.786	0.0077	1.810	0.0084	1.834	0.013	d W1/4
W1 1/2			1.901	0.027			1.929	0.018	1.914	0.024	W1 1/2
W2/3	2.058	0.013	2.145	0.018	2.120	0.010	2.099	0.011	2.052	0.013	W2/3
W2 1/2	2.169	0.013	2.267	0.011	2.210	0.0058	2.174	0.0068	2.134	0.0096	W2 1/2
ce W1/4			1.822	0.024	1.827	0.019	1.801	0.017	1.870	0.024	ce W1/4
W2 1/2			2.282	0.046	2.179	0.018	2.131	0.020	2.078	0.027	W2 1/2
bf W1/4			1.836	0.027	1.841	0.015	1.820	0.017	1.874	0.024	bf W1/4
W2 1/2			2.282	0.031	2.201	0.018	2.180	0.022	2.069	0.026	W2 1/2
ag W1/4	1.711	0.024	1.848	0.027	1.854	0.015	1.825	0.017	1.870	0.024	ag W1/4
W2/3	2.143	0.022									W2/3
W2 1/2	2.233	0.026	2.323	0.020	2.246	0.0075	2.207	0.0094	2.136	0.016	W2 1/2
h W1/4			1.860	0.036	1.865	0.022			1.931	0.034	h W1/4
W2 1/2			2.299	0.046	2.182	0.026	2.156	0.028	2.080	0.037	W2 1/2

number of parameters being fitted. The observed standard errors (see table 5) agreed well with the expected values calculated in § 4 (1), from which it was assumed that the error distribution was reasonably normal and the theoretical function a satisfactory fit to the points.

The macroscopic flux distributions vary little from core to core. The radial distributions are all nearly flat, fitting an I_0 function in cores 1-4 and a J_0 in core 5. The quoted errors in K correspond to uncertainties in the ratio of peripheral to central flux of 1/5%. The measurements are least accurate for core 1, partly because the large migration area results in a small equilibrium region and partly because there were teething troubles with the experimental technique. The vertical distributions demonstrate a constant upper extrapolation distance, apparently unaffected by the presence or absence of moderator in the fuel clusters above the level of the D_2O in the tank. The lower extrapolation distance (or reflector savings) did however vary according to the composition of the inner zone.

The fine structure factors are plotted in figures 7-10. The radial fine structure in the fuel increases as the amount of moderator in the fuel cluster increases, but the overall maximum to minimum flux ratio in the cell varies little from core to core. An important consequence of square cell geometry is the flux variation along the cell side, amounting to ~30% in the air core and 16% in the H_2O core. Attempts to discover an analogous circumferential fine structure in the fuel cluster were unsuccessful.

In addition to the measurements with gold-manganese foils, the radial hyperfine flux distribution through the fuel rods was measured with a strip of manganese ribbon 3/16 inches wide, 0.005 inches thick. The results for core 3, which agree well with the fine structure measurements, are shown in figures 11 and 12. The plotted curves are smoothed and represent the best fit to the experimental points consistent with the conditions of symmetry imposed by the fuel rod geometry. Core 3 (H_2O coolant) shows a greater hyperfine effect than any of the other cores. Even then the ratio of maximum to minimum flux in the uranium oxide is only 1.04 with an uncertainty of at least $\pm .01$. Experimental errors in the observations were such that it was possible to estimate the approximate ratio of maximum to minimum flux, but not the exact shape of the flux variation.

It should be emphasized that the graphs show manganese reaction rates and not neutron flux or density. Because of the slight departure of the manganese cross section from a $1/v$ law in the epithermal region, the depression in total neutron density through a cell will be greater than the observed depression in manganese reaction rate. On the other hand the constants K , α , β which describe the macroscopic distribution of manganese reaction rate apply directly to all groups of neutron energies. Thus any convenient detector would have served just as well as manganese for the purpose of finding K , α and β .

(iv) Material Buckling and Reactivity

The critical equation relating reactivity of the lattice to the observed macroscopic flux distribution is, in the two group approximation,

$$k_{\infty} = [1 + \alpha^2 L_{MZ}^2 \pm K^2 L_{MR}^2] [1 + \alpha^2 L_{EZ}^2 \pm K^2 L_{ER}^2],$$

where L_{MZ}^2 and L_{MR}^2 are the axial and radial thermal diffusion areas, and L_{EZ}^2 and L_{ER}^2 are the axial and radial slowing down areas. If the radial distribution is $I_0(Kr)$ the negative sign is taken, if $J_0(Kr)$ the positive.

The measured values of α and K were sufficiently small for the cross terms in α^4 , K^4 etc. to be neglected and it is therefore possible to use the one group formula for k_{∞} , without introducing an error greater than 0.05% in k_{∞} .

$$\text{Thus } k_{\infty} - 1 = M_Z^2 \left(\alpha^2 \pm \frac{M_R^2}{M_Z^2} K^2 \right)$$

No experimental values of M_Z^2 or M_R^2 were available and recourse was therefore had to the lattice calculations mentioned in §.10 of ref. 1. These calculations both gave $\frac{M_R^2}{M_Z^2} = 0.933$ for all lattices except core 1, for which a value of ~ 0.73 was obtained.

Using these calculated values of M_Z^2 and M_R^2 , the material bucklings, defined as $\frac{k_{\infty} - 1}{M_Z^2}$, have been derived from the measured α 's and K 's and are quoted in table 5. The quoted errors do not allow for error in $\frac{M_R^2}{M_Z^2}$, which will be impor-

tant where $\alpha \approx K$ (core 3, core 1), but insignificant in cores 4 and 5 where $\alpha \gg K$. Except for core 1, the errors are all about $0.05 m^{-2}$ and are not very dependent on the value of the buckling.

The values of k_{∞} derived from these measurements, using calculated values of M_Z^2 , have been compared with the results of the Pease-Cobb and modified P.80 calculations. The values of M_Z^2 used are as follows:

Calculation	Core 1	Core 2	Core 4	Core 5	Core 3
Pease-Cobb	.0817	.0367	.0303	.0257	.0176
Modified P.80	.0645	.0275	.0232	.0201	.0147

Both calculations have been corrected to allow for the measured neutron

temperatures in the fuel cluster: the changes involved amount to <0.5% in k_{∞} . The Pease-Cobb results differ from those reported in M727; an error in the calculation of effective resonance integral has been eliminated, causing the predicted values of k_{∞} to rise by 4 - 8%.

The values of k_{∞} calculated and derived from experiment are plotted in figures 6a and 6b. The horizontal scale is a measure of the ratio of moderation to absorption in the fuel cluster, hydrogen atoms being given unit weight and deuterium atoms a weight (= 0.177) proportional to their moderating power relative to hydrogen (see ref. 2). In each case the values of M_Z^2 used to derive the measured k_{∞} were those from the appropriate lattice calculations. For cores 2, 3, 4 and 5 the calculated and measured values of k_{∞} agree to within 1%, which must be regarded as satisfactory in view of the radical simplifications in both the lattice calculations. In core 1, both the calculated values of k_{∞} are much smaller than that deduced from experiments. The high derived value is inconsistent with the trend of the other results. This suggests that the value of M_Z^2 used to derive the measured value of k_{∞} is too high. Since large streaming corrections have been applied to the calculation for core 1 there is considerable doubt about the correct value of M_Z^2 and the migration area asymmetry. It therefore appears reasonable to assume that the measured α and K are correct and to examine the effect of altering M_Z^2 and M_R^2/M_Z^2 . The values of k_{∞} derived from a range of values of these parameters is given below:

M_Z^2 \ M_R^2/M_Z^2	M_Z^2	.040	.045	.050	.055
1.00		1.0273	1.0307	1.0341	1.0375
0.90		1.0318	1.0358	1.3097	1.0436
0.80		1.0363	1.0408	1.0453	1.0498
0.70		1.0407	1.0458	1.0509	1.0560

Several combinations of M_Z^2 and $\frac{M_R^2}{M_Z^2}$ in this table yield a value of k_{∞} in

agreement with that predicted by the Pease-Cobb calculations (1.0336). Remembering that the asymmetry is small when the streaming corrections (and hence M_Z^2) are small, and vice versa, a plausible combination is $M_Z^2 = .045 \text{ m}^2$, $\frac{M_R^2}{M_Z^2} = 0.9$. This implies an overall axial streaming factor of ~ 1.3 .

In order to force agreement with the value of k_{∞} predicted by the P.80 calculation (1.0134) a value M_2^2 less than 0.02 m^2 is required. This is quite unrealistic and suggests strongly that the predicted k_{∞} from this calculation is too low.

(v) Gold-Manganese Ratio Ref. 1., Section 13, paragraph (e)

At equivalent cell positions throughout the constant spectrum region of the core, the gold and manganese reaction rates should follow the same macroscopic distribution. Within the cell, however, they will differ due to hardening of the spectrum in the fuel, and the gold-manganese ratio is a direct measure of the change in the relative densities of thermal and epithermal neutrons. By using calibrated gold-manganese alloy foils, the measured ratio is independent of monitor foils, macroscopic flux distributions and errors of relative positioning. It is only necessary to know the self screening factors and what ratio the foils would give in a known spectrum.

Experiments to determine the self-screening factors are described in Appendix IV of this report. The gold-manganese ratios resulting from activations in known spectra are given below. These ratios are based on the humped joining function of Westcott (S4 of ref. 11).

Gold-manganese Ratio	Westcott "r"
1.005	0.000 at 20°C
1.888	0.083 at 60°C

Table 7 gives the observed gold-manganese ratios in each of the five cores, together with their statistical errors. Figures 13 and 14 show radial and axial plots of the gold-manganese ratio in a single cell for each of the cores. In all of the radial plots except the air-filled core, the ratio decreases more in the fuel region than in the moderator. In the axial direction the change in ratio occurs mostly in the aluminium end plates.

Figures 4 and 5 show macroscopic distributions of gold-manganese ratio as functions of core radius and height. It is seen that the air-filled and D₂O-filled cores have a distinctly smaller equilibrium region than the other cores. Graphs similar to these were used to determine the region in each core which would be used for detailed measurements of spectrum and flux. Table 5 gives the dimensions of the equilibrium regions actually used in each of the five cores.

(vi) Lutecium-manganese Ratio Ref. 1, Section 13, paragraph (e).

This ratio is a convenient measure of the effective neutron temperature of the thermal spectrum. Like the gold-manganese measurements, it is independent of monitor foils, macroscopic flux, and errors of relative positioning.

TABLE 7

Gold manganese ratio fine structure factors

Foil Position	Core 1B		Core 2B		Core 4		Core 5		Core 3	
	R	σ_R	R	σ_R	R	σ_R	R	σ_R	R	σ_R
d 0	2.444	.061	2.471	.062						
1a	2.458	.034								
1	2.424	.026	2.240	.012	2.132	.008	2.033	.010	1.744	.009
2	2.389	.021	2.213	.009	2.086	.008	1.946	.013	1.717	.007
3	2.408	.027	2.172	.010	2.023	.010	1.907	.009	1.681	.006
4	2.328	.019	2.081	.011	1.952	.008	1.818	.012	1.623	.006
5			2.023	.013	1.857	.009	1.745	.007	1.571	.009
6	2.241	.018	1.993	.013	1.826	.013	1.696	.017	1.514	.016
c, e, 0										
1a	2.499	.036								
1	2.350	.019	2.211	.009	2.110	.008	2.007	.009	1.733	.007
2	2.396	.025	2.196	.011	2.054	.006	1.952	.008	1.713	.006
3	2.317	.024	2.155	.008	1.996	.010	1.912	.008	1.673	.006
4	2.324	.017	2.079	.010	1.938	.007	1.824	.010	1.641	.007
5			1.992	.008	1.870	.011	1.750	.010	1.552	.006
6	2.248	.040	1.974	.022	1.805	.013	1.713	.012	1.510	.012
b, f, 0										
1a										
1	2.400	.030	2.214	.031	2.076	.030	1.980	.028	1.697	.024
2	2.438	.034	2.143	.014	2.038	.016	1.938	.011	1.663	.008
3	2.365	.030	2.114	.030	1.978	.027	1.884	.024	1.647	.021
4	2.341	.026	2.080	.026	1.885	.033	1.819	.025	1.571	.020
5			2.012	.025	1.864	.021	1.729	.020	1.549	.013
6	2.223	.039								

TABLE 7 (Cont.)

Gold manganese ratio fine structure factors

Foil Position	Core 1B		Core 2B		Core 4		Core 5		Core 3		
	R	σ_R	R	σ_R	R	σ_R	R	σ_R	R	σ_R	
a, g, 0											
1a	2.354	.059									
1	2.314	.058	2.100	.021	2.004	.023	1.898	.020	1.656	.019	
2	2.334	.041	2.134	.030	1.964	.022	1.892	.021	1.650	.017	
3	2.370	.042	2.080	.028	1.924	.027	1.801	.025	1.617	.022	
4	2.300	.058	2.020	.023	1.893	.022	1.801	.021	1.583	.022	
5			2.016	.023	1.850	.023	1.731	.022	1.547	.018	
6	2.217	.029									
d	W1/4	2.165	.023	1.945	.007	1.814	.022	1.672	.010	1.517	.011
	W1 $\frac{1}{2}$ /3 $\frac{1}{2}$			1.908	.034			1.669	.030	1.469	.026
	W2/3	1.998	.005	1.833	.010	1.734	.013	1.614	.009	1.496	.009
	W2 $\frac{1}{2}$ /ST	1.950	.006	1.830	.006	1.698	.004	1.613	.007	1.469	.006
c, e,	W1/4			1.912	.034	1.791	.044	1.655	.029	1.536	.027
	W2 $\frac{1}{2}$ /ST			1.844	.046	1.704	.030	1.586	.028	1.505	.027
b, f,	W1/4			1.861	.033	1.820	.046	1.700	.030	1.487	.026
	W2 $\frac{1}{2}$ /ST			1.817	.032	1.777	.031	1.659	.029	1.516	.027
a, g,	W1/4	2.111	.037	1.924	.028	1.829	.027	1.684	.025	1.552	.022
	W2/3	1.944	.025								
	W2 $\frac{1}{2}$ /ST	1.946	.008	1.821	.014	1.704	.007	1.599	.009	1.482	.011
h,	W1/4			1.884	.047	1.820	.046			1.556	.039
	W2 $\frac{1}{2}$ /ST			1.833	.046	1.649	.041	1.631	.041	1.509	.038

The lutecium foils were calibrated by irradiation in a known Maxwellian spectrum.

The axial variation of neutron temperature within the cell was found to be negligible and nearly all measurements of the lutecium-manganese ratio were made in the mid-plane of the cell, the "d" level.

Figure 16 shows the radial fine structure of the lutecium/manganese ratios for the various cores. The greatest change in neutron temperature occurs in the air filled core, and the least, as might be expected, occurs in the H₂O filled core. The H₂O filled core is also the best moderated, and therefore has the lowest lutecium/manganese ratio among the five cores. For comparison the lutecium/manganese ratio in a pure thermal flux at 20°C is 1.748 and the ratio changes by ~1% for 3°C change in neutron temperature.

Neutron temperatures deduced from the lutecium-manganese ratios are given in table 8 and figures 17 and 18 and the results for core 3, compared with the results from the fine structure stack, are given in table 13 and figure 26.

(vii) Rhodium reaction rate distributions

The rhodium measurement technique described in ref. 1 was modified during the course of the DIMPLE experiments. It was found that improved accuracy could be obtained by more careful correction for the thermal activations of impurities in the rhodium foil, and a more satisfactory standard was used for checking the counter sensitivity and channel gain. The modified techniques are described in detail in ref. 10.

The rhodium measurements in DIMPLE were mainly confined to measurements of the radial fast flux fine structure within the equilibrium spectrum region of zone 1. The comparatively low accuracy of the rhodium measurement made them less suitable as an indicator of spectrum non-equilibrium than gold manganese ratios. The decision to concentrate on radial fine structure, at the expense of axial, reflected not only the greater importance of the radial fine structure to the fast fission factor, but also the possibility of comparing radial measurements with Monte Carlo calculations. These calculations could not be extended to axial variations.

The observed saturation activities of the rhodium foils have been normalized so that they refer to a standard source strength of fission neutrons. First the foil activities from the different irradiations on a particular core have been normalized relative to the irradiation weighting factor of the first irradiation on that core. Secondly, the thermal flux and "r" value (see § 5) at the monitor foil position have been calculated from the known absolute calibration factor from the monitor foils (ref. 9). Then, using the measured fine structure factors for flux and "r", the fission rates in the fuel rods due to thermal and epithermal fission (but not due to U²³⁸ fission) have been calculated. The rates for all 90 rods are then summed to give the total fission rate per lattice cell over unit length. The foil activities have then to be reduced to the form: saturation c.p.m./fission/sec. per cell per cm. length. The quantity is plotted in figure 16.

It will be seen that the fast flux shows marked fine structure across the

cell and that the flux is substantially higher in core 1 than in the other cores. These results are discussed in more detail in a separate report (10) and they are there compared with the results of the Monte Carlo calculation SPEC and with measurements of U^{238} fast fission.

5. Spectrum Characterization by Integral Methods

The form of the thermal and epithermal neutron spectra in the S.G.H.W. reactor is complicated by several features of the lattice cell. These include:

- (i) the presence of two separate moderators which affect the thermalization process and the shape of the thermal spectrum,
- (ii) the high neutron absorption of the fuel bundle and the high temperature of the coolant which results in a thermal neutron spectrum whose effective temperature varies across the bundle,
- (iii) the axial variation of coolant density, resulting in hard spectra near the top of the core,
- (iv) the large diameter of the fuel bundle relative to the lattice pitch which with (i) and (ii) above results in a marked epithermal flux fine structure.

The variation of neutron spectrum through the fuel bundle and the hardness of the spectrum in regions of low coolant density make accurate characterization necessary for reactivity and flux peaking calculations.

In the absence of a neutron spectrometer, integral methods were used to characterize the spectrum. Measurements were made, at a number of different positions in the cell, of various reaction rate ratios which depend critically on the form of the neutron spectrum. Both foil activation and fission chamber measurements were made, and in addition, a few cadmium ratios were obtained with a boron ionization chamber. The foil activation measurements formed part of the normal foil irradiation programme, except for the vanadium irradiations which were carried out separately because of the short half-life of the induced activity. These measurements are detailed in table 8 with the results of the interpretation given below.

The preliminary interpretation consisted of comparing the measured reaction rates with those predicted from simple empirical spectra defined by Westcott (11). The empirical spectra consisted of a Maxwellian thermal distribution, a dE/E epithermal flux and a joining function of given shape covering the range 0.1 - 0.5 eV. The spectra were defined by three parameters: 'r', the intensity of the epithermal component relative to the thermal; T, the temperature of the Maxwellian; and the joining function. Three different joining functions were examined; they were the 2.8 kT Campbell-Freemantle join (12) and S_2 and S_4 ref. 11. Values of g and s from ref. 11 were used to deduce values of r and T from different measurements. The preferred joining function was that which gave the most consistent estimate of r and T from the different measurements of Table 8.

The analysis of the different measurements in terms of these spectrum models is discussed below.

TABLE 8 (Cont'd)

Core	1		2		4		5		3			
	Air		D ₂ O		20% H ₂ O		40% H ₂ O		H ₂ O			
	d3	s.t.	d3	s.t.	d3	s.t.	d3	s.t.	d3	s.t.		
DERIVED VALUES												
(1) From U235, V and B10 cadmium ratios	$r \sqrt{\frac{T}{T_0}}$.190	.114	.148	.0902	.131	.0775	.115	.0718	.0736	.0596	
(2) Combining $r \sqrt{\frac{T}{T_0}}$ with L and assuming												
a) 2.8 kT epithermal cut off Campbell & Freemantle (12)	T (°C) $\frac{U_g \text{ calculated}}{U_g \text{ experimental}}$	{ 90 rod cluster 89 " "	94 .980	47 .998	63 .918 .933	36	63 .959	33 .945	47 .959 .968	26 .971	39 .959 .965	24 .997
b) 3.67 humped epithermal cut off. (S ₄ of ref. 11)	T (°C) $\frac{U_g \text{ calculated}}{U_g \text{ experiment}}$	{ 90 rod cluster 89 " "	162 1.067	73 1.055	105 .984 1.000	52	98 1.020	44 .978	73 1.013 1.023	37 1.002	51 1.009 1.015	27 1.020
c) 5.04 kT epithermal cut off (similar to S ₂ of ref. 11)	T (°C) $\frac{U_g \text{ calculated}}{U_g \text{ experimental}}$	{ 90 rod cluster 89 " "	161 .995	79 1.008	109 .931 .946	60	103 .972	52 .960	79 .969 .978	44 .988	58 .989 .995	37 1.015

Note: (1) The normalisation of bare ratio measurements is taken as g_1/g_2 at 20°C, i.e. $R = 1.005$, $L = 1.748$, $U_g = 1.077$, $U_3 = 1.037$

(11) The values of U_g in cores 2 and 4 are less accurate than the rest, say $\pm 2\%$.

(1) Interpretation of the gold-manganese ratio

Using Westcott's notation the gold-manganese ratio is:-

$$R = \frac{s_{Au} + r s_{Mn}}{s_{Mn} + r s_{Au}}, \text{ assuming a normalization to } R = \frac{s_{Au}}{s_{Mn}} = 1.005 \text{ in a pure}$$

thermal flux at 20°C.

$$\text{Rearranging, } r = \frac{R s_{Mn} - s_{Au}}{s_{Au} - R s_{Mn}}$$

Writing $s = \sqrt{\frac{4T}{\pi T_0}} \frac{\sigma_r}{\sigma_0}$, where σ_r is the resonance integral above $\frac{1}{v}$,

$$r \sqrt{\frac{T}{T_0}} = \frac{R s_{Mn} - s_{Au}}{\sqrt{\frac{4}{\pi} \left(\frac{\sigma_r Au}{\sigma_0 Au} - R \frac{\sigma_r Mn}{\sigma_0 Mn} \right)}}$$

where the L.H.S. is temperature independent, neglecting the small variation of s_{Au} (0.1%/20°C).

Hence the parameter $r \sqrt{\frac{T}{T_0}}$ can be extracted from the gold manganese ratio, without knowledge of the neutron temperature or the joining function, since σ_{rMn} and σ_{rAu} are independent of both.

However, this simple analysis is complicated by the following effects:

- (i) a reduction in the effective value of s_{Au} caused by the use of foils which are opaque at the gold resonance,
- (ii) a similar effect for manganese,
- (iii) a higher effective value of r at the 337 eV manganese resonance, due to the depression of the epithermal flux at lower energies by U^{238} absorption,
- (iv) an anomaly in the flux spectrum near the 4.9 eV gold resonance, presumably due to a Placzek discontinuity arising from oxygen scattering of neutrons with energies in the range affected by the 6.6 eV resonance in U^{238} . The discontinuity is at 4.95 eV, very close to the gold resonance.

Subsidiary experiments in LIDO (see Appendix IV) have yielded self shielding factors for the foils employed and these factors have been used to correct for effects (i) and (ii). The gold self shielding factor is important; it is about 0.6. That for manganese is nearer unity, and because s_{Mn} is only one twentieth of s_{Au} (effective) it has only about a 7% effect on r . The higher flux at 337 eV is comparatively unimportant, a 20% increase altering the calculated r by only 4%; since the experimental evidence for this effect is contradictory no correction has been made.

Effect (iv) is difficult to calculate but it is believed to account for the discrepancies between the values of r deduced from these measurements and those obtained from the cadmium ratios of $1/v$ materials such as vanadium and boron. Using values of $\sqrt{\frac{T}{T_0}}$ deduced from lutecium measurements, values of r deduced from different measurements are plotted in figures 17 and 18. In the moderator, the discrepancy between the values based on gold and the other values is barely significant in view of the quoted errors. In the fuel the discrepancy is large in the air core, where the proportion of scattering by oxygen is high; as the proportion of oxygen scattering decreases so does the discrepancy and in the H_2O core it is negligible.

(ii) Interpretation of the lutecium manganese ratio

The lutecium manganese ratio is given by

$$L = \frac{g_{Lu}(T) + r s_{Lu}(T, \text{joining function})}{g_{Mn} + r s_{Mn}(T)}$$

where L is normalized so that, in a pure Maxwellian at $20^\circ C$

$$L = \frac{g_{Lu}(20^\circ C)}{g_{Mn}(20^\circ C)} = 1.748$$

Because of the large resonance at 0.142 eV g_{Lu} is large and varies rapidly with temperature, while s_{Lu} includes a contribution from the upper part of this resonance and consequently depends on the form of the joining function. The higher resonances are small and s_{Lu} is therefore a small positive number at low T , becoming negative at T increases. L therefore shows a weak dependence on r and on the choice of joining function. Values g_{Lu} and s_{Lu} have been calculated for the three joining functions defined above, using the cross section data discussed in ref. 13. The values differ slightly from those recommended by Westcott (ref. 11).

The determination of temperature from measured L value requires a knowledge of $r \sqrt{\frac{T}{T_0}}$ at the point of measurement. This is obtained from cadmium ratios (see below.) A particular form of joining function is next assumed and values of $s_{Lu}(T)$ may then be calculated, as well as $g_{Lu}(T)$. L as a function of temperature is then calculated, for the measured value of $r \sqrt{\frac{T}{T_0}}$, and plotted. The required temperature can then be read off.

The choice of joining function is made by comparing the measured values of U_0 with that calculated from the spectrum parameters derived from L and $1/v$ cadmium ratios. The joining function which gave closest agreement in core 1 (air core) is that equivalent to a $5kT$ cut off; in the other cores the $3.67 kT$ humped out off was preferred. The accuracy of the data did not permit more detailed conclusions to be drawn about the shape of the joining function. (See table 8).

The calculated values of T are plotted for the d_3 and $w_{2\frac{1}{2}}/3T$ position in :

figures 17 and 18. Values of L at other positions are given in figure 15.

(iii) Manganese cadmium ratio

The manganese cadmium ratio was measured in all cores at the d3 and W2₂/ST positions using standard gold manganese foils and, in some cases, 90% manganese/nickel foils. Additional measurements in the fuel region were made in certain cores. The foils were irradiated first bare, then under 0.030 inch cadmium in flat boxes. The flux impinging on the boxes was assumed to be isotropic and the transmission was calculated using Bothe's formula (ref. 14). For a 1/v absorber the effective sharp cut-off was taken as 0.544 eV (of 0.622 eV adopted by Westcott). The reduction in epithermal flux due to local depression of the fast neutron source was estimated by a multigroup diffusion theory calculation. The effect was less than 0.6% in the water filled fuel cluster, for a cadmium sleeve 0.3 inches in diameter and 3 inches long.

Using the Westcott notation:

$$\text{Cadmium ratio (C.R.)} = \frac{\sigma_0 (k + rs)}{r \sqrt{\frac{4T}{\pi T_0}} I}$$

where I = resonance integral above the cadmium cut off. Putting $s = \sqrt{\frac{4T}{\pi T_0}} \frac{\sigma_r}{\sigma_0}$, where σ_r is the resonance integral above 1/v, previously defined,

$$r \sqrt{\frac{T}{T_0}} = \frac{k}{\sqrt{\frac{4}{\pi}} \frac{I(\text{C.R.}) - \sigma_r}{\sigma_0}}$$

The values of $I(\approx 2 \sigma_r)$ and σ_r were calculated from a measured resonance integral which gave values of r in LIDO consistent with those from 1/v cadmium ratios; they were corrected for self shielding in the resonance (see Appendix IV).

The values of $r \sqrt{\frac{T}{T_0}}$ calculated from this cadmium ratio were expected to be higher than those from the vanadium or boron cadmium ratios, because of the higher flux at 337 eV. The results in figures 17 and 18 show that no significant trend was observed. This is surprising; possible explanations are depression of the flux near 337eV due to a U²³⁸ resonance or a large error in the value of σ_r deduced from measurements in LIDO. Uncertainties in the calculation of self shielding prohibited the use of a resonance integral calculated directly from the cross section data.

(iv) Gold cadmium ratio

The gold cadmium ratio was measured in all cores at the d3 and W2₂/ST positions using standard gold manganese foils. Some additional measurements were made with foils of different effective thicknesses.

The experimental technique and the analysis was the same as for the manganese cadmium ratio measurements. Corrections were applied for self shielding in the 4.9eV resonance and values of $r \sqrt{\frac{T}{T_0}}$ were obtained, inde-

pendent of the neutron temperature or the joining function. These values were in close agreement with the values of $r \sqrt{\frac{T}{T_0}}$ deduced from gold manganese ratio measurements (see figures 17 and 18). The consistent difference between r values deduced from gold activation and from $1/v$ detectors supports the hypothesis of spectrum anomalies in the region of the gold resonance.

(v) Vanadium cadmium ratio

V^{51} exhibits a $1/v$ cross section variation at low energies and its resonance integral is very small ($s \approx 0.045$, cf. $s_{Mn} = 0.64$). The cadmium ratio therefore defines a value of $r \sqrt{\frac{T}{T_0}}$ which is not dependent on corrections for self shielding or U^{238} resonance absorption effects, but is determined simply by the flux just above the cadmium cut-off.

Natural vanadium is 99.75% V^{51} and 0.25% V^{50} . The latter has an absorption cross section of 100 barns for the formation of stable V^{51} . The 2200 m/s cross section of V^{51} is 4.9 barns, leading to V^{52} which decays with a 3.7 minute half-life, emitting a 2.5 Mev β particle and a 1.4 Mev γ ray. Vanadium foils, $\frac{1}{4}$ inch diameter and 0.010 inch thick, were punched from high purity sheet and weighed. They were irradiated, bare and under 0.030 inch cadmium, at the 3d level in a search tube and in foil positions on rods 1, 3 and 5 in all cores except 1b and 2. Foils were also irradiated inside two of the special fuel rods used for the resonance capture measurements. In this case the cadmium thickness was 0.040 inch. Four foils were irradiated at a time for a period of 15 mins., which was sufficient to saturate the V^{52} activity. The flux was usually between 3×10^7 and $10^8 n/cm^2$ sec. but some under-cadmium irradiations used fluxes of up to $2 \times 10^8 n/cm^2$ sec.

Special procedures were used to unload the foils and transport them to the counting laboratory (a mile distant) in less than 12 minutes from the end of the irradiation.

Four NaI scintillation counter channels were used, one to each foil, and the counting arrangements were identical with those used for manganese (ref. 1). The activities were followed for 4-5 half-lives using gradually increasing counting intervals. Totals of 10,000 to 20,000 counts were obtained for the least active foils under cadmium. Non-linearity of decay during the counting interval was allowed for and the data were analysed using a Mercury Autocode programme (ref. 15).

Calibration irradiations on LIDO established that

- (i) the activation of each foil was proportional to its mass.
- (ii) the channel counting efficiency for vanadium was proportional to that for the cobalt standard.

- (iii) the vanadium activity has a half-life of $3.76 \pm .01$ minutes over nine half-lives from 3 minutes after the end of the irradiation.

The cadmium ratio was measured in LIDO to confirm the chosen value of 's'.

The statistical accuracy obtained was 1% for foils irradiated under cadmium and $\frac{1}{2}$ % for foils irradiated bare. An error in the half-life would tend to cancel in the cadmium ratio, but an error of 3 seconds in timing or in chronometer intercalibration would result in a 1% error in the corrected activity. The monitor foils determine the power of an irradiation to $\frac{1}{2}$ %. Assuming 1 second timing errors the standard error on the cadmium ratio becomes 1.5%.

Values of $r \sqrt{\frac{T}{T_0}}$ were deduced from the measured cadmium ratios, using the formulae of section (iii); these values were independent of joining function and neutron temperature and they agreed, within the accuracy of measurement, with the boron, indium and U^{235} cadmium ratio measurements. The average values of r deduced from all these measurements, assuming the values of T deduced from lutecium, are plotted in figures 17 and 18.

(vi) Indium cadmium ratio

The cadmium ratio of 0.005 inch indium foil was measured in all five cores. In^{115} has a large resonance at 1.456eV which contributes 97% of the episcadmium activation and the cadmium ratio is therefore a measure of the epithermal flux at this energy.

Neutron capture by In^{115} leads to In^{116} , which decays with a half-life of 54 minutes, emitting a β particle and γ rays of energies 2.1, 1.5, 1.27 and 1.09 MeV. With the counting arrangements used neither the 13 second activity from In^{116} nor the two activities due to capture in In^{113} (4.2% abundance) contributed significantly to the measured activity.

Foils, $\frac{1}{4}$ inch in diameter, were punched from a sheet of 0.005 inch pure indium foil sandwiched between 0.002 inch aluminium foils. The need for intercalibration was avoided by using the same foils for bare and subcadmium irradiations. The foils were irradiated at the d level in a search tube and on rod 3 in the equilibrium zone. Some additional measurements were made in other rod positions. The indium foils were irradiated in the course of the normal irradiation programme, usually at fluxes between 3×10^7 and 10^8 n/cm². sec., and the counting arrangements were identical with those used for manganese. The same cadmium boxes were used. Examination of the count rates obtained from one foil in different channels established that the channel counting efficiency for indium was proportional to that for the cobalt standard. The half-life was measured over six hours and agreed with the published values. The count rate data was analysed using a Mercury Autocode programme (ref. 15).

The statistical accuracy obtained was always better than 1/3%, but some of the bare foils had count rates of up to 40,000 c.p.s. which involved a dead time correction of 10%. This could only be made to 10% accuracy and the activity of these foils was therefore known to 1%. Assuming that the monitor

foils determined the flux in each irradiation to $\frac{1}{2}\%$, the error on the cadmium ratio amounts to 1.5%.

Values of $r\sqrt{\frac{T}{T_0}}$ were deduced from the measured cadmium ratios using the formulae of section (iii). Because the foils were thick it was necessary to apply a large self shielding correction to the resonance integral used in the calculation; this correction was determined by measuring the cadmium ratio in the known spectrum at the centre of LIDO. The indium cross section is not exactly $\frac{1}{v}$ in the thermal region and the value of $r\sqrt{\frac{T}{T_0}}$ therefore varies slightly according to the temperature assigned to the Maxwellian, 'g' altering by 0.4% per 20°C temperature rise. The shape of the joining functions also has a small effect on $r\sqrt{\frac{T}{T_0}}$, but this was small enough to be neglected. When these corrections had been applied the values of 'r' derived from indium agreed, within the error introduced by poor cross section data, with those from vanadium, boron and U²³⁵.

(vii) Fission chamber measurements

U²³⁵, U²³³ and Pu²³⁹ fission chambers were used to obtain cadmium ratios and reaction rate ratios in the fuel and moderator of all five cores. The fission chambers were $\frac{1}{8}$ inch diameter and had walls of stainless steel or inconel. They were located in the core inside blind ended aluminium tubes. One of these tubes was positioned centrally in a D₂O filled search tube so that the fissile material in the chamber was at the 3d level in the third ring of fuel in the cluster. To estimate the flux perturbation caused by replacing a fuel rod by an aluminium tube containing a fission chamber, some measurements were also made with bare U²³⁵ and Pu²³⁹ fission chambers inserted through small holes in the cluster plates, between the second and third fuel rings. No significant perturbation was observed in the U²³⁵/Pu²³⁹ reaction rate ratio.

Cadmium ratio measurements were made by determining the count rate first bare, then with the fission chamber inserted into a blind ended cadmium tube 1.125 inches long, of 0.040 inch wall. The flux level was monitored with a second chamber, and bare and sub-cadmium measurements were alternated until it was evident that there were no drifts in channel gain or bias. A small correction was applied for neutrons reaching the fissile material through the open end of the cadmium sleeve.

The reaction rate ratios, $U_9 = \frac{\text{Pu}^{239} \text{ fission rate}}{\text{U}^{235} \text{ fission rate}}$ and $U_3 = \frac{\text{U}^{233} \text{ fission rate}}{\text{U}^{235} \text{ fission rate}}$ were measured, normalized so that the same ratios in a pure Maxwellian spectrum at 20°C were equal to $\frac{g_9}{g_5}$ and $\frac{g_3}{g_5}$. The results are quoted in table 8.

To eliminate the counter efficiencies from these ratios it was necessary to ensure that the discriminator bias levels were reproducible. The operating bias level was defined by reference to the Pu²³⁹ α -particle pulse distribution, and was critical because the slope of the bias curve was about 2%/Volt at the working point (25V) and varied from chamber to chamber.

During the course of the experiments it was found that pile-up was affecting the α -particle pulse distribution. Changes in amplifier time constants or cable capacities caused shifts in the pulse distribution which altered the working point on the bias curve. Eventually satisfactory calibration factors were obtained by irradiating the chambers in a thermal flux in the DIMPLE reflector and controlling the electronic conditions rigidly. However, a method of calibration which avoided the use of the α -particle pulse distribution altogether would have been preferable.

Following the treatment of the lutecium-manganese and gold-manganese ratios we may write:

$$U_9 = \frac{g_9 (T) + r s_9 (T, \text{ joining function})}{g_5 (T) + r s_5 (T)}$$

where g and s refer to fission.

The calculated value of U_9 was compared with experiment for three separate joining functions using the values of r and T derived from $1/v$ cadmium ratios and lutecium-manganese measurements (see table 8 and B 5 (ii)).

The ratio U_3 shows a small variation with neutron temperature due to a change of $0.02\%/^{\circ}\text{C}$ in g_5 ; because of the low values of s_5 and s_3 it varies only slowly with r . It is therefore a poor spectrum indicator. Values of U_3 were calculated for the various cores, using the values of r and T deduced from more sensitive measurements, and disagreed with experiment by a little more than the expected errors. No useful data were therefore obtained from the measurements of U_3 .

Using a value of s derived from measurements in a known spectrum, $r\sqrt{\frac{T}{T_0}}$ calculated from the U^{235} cadmium ratio agrees closely with that deduced from boron, vanadium, and indium, cadmium ratios.

The plutonium cadmium ratio is very sensitive to the cadmium cut-off because of the resonance at 0.3eV . The measured values of R_9 are consistent with a resonance integral of 320 barns when screened by a 0.040 inch cadmium box, in an isotropic flux.

(viii) Boron Chamber Measurements

The boron ionisation chamber used for these measurements was of similar construction to the fission chambers described above, and contained about 1 mg of B^{10} . The $\text{B}^{10}(n,\alpha)\text{Li}^7$ reaction releases only 2.8 Mev of kinetic energy which is shared between the Li^7 and the α particle. Since the boron is coated on the walls of the chamber only one of these particles causes a track in the gas and the largest pulses are therefore less than half the height of U^{235} α -particle pulses. The pulses were fed into a specially built preamplifier which has a noise level equivalent to only 500 ion pairs (16). A continuous pulse height distribution was obtained at the main amplifier output from noise (at 10V) to a maximum of 50 V. There was no plateau.

Reproducible results were only obtained because of the high stability of the amplifier and discriminator.

Boron has a $1/v$ cross section which extends to 0.1 MeV; thus it is one of the few materials whose epithermal cross-section is well known. Most of the epi-cadmium reaction rate occurs at a few eV and the interpretation of these measurements is dependent on the effective energy of the cadmium cut off. A change of 10% in the effective cadmium cut off would change the boron epi-cadmium reaction rate by 5%. However the cadmium cross-section is well known and the chamber geometry simple and the attenuation of neutrons into the chamber is therefore calculable.

Measurements of the boron cadmium ratio were made in the same positions as the fission chamber measurements in cores 1 and 5. The values of $r \sqrt{\frac{T}{T_0}}$ deduced from these measurements agreed with the results of vanadium, indium, and U^{235} , measurements.

(ix) Summary

The spectrum parameters deduced from the integral measurements are presented in figures 17 and 18.

The inherent limitations of the integral method dictate the use of a simple model for the spectrum and the discrepancies in the gold and manganese measurements show that this model is not adequate to describe the spectrum, particularly the effects of U^{238} absorption, completely.

However analysis of the measurements recorded in table 8 leads to the following conclusions.

- (i) The values of r and T vary, from core to core and within the lattice cell, so as to show the expected dependence on the ratio of absorption to moderating power.
- (ii) The most appropriate form of joining function for all cores except core 1 - the hardest spectrum - is S_4 of ref. 11, i.e. that preferred by Westcott for a wide range of well moderated lattices. In core 1, S_2 of ref. 11. ($5kT$ cut-off) is better.
- (iii) The uncertainty in plutonium reaction rate due to lack of detailed knowledge of the joining function is unlikely to exceed 3% at any point.
- (iv) The calculated spectrum parameters, r and T , are adequate to determine η and f to the necessary precision for calculating neutron balance.

It should be emphasized that these conclusions apply to a system free of plutonium, or other non $1/v$ absorbers, and at uniform temperature. They would not necessarily apply to a hot, burnt-up power reactor lattice.

6. Perturbation Measurements

(i) Cadmium Absorber Effectiveness

The changes of reactivity produced by inserting a cadmium rod into the core at different radii were measured in cores 1, 4 and 5. Empty search tubes were inserted in positions 12 ($r = 0$ cm.), 13 ($r = 21.3$ cm.), 19 ($r = 42.5$ cm.), 14 ($r = 63.8$ cm.), 22 ($r = 85.1$ cm.) and 3 ($r = 109.5$ cm.) and the change in critical height was measured as a standard cadmium tube (24 inches long, 0.75" diameter) was lowered successively into the different search tubes so that its centre coincided with the core mid plane. Using the measured values of $d\rho/dH$, the change in critical height was converted to reactivity. The results are plotted in fig. 19. As is to be expected the cadmium is most effective at a radius of 90 cm., corresponding to a position in zone 2. In core 1 the effectiveness at the centre of zone 1 is relatively low, due to the low thermal flux observed there. The difference between measurements in cores 4 and 5 is not understood and does not correspond to measured or calculated differences in fluxes or adjoints.

(ii) Void Coefficient

The changes in reactivity produced by inserting an air filled search tube at different radii were measured in cores 3 and 5. The perturbations were very small (2 mm in critical height) and the accuracy obtained was low. The results are plotted in figure 20.

7. Engineering and Operational Features

(i) Fine control rod

(a) Description

DIMPLE is designed to be controlled during normal operation with the fine control pump, which is a variable speed, reversing, positive displacement pump with a maximum capacity of 5 g.p.m. Because water leaks back slowly through this pump when it is not operating, the pump must be run almost continuously if the D_2O height in the tank is to be maintained and the reactor power kept constant. To reduce wear it was normal practice to valve off the control pump on reaching the required power level, subsequently controlling the reactor with a cadmium fine control rod. This consists of a cadmium tube, 8 inches long and $\frac{1}{2}$ inch diameter, suspended from a fine cable in an empty search tube in position 22, four lattice pitches from the reactor centre. The cable was suspended from a drum driven by a constant speed reversing motor. In its lowest position the control rod was 143 cms above the tank bottom; in normal use it was placed at elevation 185 cm., which is about mid-way between the reactor centre plane and the top of the fuel clusters. In this position its reactivity worth is approximately 0.02% $\delta k/k$; this was small enough for the rod drive not to require interlocking with the safety circuits. The normal operating practice was to bring the reactor to the required power using the control pump, the fine control rod being near the middle of its range of travel, then to valve off the control

pump and maintain the demanded power by small rod movements (usually less than 2 cm.).

(b) Effect on reactor flux distributions

Three $\frac{1}{8}$ inch diameter, 4 ft. long fission chambers were used to observe changes in neutron flux as the fine control rod was moved from its fully out position to its normal operating position. The three fission chambers were centrally located in dry vertical search tubes at the following radial positions:

S.T. 12 - Reactor centre.

S.T. 19 - 2 lattice pitches from the centre, on a radius with the fine control rod.

S.T. 14 - 3 lattice pitches from the centre, on a radius perpendicular to the above radius.

Observations of neutron flux were made at 6 different elevations in search tubes 12 and 19, while the fission chamber in S.T. 14 was kept at a fixed level. All measurements were made with the reactor operating at a nominal level of 1% of 9×10^7 n/cm²-sec. The "Deviation Channel" was used, and corrections to the nominal level could be made with a maximum error of 0.1%. In effect all measurements were relative to a constant neutron flux in the "Deviation Channel" ion chamber. It should be noted that the ion chamber is in the graphite reflector approximately 2 lattice pitches from the fine control rod, at an elevation of 80 cm. above the tank bottom. Consequently when the fine control rod is inserted, it is expected that all fluxes at positions greater than about 2 lattice pitches from the fine control rod will increase. The increase should be greatest at the reactor boundary farthest from the fine control rod.

(c) Measured flux distortions

The fission chamber in S.T. 14 at a fixed level of 121.3 cm. above the tank bottom gave the following result:

Ratio of counting rates: $\frac{\text{fine control rod in}}{\text{fine control rod out}} = 1.0061 \pm .0010$

The quoted value and standard error result from averaging twelve observations. The corresponding ratios for the fission chambers in the other search tubes at the different elevations are listed below. The standard error of each ratio is estimated to be 0.0022 from the statistics of the observations in S.T. 14.

TABLE 9

Perturbations due to fine control rod

Elevation cm.	Ratio: $\frac{\text{Control rod in}}{\text{Control rod out}}$		
	S.T. 12	S.T. 19	S.T. 14
103.5	1.0050	1.0015	-
121.3	1.0048	1.0017	1.0061
139.0	1.0074	1.0000	-
156.8	1.0088	0.9995	-
174.6	1.0067	0.9992	-
192.4	1.0139	1.0021	-

Note: The 139.0 cm. level is the mid horizontal plane of the UO₂ fuel. The levels at 121.3, 139.0 and the positions used for manganese monitor foils in S.T. 14 and 19 throughout the foil irradiation programme.

In addition to the evidence of the above experiments, it was noticed during normal foil irradiations that the "Linear channel" ion chamber current increased by 0.8% when the fine control rod was inserted and the "Deviation Channel" current kept constant. The "Linear channel" ion chamber is situated in the reflector, opposite the "Deviation Channel" at a height of 80 cms. above tank bottom.

(d) Conclusions

As expected, the flux level increases in S.T.'s 12 and 14 and at the linear ion chamber when the fine control rod is inserted; these locations are all more than two lattice pitches from the rod. The increase is about 0.5% on the reactor centre plane, possibly increasing at the top of S.T. 12 to ~0.75%. No effect is noticed at any height in S.T. 19, which is exactly two lattice pitches from the rod.

Thus when the fine control rod is inserted three of the monitor foil activation will remain constant and three will increase by 0.5%; the average will increase by 0.25%. Ignoring local flux depressions in pressure tubes E9 and F9 the average flux in Zone 1 will increase by about 0.5%. A net error of 0.25% is therefore to be expected. This is barely significant since the errors on individual foil measurements are ~1.5%.

(ii) Flux scanning device

This device was described in ref. 1. It was originally fitted with four aluminium wires to which foils could be attached at any height throughout the core. The tensioning devices for these wires proved unsatisfactory in operation and they were replaced by double lengths of 6 lb. nylon fishing line. A fifth line was also added at the centre of the cell side. The positions in the cell accessible to the flux scanning device are shown in fig. 3.

The accuracy of positioning of foils on the flux scanning device was checked at the end of the experiments when the core was being dismantled. It was found that foils on the wire farthest from the axis were located vertically within $\frac{1}{8}$ inch of the nominal height and within $\frac{1}{16}$ inch in the direction normal to the plane of the wires. In the radial direction the accuracy was $\frac{1}{8}$ inch. Errors due to positioning were therefore less important than counting errors.

Inserting the flux scanning device into the reactor caused a small reduction in reactivity, and therefore an increase in critical height, and a local perturbation of the thermal flux. The flux perturbation was examined in core 5 by measuring the change in fission chamber count rates when the flux scanning device was inserted in the reactor. Fission chambers were inserted in S.T. 12 and pressure tube E 6 in the positions used for spectrum characterization and in an empty search tube in position 19. On inserting the flux scanning device the critical height increased by 0.8 cms. and the fluxes in S.T. 12 and E 6 decreased by 0.75%. The flux in S.T. 19 increased slightly. The fission chamber in this channel was above the centre plane and the increase was ascribed to the shift in vertical flux distribution with increasing critical height. It was concluded that the nearest foils to the flux scanning device might experience flux depressions of up to 1% and that foils more than 1 lattice pitch distant would not be significantly affected. The foil irradiations were planned so as to minimise the number of foils irradiated near the flux scanning device.

(iii) D₂O Handling

In addition to the normal transfer and handling of the DIMPLE moderator, the S.G.H.W. experiment involved the preparation and handling of several batches of D₂O and D₂O/H₂O mixtures for use as moderator and coolant simulant inside the pressure tubes. The liquids present inside the Zone 1 and Zone 2 pressure tubes throughout the experiments are listed in Appendix I. The handling techniques adopted are described below.

(a) Zone 1 pressure tubes

Special precautions were necessary in filling the Zone 1 pressure tubes with liquid to ensure that the metal surfaces were dry before filling and to ensure that no air was trapped by the narrow clearances between fuel rods and cluster plates and between cluster plates and the pressure tubes.

The filling procedure was to connect each tube, already loaded with fuel, in turn to a vacuum pump; to evacuate the tube to a pressure of

3 cm Hg; to isolate and ensure that the pressure did not double in less than two minutes; to re-evacuate to 3 cm. Hg and to admit the required coolant to the evacuated tube from a polythene bottle containing the correct volume (16.8 litres) of liquid. The partial vacuum was then broken by admitting dry nitrogen to one atmosphere pressure.

The method of emptying was to remove the fuel clusters, allowing them to drain into a tray on the reactor top. The drainings were subsequently recovered and used to make up D₂O/H₂O mixtures of lower concentration. The remaining coolant was then removed from the tube by suction into a stainless steel drum, using a vacuum backing pump. Finally, the tube was dried with lint-free cotton swabs and with swabs wetted with acetone.

Initially the pressure tube caps were bolted to the pressure tubes to form an air-tight seal, but when corrosion and gas evolution were discovered all the caps were drilled with a 3/16" diameter hole to allow continuous venting. After corrosion had been discovered in core 2a all the pressure tubes were emptied and they and the cluster plates were subjected to acid-alkali cleaning. The fuel rods were washed in demineralised water and dried with acetone. When the fuel was reloaded fresh D₂O was used in the pressure tubes and the initial batch was filtered and deionized to remove the corrosion products (see § 10).

The coolant simulant used in core 3 was H₂O. The filling procedure was to empty and dry the pressure tube in the normal manner, then to pour in 16.8 litres of deionized H₂O. The fuel cluster, after draining, were rinsed in H₂O and then loaded into the pressure tubes. Difficulty was experienced locating the lower cluster under several feet of water but the method was quicker than that used for the D₂O mixtures. The fact that the clusters were wet on being loaded prevented large volumes of air being trapped inside them.

The coolant simulant for core 4 was obtained by mixing a fraction of the filtered D₂O used in core 2a with deionized H₂O. Five drums of mixture were prepared and to ensure uniform composition the drums were connected in series and the mixture circulated with a small pump for four hours. The isotopic purity of several samples was checked before the mixture was used and a value of $79.83 \pm .02\%$ W/W D₂O obtained. At the end of the programme on core 4 samples were taken from several tubes which had been opened frequently and a value of $79.59 \pm .07\%$ W/W D₂O was then obtained. The average composition during the irradiations with this core was then taken to be $79.7 \pm .1\%$ W/W D₂O.

The filling procedure for core 4 was similar to that for core 2 (see above). The fuel clusters were removed and dried by compressed air blasts, by portable hot air driers and by being placed in a hot cupboard attached to the DIMPLE freezer drier unit. Not more than 6 clusters were removed from the reactor at any time.

At the end of the irradiations on core 4 the tubes and the fuel clusters were emptied and dried and a short series of experiments were carried out in the air filled core (core 1c). During this period a

proportion of the degraded D₂O from core 4 was further degraded and, after thorough mixing, an average isotopic purity of 60.21 ± .07% W/W D₂O was obtained.

The filling procedure for core 5 was similar to that for core 2. At the end of the irradiation programme the top two clusters were removed from each pressure tube and the liquid level lowered by suction to the top of the third cluster. The top two clusters were then replaced. After one week of operation in this condition, all the fuel was removed and all the liquid extracted using the procedure for core 2. Further measurements of isotopic purity made at the end of the programme yielded a value of 60.0% W/W D₂O. The average composition during the irradiations was therefore taken to be 60.1 ± .1% W/W D₂O.

(b) Zone 2 pressure tubes

Liquid handling in Zone 2 was simplified by the construction of the fuel boxes, which made it possible to pour D₂O over them in situ or to lower them into place through several feet of D₂O without in either case trapping large air bubbles. Furthermore, as the liquid composition did not change throughout the experiments much less handling was required.

The filling procedure for Zone 2 was as follows:- All pressure tubes were loaded with fuel. The correct volume (30.5 litres) of D₂O was transferred to a polythene bottle, a pressure tube was purged with dry nitrogen for five minutes and the contents of the bottle were then poured into the tube. This process was then repeated for all the pressure tubes. Initially the tube caps were screwed down to form an air tight seal, but when gas evolution was observed the caps were drilled and a dead weight relief ball valve fitted to permit excess gas pressure to be dissipated while limiting D₂O exchange with the atmosphere. When corrosion was discovered, the same cleaning treatment was applied to the zone 2 tubes and fuel at to zone 1. The initial batch of D₂O was removed and stored and, after cleaning and reloading the fuel, fresh D₂O was added to the tubes using the procedure described above. This liquid remained in the tubes until the end of the experiments. The fuel boxes were removed several times in order to vary the spike loading. The spike change was made with the boxes wet and any loss of D₂O was made up on replacing the fuel in the pressure tubes. The tubes were not purged with nitrogen on these occasions.

(c) Fine structure stack

720 Kg of D₂O recovered from the zone 2 pressure tubes at the end of the experiments on core 2a was supplied for the fine structure stack. The calandria tank was dried with the freezer drier unit and the D₂O transferred under pressure with dry nitrogen. At the conclusion of the experiments the D₂O was drained out of the calandria tank into storage drums. Losses were negligible.

(d) D₂O losses

Approximately 5% of the D₂O used as coolant simulant in the pressure

tubes was lost in the course of the experiments. Three factors contributed to this loss:-

- (i) the frequent removal of fuel clusters and "trombones" of large surface area in order to load and unload foils.
- (ii) the complete emptying and drying of the pressure tubes after the use of D₂O mixtures in cores 2a, 2b, 4 and 5 in zone 1 and cores 2a and 5 in zone 2.
- (iii) the high level of activity on the fuel during the experiments which made it vital to restrict fuel handling to the minimum.

Even if the activity of the fuel had not precluded more deliberate treatment the time penalty incurred in recovering D₂O from fuel elements and pressure tubes during coolant changes and foil loadings would have involved unacceptable delays to the programme.

8. Aluminium Corrosion

(This is based on an unpublished note by Mr. J. N. Wanklyn, Metallurgy Division, A.E.R.E., Harwell).

On June 22nd, 1960, an appreciable gas pressure was noted on loosening one of the zone 2 pressure tube caps. A sample of the gas contained 59% deuterium, the remainder being air. The pressure tubes in zone 2 had been filled with D₂O on May 18th - 19th and had remained sealed since that date. The amount of free deuterium observed indicated that appreciable corrosion had taken place and an analysis of the D₂O in the tube showed the following changes.

Quantity	Original D ₂ O	Sample from tube
pH value	6.0	5.5
Conductivity mhos.	1.0	6.2
Aluminium p.p.m.	1.0	>80.0
Iron p.p.m.	0.1	1.0
Zinc p.p.m.	0.05	0.5
Chlorides as Cl p.p.m.	0.2	7.6
Ammonia as NH ₃ p.p.m.	0.2	1.3

The suspended matter in the tube was found to contain mainly aluminium, with

some iron and traces of magnesium. On emptying the tube and examining it with an intrascope the corrosion was seen to be uniform and more sludge was noticed at the bottom, suggesting that the water analysis underestimated the aluminium loss.

The total corrosion was estimated from the gas evolution to be about 180 mg/dm^2 after 1 month, compared with typical figures for 99.5% aluminium at 20°C . of 4 mg/dm^2 . A period of incubation was observed before rapid corrosion started, varying between 7 and 32 days. Although the corrosion was not severe enough to weaken the structure, there was a risk of explosion, some loss of deuterium, and turbidity in the water which hindered fuel handling. The fact that aluminium acceptable by present specification could corrode rapidly was also disturbing.

The pressure tubes and aluminium frames were removed from the reactor, pickled in NaOH and passivated with NHO_3 , and were then replaced in the reactor and immersed in clean D_2O . Gas evolution was again observed after an incubation period of about 8 days. It then appeared that the corrosion was due neither to the inadequacy of the original cleaning treatment nor to impurities in the first batch of D_2O . A series of corrosion tests was therefore initiated by Industrial Chemistry Group.

Samples of aluminium from pressure and calandria tubes were immersed in deionized D_2O , in distilled H_2O and in deionized H_2O and their behaviour compared with a control sample of 99.5% aluminium immersed in deionized D_2O . In all three liquids the test samples started to corrode rapidly, evolving gas after incubation periods which varied between 7 and 70 days. The control sample remained inactive. The incubation period was in all cases followed by a short period (~ 10 days) of rapid corrosion and gas evolution after which the corrosion rate fell to a very low value (often less than the limits of measurement). The incubation period appeared to be influenced by the ratio of total specimen surface area to fresh out surface area and also by the water quality.

Preliminary examination of the corrosion test results suggested that the aluminium used for the pressure tubes and calandria tubes was abnormal. The absence of pitting and the extreme uniformity of the corrosion made it likely that the usual impurities in the metal and/or water were not responsible but that the material possessed some unusual difference in composition or structure from normal aluminium. Further corrosion tests and analyses were therefore put in hand in order to clarify the effects of water quality, surface conditions and heat treatment. These tests are still in progress and a possible mechanism for the observed corrosion has been suggested. If this suggestion is confirmed it should be possible to avoid a recurrence of the problem by varying the material specifications. A more detailed account of the investigation will be issued later by the Groups concerned.

The recurrence of corrosion in the reactor after the aluminium components had been repickled was not allowed to interrupt the experimental programme a second time. The corrosion rate was not high enough to affect the safety of the core structure and the risk of an explosion was made negligible by venting the pressure tubes and fitting an extract fan to the top shield. The methods of handling fuel under water were modified so as to make them suitable for use in turbid water. No difficulties were experienced due to the flocculent precipitate. As in the laboratory test the corrosion rate in the reactor appeared to decrease markedly after the initial period of activity.

9. The Fine-Structure Stack

(i) Introduction

In the experiments in DIMPLe the various coolants were all at the same temperature as the D₂O moderator, i.e. ambient. In the power reactor the temperatures will be very different, with coolant at about 280°C and moderator at about 65°C. These elevated temperatures will affect all the lattice parameters but will have most influence on the thermal neutron spectrum and the thermal flux peaking. In the fine-structure stack the coolant temperature was raised above that of the moderator and the effects on the thermal neutron distribution and spectrum were investigated. Because of limited time, manpower and money the experiments were restricted to one type of moderator and a relatively small increase in temperature.

The stack was a sub-critical assembly driven by neutrons from the LIDO core (17). It was made up of S.G.H.W. fuel channels of exactly the same type as in the DIMPLe cores, at the same pitch, in a calandria tank containing D₂O moderator.

H₂O coolant was pumped through the channels at temperatures in a range up to 87°C, and the thermal spectrum and thermal peaking were investigated by irradiating Mn/Lu and Mn/Au foils, just as in the DIMPLe experiments.

(ii) The Calandria Tank and Fuel Channels (figures 21 and 22)

The calandria was a small tank of 99% aluminium approximately 3 ft. wide by 3ft. long by 3 ft. 6 inches high, containing 16 straight-through calandria tubes of 99.5% aluminium, each 6.625 inch O.D. with walls 0.192 inch thick. The tubes were vertical in the tank on an 8.375 inch pitch in a 4 x 4 square array. In each calandria tube was a coaxial pressure tube of 99.5% aluminium, 5.25 inch I.D. with walls 0.128 inch thick. There was thus an air gap of 0.375 inch between pressure tube and calandria tube. The above dimensions, the pitch, tube radii and air gap were exactly the same as in DIMPLe. The pressure tubes were suspended by insulating fingers of tufnol under their top flanges and were centred by tufnol fingers at the bottom ends. At the top and bottom of each pressure tube were $\frac{3}{8}$ inch O.D. pipes for coolant.

Inside the calandria tank, in the moderator, at the end furthest from the source, was a cooling coil made up of $\frac{1}{2}$ inch I.D. aluminium tubing, approximately 17 ft. long.

Each channel contained three S.G.H.W. clusters, the clusters in the central four channels being of the modified type to take 'three-decker' trombones for foils (reference 1). To aid the flow of coolant water, 54 holes of $\frac{1}{8}$ inch diameter were drilled through each cluster plate, spread more-or-less uniformly over the plate.

After drying out the calandria with the DIMPLe freezer-dryer, it was filled with D₂O to within $\frac{3}{4}$ inch of the top and the space above was vented through a drying trap filled with silica gel. The trap can be seen towards the top left of figure 21. There were approximately 465 litres of D₂O in the tank.

(iii) Irradiating the stack

The neutron source for these experiments was the LIDO core, which has a side of approximately 15 inches by 25 inches high. The stack was mounted in the shielding trolley at panel B position at LIDO (ref. 17) and it was supported on a steel framework so that the centre of the front face was lined up, within an inch, with the centre of the core face. With the trolley racked into the concrete shielding round the LIDO pool, the front face of the stack was separated from the LIDO core by a few inches of pool water, two aluminium panels of total thickness 1 inch in the pool wall, the front wall of the trolley made of $\frac{1}{2}$ inch of aluminium, and a few inches of air.

A lifting cross-beam with four slings was constructed so that the entire stack, full of moderator, fuel and coolant, could be lifted for positioning in the trolley. The stack with its support and the lifting gear are shown in figure 21.

(iv) The coolant circulation system

The coolant water was heated in a 28 gallon domestic hot water tank. These tanks are, of course, made of copper but it was considered that since the total time when the coolant would be circulating would be short (several runs of a few hours) there would be very small risk of any action between copper and aluminium. Experience proved this to be correct.

Four 3-kilowatt immersion heaters were installed in the boiler, two of them controlled manually by switches and the other two controlled by a laboratory type thermostat. A small open tube was connected through the top of the boiler to avoid any build up of pressure and a simple float assembly was incorporated into the tube to measure the water level.

From the boiler the coolant was pumped to the stack through 1 inch I.D. rubber hose by a Stewart-Turner centrifugal pump, at about $1\frac{1}{2}$ gallons/min. The water was distributed to the lower ends of the pressure tubes from a short fat cylindrical header tank of aluminium, through PVC tubes of $\frac{1}{2}$ inch I.D. At the top the water was collected in another header through PVC tubes and was returned to the boiler through another 1 inch rubber hose. PVC tubing is not suitable for prolonged use at temperatures above about 80°C but it gave no trouble during the short period of the experiments. Figure 22 shows the arrangement of the top header and the plastic tubes. Both headers had valves to bleed off trapped air.

The coolant circuit contained about 25 gallons of water, exclusive of the boiler.

(v) Measurement of Temperature

All temperature measurements were made with standard Pyrotenax thermocouples of Chromel/Alumel sheathed in $\frac{1}{8}$ inch O.D. stainless steel tubing.

The moderator was monitored at eight positions, marked T1, ——— T8 in figure 23, the junctions being half way down in the tank.

Coolant temperatures were measured in the four central channels F, G, K, L of figure 23. The thermocouple tubes were passed through sliding seals in the top plates of the pressure tubes and down through the water holes in the cluster plates. One thermocouple was inserted in each of channels F, G and L and three were located in K, at different radii.

The variation in coolant temperature, as a function of height and radius in a channel, was explored in preliminary, out-of-pile, runs and it was found that once conditions had become steady the temperature was uniform to within 1°C , at all points in a channel.

All the thermocouples voltages were measured on a standard potentiometer by way of a multi-position low-resistance switch and a common cold junction was set up in melting ice.

The calibration of a typical thermocouple was checked against a mercury thermometer of sub-standard accuracy and it was found to agree with the manufacturers data within an experimental error of about 0.2°C . Accordingly, the published data was taken to apply to all the thermocouples and an error of $\pm 0.2^{\circ}\text{C}$ has been assigned to all the readings.

(vi) Operation

The hot water circuit was tested in several out-of-pile runs. To prevent air from flowing up through the annular gaps between the pressure tubes and calandria tubes, each gap was filled with a soft rubber ring near the top of the tube. The preliminary calculations had predicted that, for coolant at 85°C and D_2O at 20°C , the rate of loss of heat across the gaps would raise the D_2O temperature by about 1°C per hour and this was considered to be acceptable. However, in the testing run at high temperature the heat transfer seemed to be much larger than this and it was suspected that convection might be the cause. Since time was too short to investigate the effect it was decided to fill the annuli with sheets of very low density expanded polystyrene. With the coolant at 85°C , the heat losses across the annuli then fell to the estimated rate. It was found that by circulating ice-water through the cooling coil the bulk of this heat could be removed from the moderator and the moderator temperature could be held constant to within 1 or 2°C during any one experiment, from the beginning of the warming-up period through the irradiation.

The procedure in a typical hot-coolant irradiation was as follows.

- (a) The foils were loaded and the calandria was installed in the trolley along with its pipes and instrumentation.
- (b) Meanwhile, the water in the boiler was heated to about 90°C with the rest of the circuit closed off. The ice-water circulation was started through the cooling loop so as to lower the D_2O temperature by about 1°C below ambient.
- (c) The main circulation was started and the boiler water became mixed with the water in the rest of the circuit, with a resulting temperature of about 35 to 40°C . (This technique raises the whole coolant

temperature by about 20°C without transferring any heat to the moderator).

- (d) With all the heaters on, coolant was circulated until the temperature in the channels was near to the required value. The control thermostat in the boiler was then set to an appropriate temperature, usually about 3°C above the required channel temperature, and the whole coolant system was allowed to come to equilibrium. At one extreme, the run at 85°C required the 6 kw of ballast heat as well as the 6 kw of thermostatically controlled heat and at the other extreme, the run at 40°C was driven by the controlled 6 kw alone.
- (e) When the coolant had definitely reached equilibrium the shielding trolley was run into the cave and the irradiation was started. During the later part of the warming-up period and the irradiation itself the eight temperatures in the moderator and the six temperatures in the channels were taken at ten minute intervals. The hottest run took about 3 hours to come to equilibrium.
- (f) After the irradiation the stack was left for an hour or more inside the shielding. The levels of $\beta\lambda$ radiation then ranged from about 500 mr/hr at the source end of the stack to about 50 mr/hr at the back. The unloading of the foils was accomplished in less than 5 minutes by two people, both standing in a part of the area subject to a field of about 200 mr/hr.

(vii) Difficulties in operation

One problem was common to all the hot runs and it proved to be a stubborn one. Although it was quite simple to bleed off trapped air from the headers, through their air valves, it was extremely difficult to dislodge all the air bubbles from the small crevices inside the fuel clusters. As the system heated up this air produced large bubbles which were able to interfere with the flow of coolant and even, on two occasions, to prevent flow through several channels. Various remedies were used:

- (a) Clamping off most of the channels and diverting the whole flow to the affected ones,
- (b) Valving off the whole flow and then suddenly releasing it,
- (c) Shaking the whole system, and in very stubborn cases bouncing a whole pressure tube up and down.

These techniques proved to be successful and steady flow through all channels was always achieved but in a more permanent experiment it would clearly be worth-while to apply considerable design effort to the flow paths inside the pressure tubes.

It was realised that in some of the runs the coolant would be considerably above the range of temperatures for which the Stewart-Turner pump was designed and an air blast was arranged to cool the motor and the actual pump section. Despite this, the packing in the pump gland seized during the hottest run, but

fortunately not until quite near the end so that no great inconvenience was caused.

(viii) Flux measurements

(a) The foil loading pattern

Preliminary calculations had indicated that in the lattice with light water coolant an equilibrium spectrum would be established within about one lattice pitch from a boundary or from a source with a comparatively hard spectrum such as LIDO. The experimental evidence from core 3 in DIMPLE was in agreement.

In accordance with these arguments it was expected that there would be equilibrium in the fine-structure stack in a region round the four central channels F, G, K, L, extending vertically over the middle clusters in those channels. Accordingly, a foil pattern was arranged to cover this region, in fuel and moderator, using Au/Mn and Lu/Mn foils of the kind used in the DIMPLE experiments. It was hoped that the activations would then furnish information on the spatial variation of the total neutron density, the relative density of epithermal neutrons and the effective neutron temperature, as functions of the coolant temperature.

The number of Lu/Mn foils was limited so the experiment was designed to make one run at each of five temperatures, more or less equally spaced from about 20°C to about 90°C inclusive.

Foils were attached with 'Lassothene' to the trombones in the four central channels, at positions inside the middle cluster in each channel. The orientations of the trombones are shown in figure 23. The vertical co-ordinates are labelled b, c, d, e, f, and the radial co-ordinates 1, 2, 3, 4, 5, just as in DIMPLE, see figure 3.

In the moderator the foils were fastened to an 'umbrella' foil holder which was loaded through a 1.5 inch diameter hole in the tank lid, at the centre. The holder is shown in figure 24. It had four thin tubular arms of aluminium 25 inches long, jointed at the top. Between the arms were stretched two thin sheets of polythene, intersecting on the central vertical axis and extending between the central channels in directions North, South, East and West, see figure (23). Foils were stuck to the sheets with lassothene at heights corresponding to the positions on the trombones, at the locations (i) ——— (vii) in figure 23. Positions (iii) and (v) lie 2 inches South and North respectively from the central position. The advantages of the umbrella are:

- (a) the obvious one that it can collapse and hence be loaded into the tank,
- (b) it avoids the use of metal on the central axis where it is important that the flux should not be perturbed,
- (c) the disturbing material which it does introduce is a relatively small volume of polythene which is itself a moderator.

Each run involved 35 Au/Mn foils and 26 Lu/Mn foils, sited to provide vertical and horizontal fine-structure distributions. The most significant were:

Au/Mn Distribution

Horizontal: Across channel F and moderator (i), at height d.
 Across channel G and moderator (i), at height c.
 Across moderator at (ii), (iii), (iv), (v), (vi), at height d.

Vertical: In channel F at radius 3.
 In channel K at radius 3.
 In moderator at positions (iv).

Lu/Mn Distribution

Horizontal: Across channel F and moderator (i), at height e.
 Across channel G, at height d.
 Across moderator at (ii), (iv), (vi).
 Across channel K and moderator (vii), at height c.
 Across channel L and moderator (vii), at height d.

(b) The flux in the stack

For the equivalent DIMPLE core, No. 3, the preliminary calculations had predicted that the material buckling would be approximately zero. In the fine-structure stack the horizontal and vertical asymptotic flux distributions are effectively determined by the dimensions of the tank and should be cosines of the form $\cos \alpha (x - x_0)$, and $\cos \beta (y - y_0)$ respectively where $\alpha \sim 3.2 \text{ metre}^{-1}$ and $\beta \sim 2.8 \text{ metre}^{-1}$.

The asymptotic distribution parallel to the current from the source will be of the form $\sinh \gamma (z_0 - z)$ where γ is given by

$$\alpha^2 + \beta^2 - \gamma^2 = B_m^2$$

and B_m^2 is the material buckling. If B_m^2 is approximately zero then $\gamma \approx 4.3 \text{ metre}^{-1}$. The flux will thus fall by a factor of about 6 from the front to the second row of channels F, G, and by a further factor of about 1.7 from FG to the row KL.

In practice, the presence of source harmonics will complicate the distribution. The shape of the source distribution, that is the flux pattern from the LIDO core, is shown in reference (18), figures 4 and 5. Both the source and the tank distributions should be symmetric so the contributions from second harmonics should be very small. Since the source shape is more sharply peaked than the asymptotic cosiness in the tank the

third harmonic contributions will be positive and the flux will fall off more rapidly than the asymptotic sinh form above.

It was decided that the foils should be irradiated for the same length of time and the same flux as in the DIMPLE experiments so that when the results were compared the effects of any errors in the count-reduction procedure would be small.

Using the calculation above and the LIDO flux measurements of reference (18) it was estimated that a LIDO power of 2 KW would produce thermal fluxes of approximately 3×10^7 neutrons/cm.² sec in the fuel channels K and L. The foil activities which resulted from the irradiations were in good agreement with the prediction.

For irradiations of this kind LIDO is usually brought to power with a doubling time of about 25 seconds and is shut down at the same rate. The foils were irradiated for one hour at 2 KW power. The time was taken from 80% of power at the beginning to 80% of power at shut-down and the necessary allowances were made in calculating the foil-decay corrections so as to make the results comparable with the irradiations in DIMPLE.

(ix) Results

(a) Moderator Purity

The isotopic purity of the D₂O moderator remained constant within the limits of measurement from the beginning to the end of the experiment. It was 99.68 ± 0.003 weight per cent.

(b) Temperatures

The preliminary tests showed that once the coolant system had reached equilibrium the temperatures in a channel at any one time did not vary from the mean value by more than 0.5°C , either from top to bottom or radially. The steady drift in mean coolant temperature during an hour irradiation was at most 2°C .

Table 10 lists some thermocouple voltages in millivolts, and equivalent temperatures in $^{\circ}\text{C}$, obtained during the irradiations.

The maximum and minimum voltages are those recorded at any time during an irradiation and the mean voltage, which yields the mean temperature, is the average of all readings taken during the irradiation. For each irradiation the uncertainties in the coolant and the moderator temperatures are compounded from the following:

- (i) $\pm 0.2^{\circ}\text{C}$ in reading and calibration for each temperature.
- (ii) An error depending on the steady drift observed during the irradiation.
- (iii) For the coolant, an error of $\pm 0.5^{\circ}\text{C}$ in spatial constancy inside a pressure tube.

TABLE 10

Coolant temperatures in the fine structure stack

Run	FSS 2	FSS 3	FSS 6	FSS 5	FSS 4
Mean H ₂ O Temp.	19.4 ± 0.6	40.5 ± 0.7	55.2 ± 0.7	69.7 ± 0.8	86.8 ± 1.0
Mean D O Temp.	19.3 ± 0.6	15.9 ± 0.9	18.1 ± 0.6	17.2 ± 0.8	18.8 ± 0.9
H ₂ O EMF max.	.786	1.662	2.288	2.900	3.601
min.	.771	1.632	2.211	2.808	3.521
mean	.778	1.647	2.248	2.846	3.553
D ₂ O EMF max.	.781	.660	.745	.716	.790
min.	.767	.610	.702	.656	.719
mean	.773	.636	.725	.690	.750

(iv) The total rise in the Moderator temperature was always very small, a few degrees, and because of this and the presence of natural convection currents it was assumed that the temperature was appreciably constant over the volume of the moderator. As a check, the moderator was agitated with an electric stirrer during an out-of-pile run. It was concluded that the variation over the bulk of the moderator at any one time during an irradiation was not more than $\pm 0.5^{\circ}\text{C}$ from its mean value.

(o) Foil Activation

Foil Calibrations and Errors in Activities

The Au/Mn and Lu/Mn foils were selected from the ones used in the DIMPLE cores and they had the properties and spectral calibrations which are described in sections 4 and 5.

The total errors due to foil composition, counting statistics and counting procedure were as follows.

Activities in Au/Mn foils: Mn $\pm 1\%$, Au $\pm 1.7\%$,
leading to an error of $\pm 2\%$ in the ratio.

Activities in Lu/Mn foils: Mn $\pm 1\%$, Lu $\pm 1.25\%$,
leading to an error of $\pm 1.6\%$ in the ratio.

These uncertainties are increased by errors in positioning in the stack. The exponential-type fall in flux in the direction away from the source produces a change of about 0.3% in macroscopic flux for a position error of 1 mm in that direction.

For each mean value of a ratio which is quoted in the following tables two errors have been computed (i) using the above errors, (ii) by taking the deviations about the mean, and the error which is actually listed is the larger of the two.

The Equilibrium Spectrum

As was discussed above in § 9 (viii), it was very probable that the equilibrium spectrum was confined to the neighbourhood of the middle clusters in the four central channels. Since this region contains only four cells, (i) it was not possible to make an accurate determination of the macroscopic flux distribution and, (ii) the spectrum measurements viewed in isolation do not provide a very convincing proof that an equilibrium spectrum had indeed been established.

The question of equilibrium can be answered in the following way. The Au/Mn and Lu/Mn activation ratios in an equilibrium region are independent of macroscopic flux variation and depend only on the variation in spectrum across a cell. Hence these ratios can be compared with the measurements at equivalent positions in the cells in the light-water-coolant core in DIMPLE. The core in DIMPLE was much larger than the stack and it had been proved that an equilibrium zone was established.

Thus if the ratios in the stack are in agreement with the ratios in the DIMPLE core it can safely be assumed that the central region in the stack was in equilibrium. Strictly, this comparison can only be made for the cold-coolant case but in fact for the temperature range of the experiments the macroscopic absorption and scattering cross-sections in the stack will change by a few per cent at most and the corresponding changes in relaxation lengths will not be large enough to cause a detectable displacement in the boundaries of the equilibrium zone.

Table 11 compares the Au/Mn ratios and Lu/Mn ratios in the cold run, at the positions listed in § 9. (viii), with the values at corresponding positions in cells in DIMPLE core 3. The coolant and moderator were at a mean temperature of 22.0°C in core 3 and at 19.4°C in the stack.

In core 3 the Au/Mn ratios are for the 'd' heights and the Lu/Mn are averaged over 'c, d and e' heights and in FSS 2 both ratios are averaged over the 'c, d and e' heights.

In FSS 2 the moderator positions (i), (ii), (vi) and (vii) have been averaged and the average is labelled W1 since this is the equivalent position in the DIMPLE cores. The value for position (iv) is labelled by its equivalent DIMPLE position, W2 $\frac{1}{2}$.

Both sets of ratios are in agreement within the experimental errors and it can thus be assumed that the central region in the stack was in equilibrium.

Gold/manganese Ratios

It was found that within the errors of measurement there were no detectable changes in the Au/Mn ratios as the coolant temperature was raised. That is, at any particular position the ratio was constant to $\pm 1.5\%$ or better.

Lutecium/Manganese Ratios

Table 12 gives, for each run, the mean values of Lu/Mn ratio for five positions in a channel and two in moderator. The results are averaged vertically over c, d and e heights and the position W1 in moderator refers to an average over positions (i), (ii), (vi) and (vii).

The ratio is shown as a function of position in a cell in figure 25, for three runs, at the coolant temperatures 19.4°C, 55.2°C and 86.8°C. The moderator positions are expressed in terms of their distances from the axis of the cell but it should be remembered that the cell is square and that they both lie on the boundary.

The Determination of r and T

Using the Au/Mn ratios and the Lu/Mn ratios, values can be obtained for the spectrum parameters r and T of the Westcott convention. The technique is described in sections 4 and 5 of this report.

TABLE 11

Comparison of gold/manganese and lutecium/manganese ratios in the fine structure stack and DIMPLE

Run	Ratio	FUEL POSITIONS					MODERATOR POSITIONS	
		1	2	3	4	5	W1	W2 $\frac{1}{2}$
Core 3	Lu/Mn	1.977 \pm .033	1.964 \pm .009	1.961 \pm .009	1.937 \pm .017	1.996 \pm .033	1.879 \pm .022	1.853 \pm .014
FSS 2	Lu/Mn	1.974 \pm .015	1.964 \pm .015	1.959 \pm .015	1.932 \pm .015	1.877 \pm .025	1.867 \pm .015	1.827 \pm .021
Core 3	Au/Mn	1.748 \pm .009	1.716 \pm .007	1.681 \pm .007	1.624 \pm .006	1.566 \pm .007	1.517 \pm .010	1.469 \pm .006
FSS 2	Au/Mn	1.779 \pm .021	1.712 \pm .020	1.683 \pm .010	1.657 \pm .020	1.579 \pm .019	1.545 \pm .015	1.494 \pm .019

TABLE 12

Lutecium manganese ratios in the fine structure stack at different temperatures

Run	Coolant Temp °C	Fuel Positions					Moderator Positions	
		1	2	3	4	5	W1	W2½
FSS 2	19.4	1.974 ±.015	1.964 ±.015	1.959 ±.015	1.932 ±.015	1.877 ±.025	1.867 ±.015	1.827 ±.021
FSS 3	40.5	2.081 ±.017	2.089 ±.022	2.062 ±.016	2.049 ±.016	1.944 ±.018	1.882 ±.014	1.830 ±.020
FSS 6	55.2	2.186 ±.027	2.213 ±.025	2.161 ±.025	2.141 ±.024	2.022 ±.023	1.926 ±.015	1.870 ±.027
FSS 5	69.7	2.287 ±.023	2.292 ±.035	2.260 ±.020	2.191 ±.022	2.090 ±.018	1.950 ±.021	1.893 ±.022
FSS 4	86.8	2.320 ±.028	2.335 ±.022	2.266 ±.018	2.236 ±.018	2.109 ±.016	1.927 ±.020	1.886 ±.021

A value of 3.67 kT was chosen for the epithermal lower energy limit since this seems to give the best agreement between the various foil and fission-chamber measurements in the corresponding DIMPLE core, no. 3 (H₂O coolant).

The values of r are essentially determined by the Au/Mn ratios and the values of T by the Lu/Mn ratios.

As was stated above, there was no detectable change in the Au/Mn ratios as the coolant temperature increased. This implies that the $r \sqrt{\frac{T}{T_0}}$ values do not change. Unfortunately, the r values which are obtained from the Au/Mn ratios in the stack and in core 3 do not agree with the r values from the other types of measurement which were made in Core 3, the other determinations being consistent among themselves. The values obtained from Au/Mn are about 7% lower in a cluster (r about 0.065) and about 20% lower in moderator (r about 0.045). However, since the values of T are usually insensitive to r, and are especially so in this case since the spectrum is so soft, the resulting uncertainty in T is very small.

Table 13 gives the values of T for the fuel and moderator positions, for the different coolant temperatures. The uncertainty is on the average $\pm 2.5^\circ\text{C}$ of which less than 0.5°C is due to uncertainty in r.

The variation of T at radial positions 2 and 5 is shown graphically in figure 26.

In view of the uncertainty in r, its values are not listed here.

Manganese Distributions

The distributions of the individual activities Au, Mn or Lu are each compounded of two functions, the macroscopic flux distribution and the respective fine structure. Since the macroscopic variation cannot be obtained accurately because of the small size of the region of constant spectrum it is not possible to remove it so as to reveal the respective fine structures. The variation in an activation from run to run can thus only describe the variation in combined macroscopic and microscopic effects.

Within the errors, the shape of the Mn distribution does not change from run to run in any of the three directions, across the tank, vertically, or away from the source. The macroscopic distributions vertically and across the tank are determined to a high degree by the actual height and width respectively and by the effective extrapolation lengths for the flux into the surrounding shielding concrete. Hence both distributions are very insensitive to changes in coolant temperature and it can be assumed that they do not vary detectably over the range of temperatures observed. Thus the constancy of the Mn distributions vertically and across the tank implies that the fine structure axially and radially in a cell does not change over the temperature range. Then at each position, taking account of results from all the runs, the Mn fine structure is constant to $\pm 2\%$, or better.

TABLE 13

Effective neutron temperatures at different coolant temperatures in the fine structure stack

Run	Coolant Temp.	Moderator Temp.	T - Fuel Positions					T - Moderator	
			1	2	3	4	5	W1	W2 $\frac{1}{2}$
FSS2	19.4	19.3	55	53	52	42	36	35	28
FSS3	40.5	15.9	75	76	70	67	48	37	28
FSS6	55.2	18.1	94	98	88	83	62	45	35
FSS5	69.7	17.2	111	111	105	92	73	49	39
FSS4	86.8	18.8	116	118	107	99	76	45	38

Temperatures are in °C. The average error in T is $\pm 2.5^{\circ}\text{C}$.

(d) Additional Runs

In addition to the above runs with light-water coolant two extra runs were made to provide information for the design of future experiments. In one of them there was no coolant, as in the air core in DIMPLE, and in the other run light-water coolant was used but only the four centre channels were heated.

(i) Air Coolant

Au/Mn and Lu/Mn foils were irradiated with air coolant, at a moderator temperature of $17.5 \pm 0.5^\circ\text{C}$. The errors in Lu/Mn ratio were larger than in the previous runs since only about half the number of foils was available.

The results may be compared with the measurements in the air coolant core in DIMPLE, Core 1.

Lu/Mn ratios: The ratios in the fuel channels in the stack were about 5% lower than in the fuel channels in DIMPLE and the ratios in the moderator were about 2% lower than in DIMPLE moderator. The errors were about 1% in the moderator and from 1 to 2% in the channels.

The DIMPLE experiments were carried out at a mean temperature of 22°C . If the stack results are corrected to this temperature the ratios will be increased by about 1.5%. This will bring the moderator values into good agreement and will leave the ratios in the fuel channels about 3.5% lower than in the DIMPLE channels.

Au/Mn ratios: The ratios in the channels are consistently lower than in the DIMPLE channels, by about 2%, with error of from 1 to 1.5%. The ratios in moderator are not significantly different from the DIMPLE moderator.

(ii) Four Heated Channels

With light water coolant in all channels, the central four were heated to $80.7 \pm 1.0^\circ\text{C}$ with the remaining channels and the moderator at $14.8 \pm 0.9^\circ\text{C}$. The Au/Mn and Lu/Mn foils were irradiated, there being about half the normal number of Lu/Mn.

The results may be compared with the hottest run, FSS 4, which had coolant at 86.8°C in all channels, and moderator at 18.8°C .

Lu/Mn ratios: The difference in coolant temperature between the runs was approximately 6°C and a first-order correction would be to reduce the ratios in the FSS 4 channels by 2%. The difference in moderator temperatures was 4°C and the first-order correction to the FSS 4 moderator ratios would be a reduction by 1.3%. If these corrections are made, the results from the two runs are in agreement within the errors, which are about 1.5%.

Au/Mn ratios: The Au/Mn ratios in the channels and moderator are in agreement with the corresponding values in FSS 4 within their errors, which are about 2.5%.

10. Acknowledgements

We are indebted to Mr. B. T. Price, Dr. J. E. R. Holmes and Dr. C. G. Campbell for their guidance and advice in planning and carrying out the experiments, and to Mr. I. Johnstone and Dr. R. B. Tattersall for their help in obtaining safety clearance for DIMPLE.

The theoretical calculations have been carried out by Mr. J. Fell, Dr. D. Hicks, Dr. C. Carter, Dr. D. C. Leslie, Mr. A. Green and Mr. D. W. Holbrough, to all of whom we are indebted for helpful comments and discussion.

The experiments were carried out and analysed with the help of Mr. J. C. Fisher, Mr. J. Crabbe, Mr. C. F. Bartlett, Mr. J. Hedderly, Mr. R. P. Lay, Mr. R. Lincoln and Mr. B. J. Rogers, Mrs. S. Bunce and Miss V. Aldworth.

Mr. J. N. Wanklyn of Metallurgy Division and Mr. G. F. Aitchison of Industrial Chemistry Group, A.E.R.E., Harwell investigated the abnormal aluminium corrosion and gave advice on metal and water treatment.

We are grateful to Mr. E. J. Maunders for the loan of calibrated fission chambers

Dr. D. Hicks and Mr. J. N. Hull assisted in the start-up of DIMPLE and Mr. G. R. J. Wilkinson and Mr. D. R. Dickie in its operation.

We are grateful to Mr. W. F. Wood of Research Reactors Division, A.E.R.E., Harwell, and to the members of his Operations Group on DIMPLE and LIDO, whose enthusiasm and help made the experiments possible.

11. References

1. J. W. HILBORN (editor). First Report on the S.G.H.W. Experiment in DIMPLE. A.E.R.E. - M 727, 1960.
2. H. R. McK. HYDER. Comparison of Designs and Nuclear Parameters of the S.G.H.W. Power Reactor and DIMPLE Experiment. AEEW - M 64, 1960.
3. D. HICKS and H. R. McK. HYDER. The Experimental Programme for the S.G.H.W. Cores in DIMPLE. AEEW - M 65, 1960.
4. W. N. FOX, A. J. M. HITCHCOCK and R. G. JARVIS. Measurements of Resonance Escape Factor and Fast Fission Factor in the S.G.H.W. Experiment in DIMPLE. AEEW - R 86, 1961.
5. H. R. McK. HYDER. Standing Orders for the S.G.H.W. Experiment in DIMPLE. RG - RSCC/S46, 1960.
6. M. N. JOHN. Rod Drop Studies on DIMPLE (S.G.H.W. Core). A.E.E., Winfrith Note WCBN/28, 1961.
7. G. R. KEEPIN and T. F. WIMETT. Reactor Kinetic Functions. A New Evaluation. Nucleonics 10, 86, 1958.
8. M. W. JOHNS and B. W. SARGENT. Photoneutrons in a Heavy Water File. Can. Jour. Phys. 32, 136, 1954.
9. J. W. WEALE, H.R. McK. HYDER et al. Neutron Flux Measurements in the core of LIDO. A.E.R.E. R/R.2620, 1958.
10. D. H. DAY, W.N. FOX and H. R. McK. HYDER. Measurement and Calculation of Fast Neutron Flux in a Zero-Energy Reactor. AEEW - R 85, 1961.
11. C. H. WESTCOTT. Effective Cross Section Values for Well-Moderated Thermal Reactor Spectra. AECL 1101, 1960. CRP 960.
12. C. G. CAMPBELL and R. G. FREEMANTLE. Effective Cross Section Data for Thermal Reactor Calculation. A.E.R.E. RP/R 2031, 1956.
13. H. R. McK. HYDER, C. J. KENWARD and G. A. PRICE. Thermal Spectrum Measurements with Lutecium. A.E.R.E. M 552 1961.
14. W. BOTHE. Zur Methodik der Neutronensonden. Zeit.fur Physik 120, 437, 1943.
15. G. J. KENWARD. Mercury Programmes for the Reduction of Observations on Alloy Foils. A.E.R.E. M 893, 1961.
16. D. W. COLVIN. Private Communication.
17. H. R. McK. HYDER et al. LIDO - The Engineering and Physics Design. A.E.R.E. R/R 2340, 1957.

18. E. D. JONES. Neutron Flux Measurements on an Aluminium Panel and in the Pool of Lido. A.E.R.E. M 608, 1960.
19. G. M. Roe. The Absorption of Neutrons in Doppler Broadened Resonances. KAPL 1241, 1954.
20. W. N. SELANDER. Theoretical Evaluation of Self Shielding Factors Due to Scattering Resonances in Foils. ORT 927, 1960.

APPENDIX I
Calendar of Experiments

Date	Core	Lattice Certificate	Zone 1	Zone 2		
			Coolant Simulant	No. of Spikes	Liquid	
2nd May	1a	32	Air	0	Air	Approach to critical (sub-critical)
3rd May	1a	33	"	9	"	" " "
6th May	1a	34	"	12	"	" " "
9th May	1a	35	"	17	"	Approach to critical
18th May	1b	36	"	12	D ₂ O	Approach to critical and safety measurements
24th May- 19th June	1b	36	"	12	"	Foil irradiation: 7 L.P. 9 H.P.
20th June	2a	37	D ₂ O	12	"	Approach to critical
22nd June 2nd July	2a	38	"	11	"	Approach to critical and safety measurements
						Foil irradiation: 4 L.P.
2nd July- 19th July						Reactor unloaded; aluminium components pickled; core re-assembled.
20th July	2b	39	D ₂ O	11	D ₂ O	Approach to critical
21st July- 12th Aug.	2b	39	"	11	"	Foil irradiations: 12 L.P. 22 H.P.
14th Aug.	3	40	H ₂ O	11	D ₂ O	Approach to critical (sub-critical)
15th-20th Aug.	3	41	"	12	"	Approach to critical and safety measurements
23rd Aug.- 12th Sept.	3	41	"	12	"	Foil irradiations: 12 L.P. 4 H.P.
12th Sept.- 19th Sept.						Coolant change
19th Sept.	4	42	79.7% D ₂ O 20.3% H ₂ O	10	"	Approach to critical and safety measurements.
21st Spt.- 6th Oct.	4	42	"	10	"	Foil irradiations: 11 L.P. 7 H.P.
11th Oct.	c	43	Air	12	"	Approach to critical
12th-21st Oct.	c	43	"	12	"	Foil irradiations etc.: 4 H.P.
24th Oct.	5	44	60.1% D ₂ O 39.9% H ₂ O	10	"	Approach to critical and safety measurements
26th Oct.- 18th Nov.	5	44	"	10	"	Foil irradiations: 11 L.P. 9 H.P.
21st-24th Nov.	6	45	4 clusters only flooded as above.	10	"	Approach to critical; safety and perturbation measurements

L.P. = Low Power. H.P. = High Power.

APPENDIX II

Foil Encapsulator

To prevent errors due to corrosion or contamination all the $\frac{1}{4}$ inch foils irradiated under water in DIMPLE were wrapped in waterproof packets. Hand wrapping proved to be laborious and inefficient and a simple device was therefore designed and constructed to encapsulate foils in polythene sheets.

The apparatus is illustrated in fig. 27. It consists of a base plate to which is fixed a mild steel plate drilled with 31 $\frac{3}{8}$ inch diameter holes; a lever is pivoted on the base plate, carrying a circular copper plate also drilled with 31 $\frac{3}{8}$ inch diameter holes, $\frac{1}{4}$ inch deep. The upper surface of the copper plate is recessed to accommodate a circular electric heater. When the lever is in the horizontal position the holes in the copper and steel plates are in register and the plates are parallel and 0.010 inch apart. The heater element was fed through a Variac which permitted the temperature of the copper plate to be controlled to a few degrees within the range 120-130°C.

The method of encapsulating $\frac{1}{4}$ inch diameter 0.020 inch thick foils in 0.010 inch polythene is as follows:

- (i) the heater is switched on and the copper plate allowed to reach a steady temperature with the lever in the up position. At the correct temperature strips of polythene just melt on being pressed against the edge of plate.
- (ii) a sheet of 0.010 inch polythene is laid over the steel plate and 31 foils are positioned centrally over the holes visible through the sheet, leaving a clearance of $\frac{1}{16}$ inch round each foil.
- (iii) a sheet of 0.010 inch polythene is placed over the foils; this is covered with a sheet of 0.001 inch glossed aluminium.
- (iv) the copper plate is pressed firmly onto the foils for about 10 seconds.
- (v) the polythene sandwich is allowed to cool, removed and cut up.

The aluminium sheet was found to be essential in preventing the polythene from sticking to the copper plate. Sometimes air trapped between the two polythene sheets prevented them from welding together properly. This trouble could be reduced by "dabbing" the copper plate onto the polythene lightly two or three times before pressing it down to complete the welding. A more satisfactory solution would be to redesign the apparatus with a slightly convex copper plate and a hard rubber block in place of the mild steel plate. The addition of a thermocouple to the copper plate would make the apparatus easier to operate and permit the use of thinner polythene sheets.

With the apparatus in its present form it proved possible to process 400 foils a day reliably into transparent, watertight capsules.

The apparatus was designed by B. J. Rogers.

APPENDIX III

Least Squares Fitting Programme

Observed manganese reaction rates were initially fitted to functions of the form $A_i I_0 (\kappa r) \cos (\alpha z + \beta)$ using a conventional least squares programme written for the Mercury computer. The programme uses methods of linear algebra to find the best values of parameters A_i , κ , α , β , together with their statistical errors. Storage capacity limited the input to 100 experimental points and 20 parameters.

Since the experimental cases being considered each had approximately 250 points and 35 parameters, the computer programme required extensive modification. This turned out to be a formidable task and an alternative scheme was adopted. To simplify the problem it is assumed that the algebraic sum of the relative deviations of the observed points from the fitted function is zero for each group of points defining a fine structure factor A_i . Thus for a given κ , α , β , the factor A_i equals $\frac{1}{n} \cdot \Sigma \frac{\phi \text{ observed}}{I_0 (\kappa r) \cos (\alpha z + \beta)}$ where summation is over all n observed points in the i^{th} group. Although this condition is not strictly the same as the least squares condition, the resulting A_i values from the two methods are identical for all practical purposes. The fitting problem is therefore reduced to finding values of κ , α , β which minimise

$$F (\kappa, \alpha, \beta) = \left(\frac{A_i I_0 (\kappa r) \cos (\alpha z + \beta) - \phi_{\text{ob}}}{A_i I_0 (\kappa r) \cos (\alpha z + \beta)} \right)^2$$

where A_i are defined as above, and summation is over all experimental points.

Preliminary runs on selected groups of points using the 100 point programme showed that κ , α and β did not vary too much from core to core, and approximate values could be found quite easily. Therefore a simple "trial and error" computer programme was written which varied κ , α and β by small steps in all possible combinations until $F (\kappa, \alpha, \beta)$ reached a minimum. The method was thoroughly checked by comparison with the original matrix method, and would optimise κ , α and β for 250 experimental points in approximately one hour of computer time.

The statistical errors of the parameters were calculated by means of a second computer programme which used the final results of the first programme. This second routine was based on the original matrix method for solving linearized versions of the least-squares equations.

APPENDIX IV

Determination of the resonance self shielding factors in gold and manganese

In order to obtain adequate sensitivity with the low fluxes available in DIMPLE it was necessary to use gold and manganese foils which exhibited appreciable resonance self shielding. The standard alloy foils in fact contained 17.4 mg/cm² of gold and 69.5 mg/cm² of manganese.

The appropriate self shielding factors for these foils were determined by a series of subsidiary measurements in LIDO, where the flux is both intense and well characterized. The value of 'r' in LIDO has been measured using several different "thin" foils and the epithermal spectrum is believed to be close to $\frac{dE}{E}$ in the region 2-300 eV, since leakage effects are comparatively small and, in the absence of U²³⁸, epithermal absorption is negligible.

Foils of four different thicknesses were irradiated in LIDO, bare and under cadmium, and the results are as follows:-

<u>Material</u>	<u>Au/Mn ratio</u>	<u>Au Cadmium Ratio</u>	<u>Mn Cadmium Ratio</u>
0.001" Au foil } 0.005" 90% foils }	1.519	2.41	10.96
1.5% Au 5.5% Mn alloy 0.015" thick	2.105	1.72	9.58
5% Au 20% Mn alloy 0.015" thick	1.848	1.95	10.75
15% Au 60% Mn alloy 0.015" thick	1.505	2.51	11.72

Defining the self screening factor, F, for a thick foil as follows:-

$$F = \frac{\text{Epicadmium activation of thick foil}}{\text{Epicadmium activation of thin foil in same flux}}$$

we have
$$F = \frac{(\text{Cd Ratio} - 1) \text{ thin}}{(\text{Cd Ratio} - 1) \text{ thick}}$$

Using the published value for the cadmium ratio of thin gold in LIDO (9), it was possible to obtain values of F for gold without making further assumptions. The Au/Mn ratios and manganese cadmium ratios were analysed using the spectrum parameters $r = 0.083$ and $T_n = 60^\circ\text{C}$ for the centre of LIDO. The results, given below, are virtually independent of the form of cut-off assumed.

The shielding factor for gold has been estimated using Roe's theory (19) but the neglect of resonant scattering effects appears to lead to error. The self

shielding in the manganese resonance has been calculated by Selander (20) and this is combined with a resonance integral calculated from resonance parameters but again the agreement with experiment is not good. These results are also given below.

Material	Gold					Manganese	
Foil Dimension	F-self shielding above Cd			$\frac{RI > Cd}{\sigma^0}$		$\frac{RI > Cd}{\sigma^0}$	
	From Cadmium Ratios	From Bare Ratios	Weighted Mean	Observed	Calculated (Roe)	Observed from C.R.	Calculated (Selander)
0.001" Au foil) 49 mg/cm ²) 0.005" 90% Au foil) 84.7 mg/cm ²)	.422	.401	.408	6.477	6.153	.964	1.118
1.5% Au 5.5% Mn alloy) 0.015" thick) (5.2 mg/cm ² Au,) 19.1 mg/cm ² Mn))	.826	.814	.818	12.99	12.02	1.119	-
5% Au 20% Mn alloy) 0.015" thick) (17.4 mg/cm ² Au,) 69.5 mg/cm ² Mn))	.626	.625	.625	9.923	8.764	.985	-
15% Au 60% Mn alloy) 0.015" thick) (52 mg/cm ² Au,) 210 mg/cm ² Mn))	.394	.387	.389	6.176	-	.896	-

Thus for the standard 5% Au - 20% Mn alloy the following parameters are calculated.

T (°C)	Gold		Manganese
	g	S	S
20	1.005	10.79	.625
40	1.006	11.15	.645
60	1.008	11.39	.666
80	1.009	11.83	.685
100	1.010	12.17	.705
120	1.011	12.47	.724
140	1.012	12.79	.742
160	1.013	13.09	.760

APPENDIX V

The Foil Irradiation Scheme

1. Gold manganese foils

The positioning of the gold manganese foils was conceived as a factorial experiment, the primary variables being the position of the cluster, the position of the foil in the vertical direction within the cluster, and in the horizontal direction within the cluster.

In the zone of equilibrium spectrum, it was decided to give each cluster position equal weight, after allowing for quadric symmetry, except that some check reflections about the centre were carried out in order to confirm that the flux was indeed symmetric. Horizontally within the cluster, the five rings of fuel rods provide an obvious set of five positions, and these were given equal weight. Originally it had been intended that the number 6 position, on the outside of the pressure tube, should be given the same weight as the five within the cluster, but the high level of radiation experienced on lifting the pressure tube to load foils in this position made it desirable to reduce its weight. In the moderator, the search tube position at the corner of the lattice cell was given a high weighting and the mid point of the cell side a rather lower one.

In the vertical direction, it was felt that the axial fine structure was of less interest and foil positions were therefore chosen so as to indicate the limits of the zone in which axial fine structure was negligible. These were the c and e levels, equally spaced above and below the d level, which was at the centre of the fuel cluster. The a, b, f and g levels covered the zone of appreciable fine structure.

The weightings finally adopted for the various foil positions within the cell are shown below:

Position within cell		Weighting
Vertical	Horizontal	
d	Fuel 1 - 5	3
d	Pressure tube 6	$1\frac{1}{2}$
d	Moderator $W\frac{1}{2}/ST$	6
d	Moderator $W\frac{1}{4}$	$1\frac{1}{2}$
c + e	Fuel 1 - 5	4
c + e	Pressure tube 6	1
c + e	Moderator $W\frac{1}{2}/ST$	$1\frac{1}{2}$
c + e	Moderator $W\frac{1}{4}$	$\frac{1}{2}$
b+f, a+g	Fuel 1 - 5	1
a + g	Moderator $W\frac{1}{2}/ST$	3
b+f, a+g	Moderator $W\frac{1}{4}$	$\frac{1}{2}$

Other positions in the cell were measured with a lower weighting. Unit weighting corresponded to about 6 foil measurements in core 2 - 5, that is a total of about 200 foils measurements per core, in the equilibrium zone.

Insofar as the system of weighting permitted, the foils were distributed throughout the equilibrium zone on the 'Latin square' principle, each foil contributing information on radial and axial macroscopic distributions as well as radial and axial fine structure.

The final errors obtained on the fine structure factors in the 37 cluster positions and the very reasonable limits of error obtained on the macroscopic flux parameters justify this choice of irradiation scheme, as opposed to the apparently simpler method of measuring the flux along straight lines.

The foil positions having been determined, it remained to break down the scheme into a series of irradiations, and here the principle was adopted that so far as possible all the foils to be irradiated in one channel should be covered in one, or at most in two, irradiations. Standard formats were prepared on which the identifying mark of each foil loaded, the number, date, and time of irradiation, were recorded during loading and checked during unloading.

Within the moderator a somewhat less systematic line was taken, the flux being measured in search tube positions along a diameter parallel to the lattice direction and along a half diameter inclined at 45° to this. The flux plotting device was used to fill in the gaps in these positions and the irradiations were planned so that the flux plotting device was not inserted close to a cluster in which foil irradiations were occurring.

Outside the equilibrium zone measurements at the a, b, f and g levels were not made, but a very rough attempt was made to cover the flux variations across positions 1 - 5 at the c, d and e levels. Each recognisably different channel in the lattice was investigated, though in the outer ring of channels the total number of foils inserted per channel never exceeded ten.

2. Manganese lutecium foils

The scheme just described was adapted for the smaller number of manganese lutecium foils by omitting the a, b, f and g levels almost entirely and by restricting, even more heavily, the number of measurements in the non-equilibrium zone. Within these limits, however, the same principles were applied, though necessarily in a somewhat ad hoc fashion.

3. Rhodium foils

Rhodium foil measurements were restricted entirely to the equilibrium zone and almost entirely to the fuel and search tube positions at the d level. Because of the large thermal absorption cross section of rhodium, it was particularly important to keep other foils well away from it.

KEY



FOIL POSITIONS IN FUEL



FOIL POSITIONS IN SEARCH TUBES (MODERATOR)



MANGANESE MONITOR POSITIONS



FOIL POSITIONS ON FLUX SCANNING DEVICE (MODERATOR)

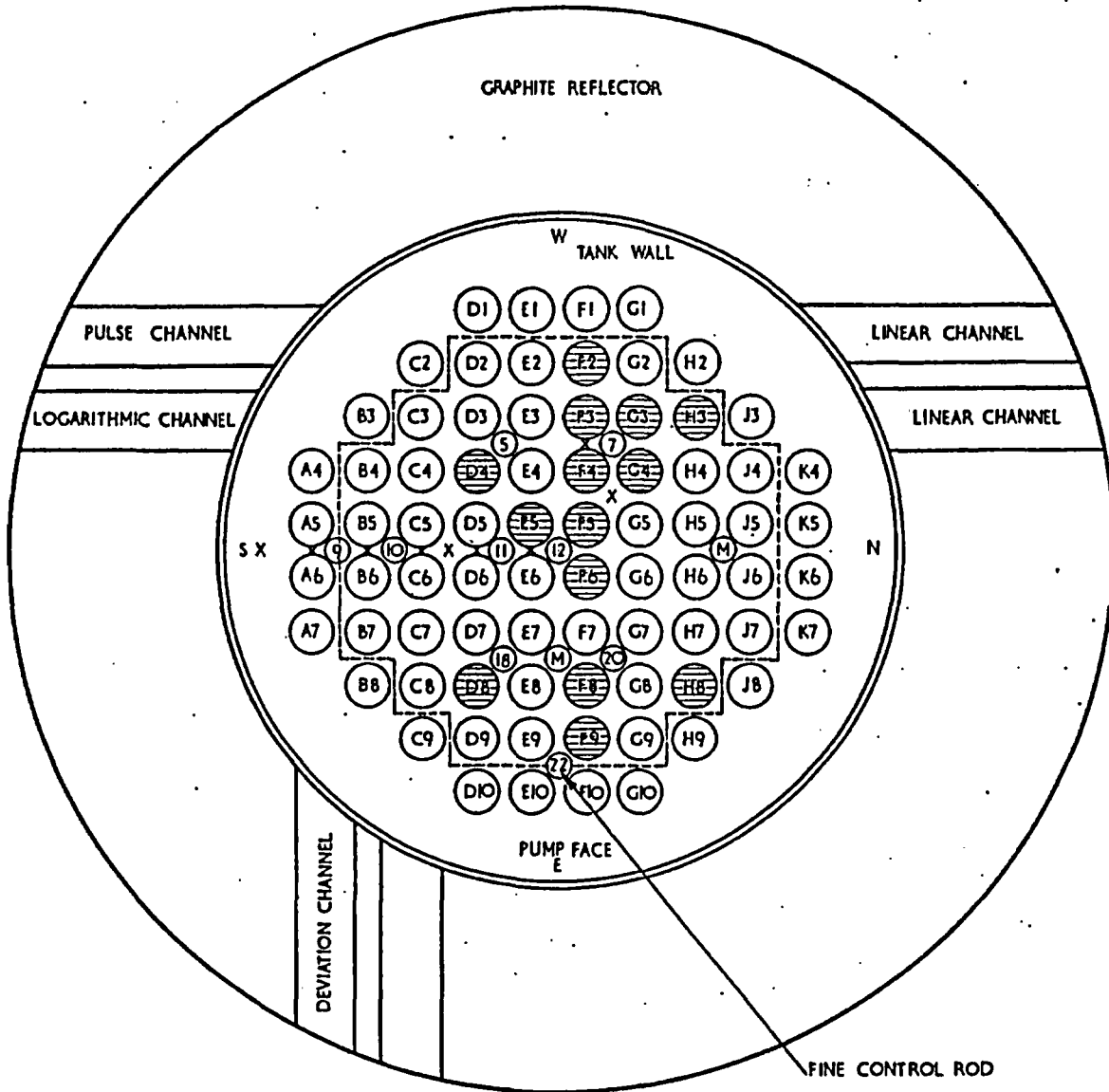
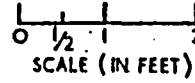
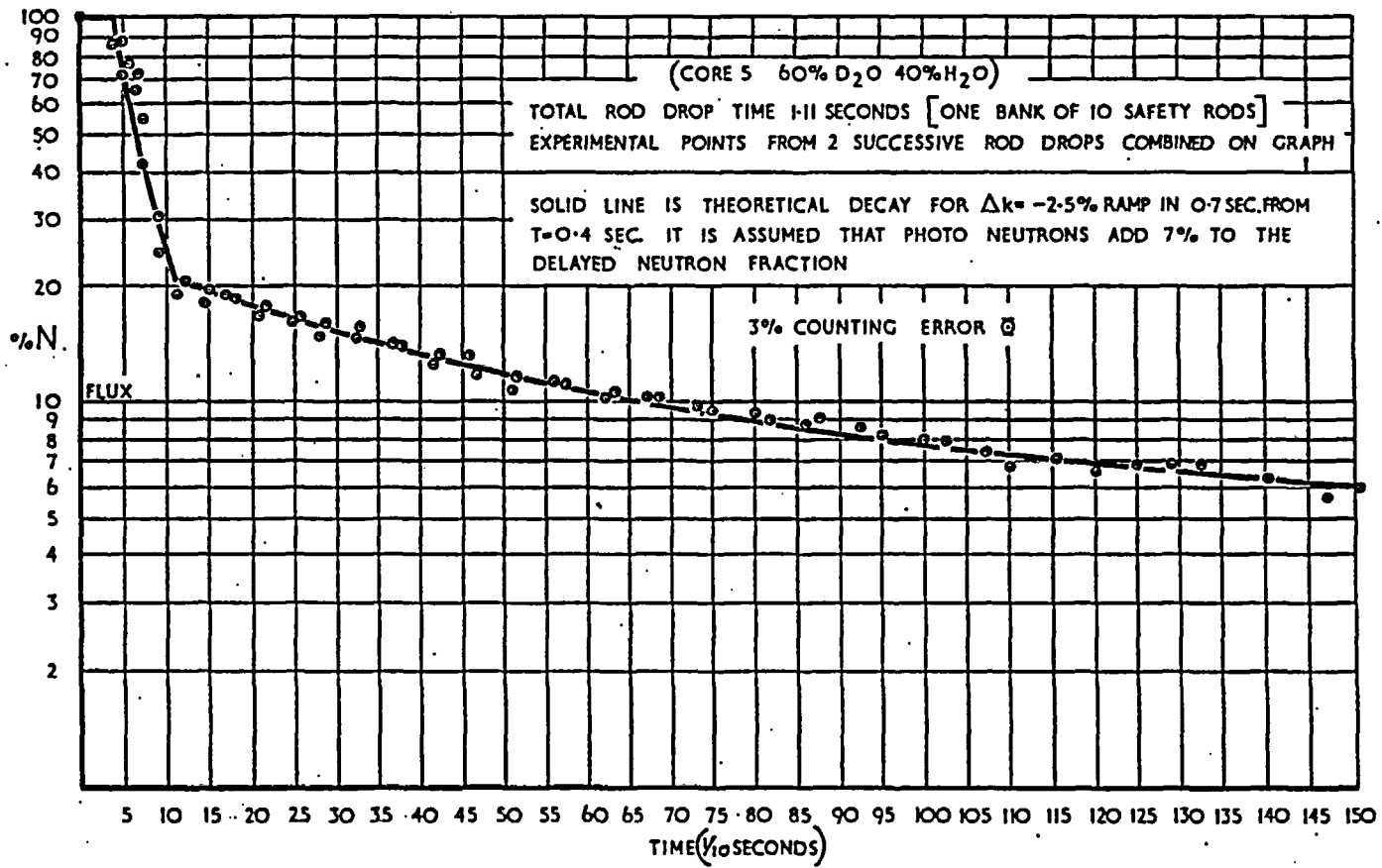


FIG. 1. PLAN OF REACTOR CORE

FIG. 2. MEASURED AND CALCULATED FLUX DECAY CURVES



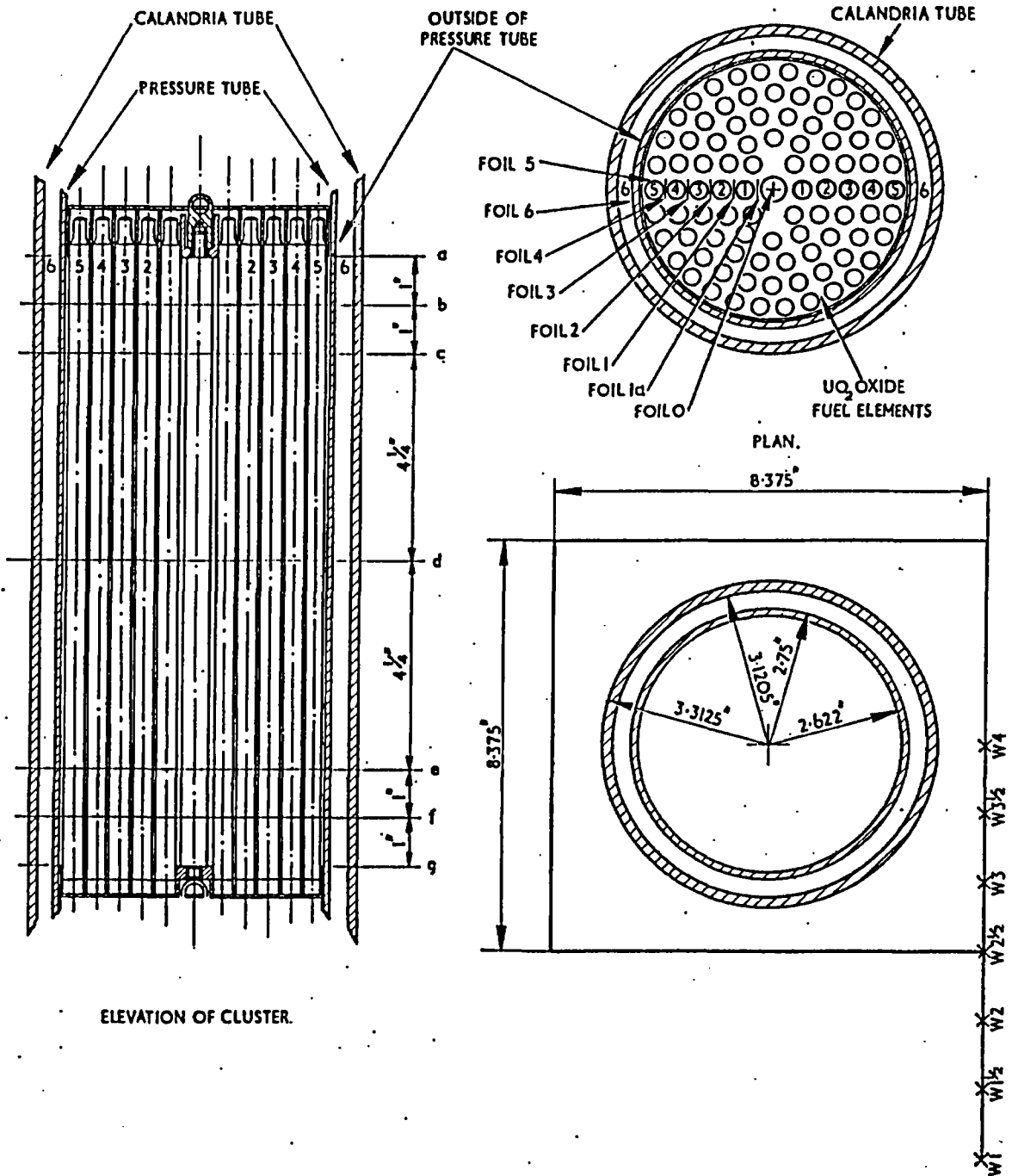
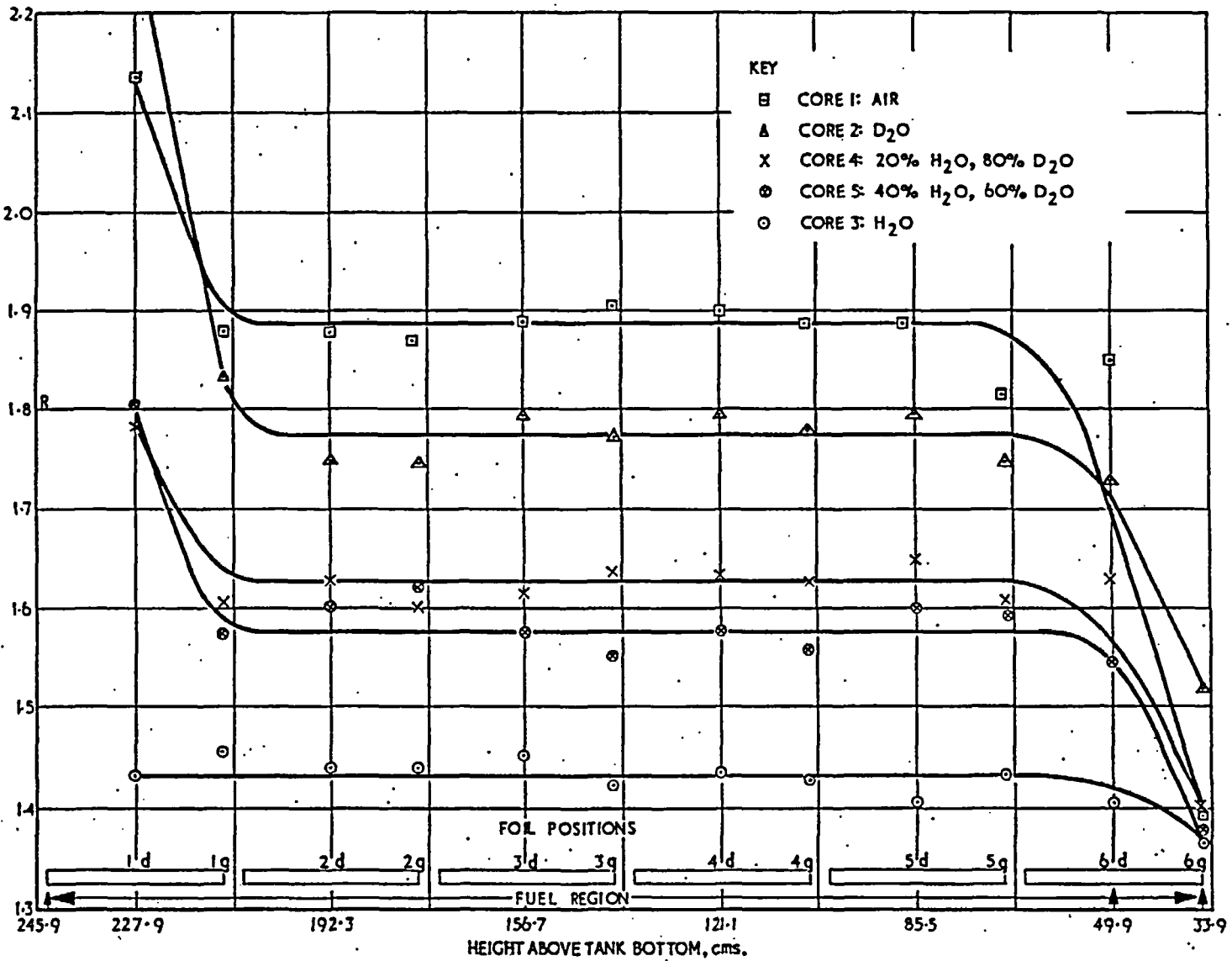
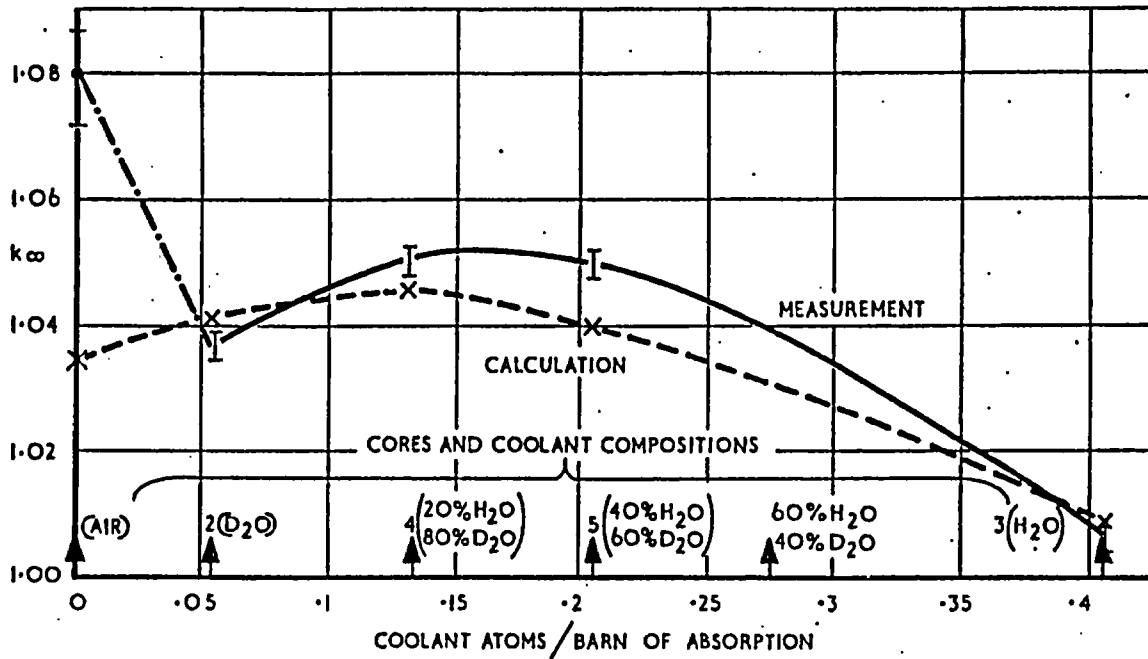


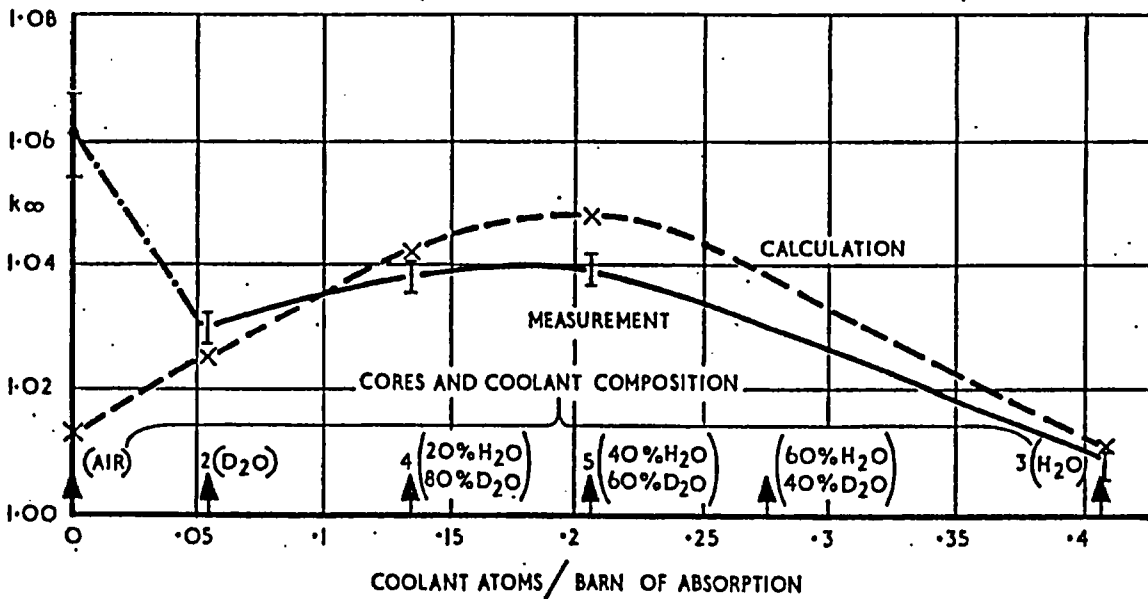
FIG. 3. FOIL POSITIONS IN A LATTICE CELL.

FIG. 5. MACROSCOPIC AXIAL DISTRIBUTION OF GOLD/MANGANESE RATIO.





a. MEASURED AND CALCULATED k_{∞} (PEASE-COBB CALCULATION)



b. MEASURED AND CALCULATED k_{∞} (P80 CALCULATION)

FIG.6. COMPARISON OF MEASURED AND CALCULATED VALUES OF k_{∞}

KEY		
CORE	COOLANT	
□	1	AIR
△	2	D ₂ O
X	4	20% H ₂ O, 80% D ₂ O
⊗	5	40% H ₂ O, 60% D ₂ O
⊙	3	H ₂ O

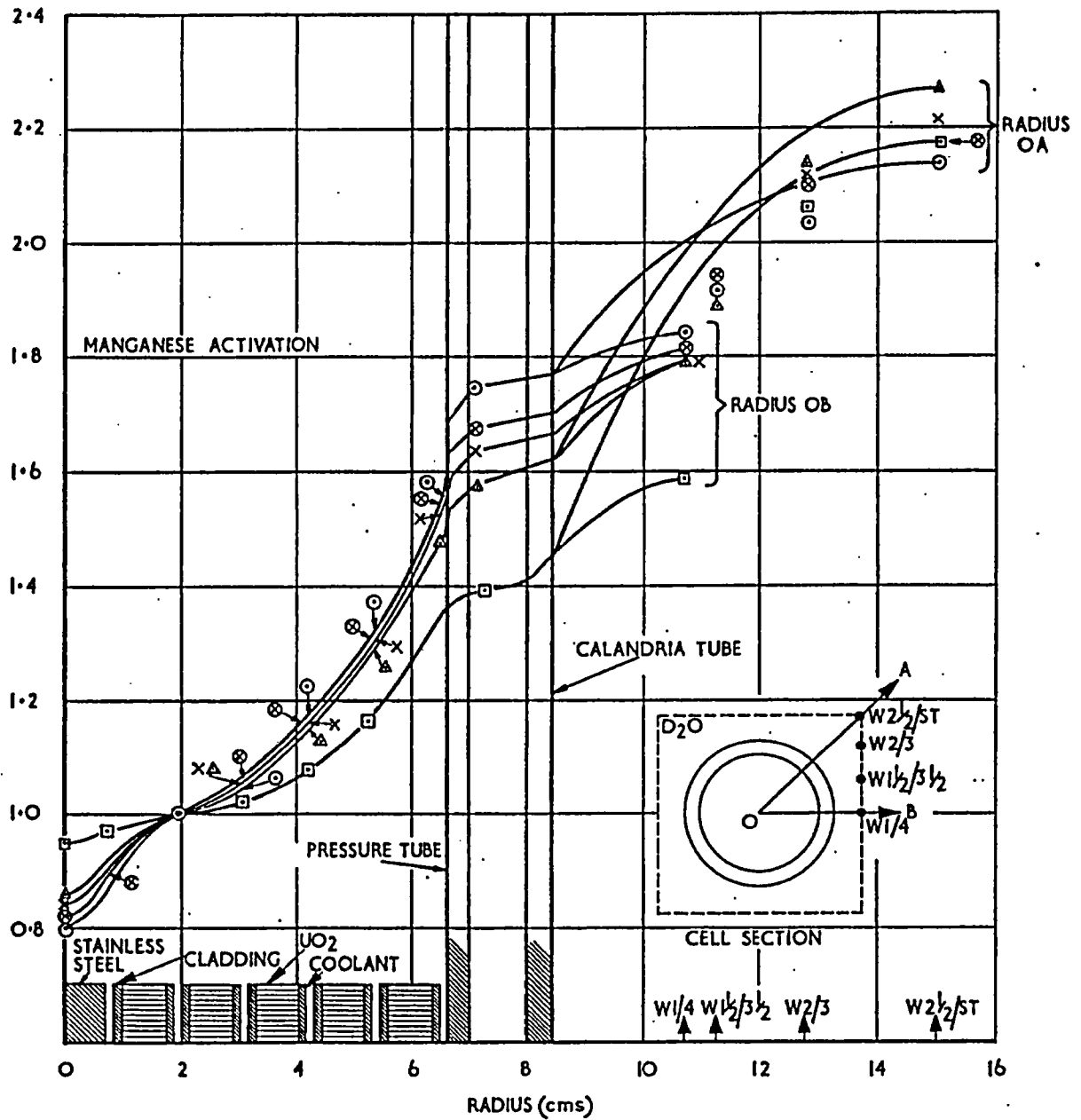
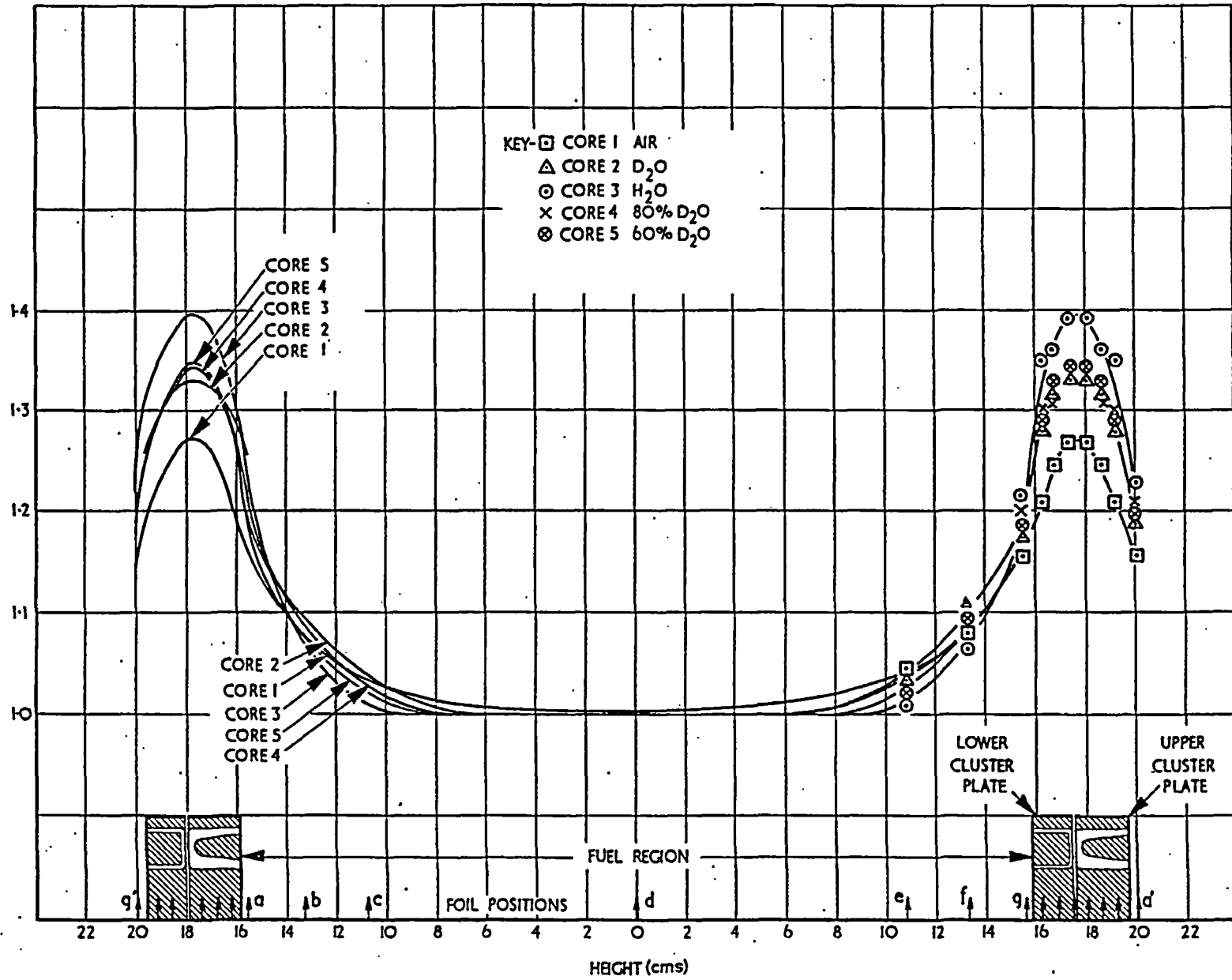


FIG. 7. RADIAL FINE STRUCTURE OF MANGANESE ACTIVATION IN CORES 1-5

FIG. 8 AXIAL FINE STRUCTURE OF MANGANESE ACTIVATION IN CORES 1-5



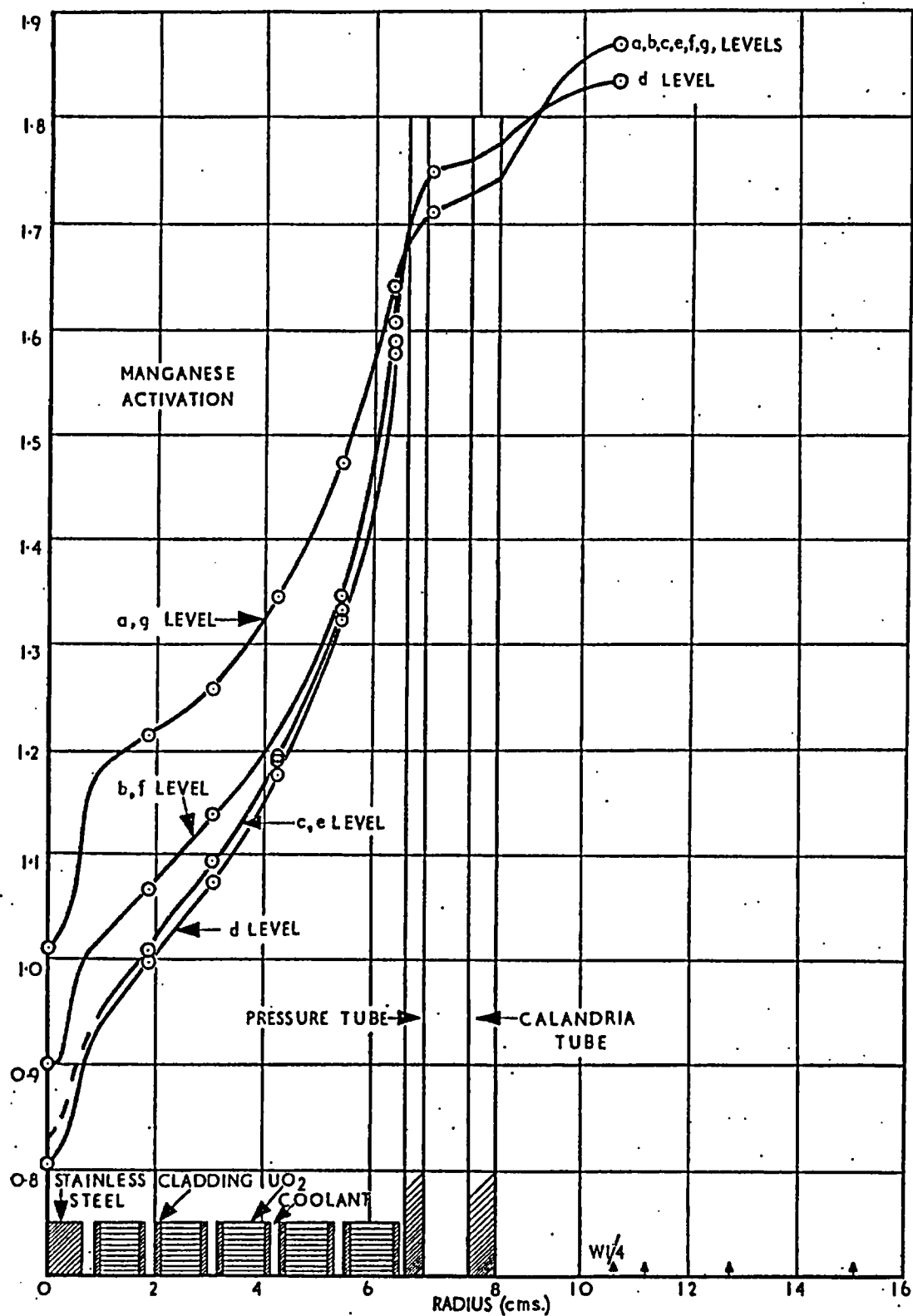


FIG. 9. RADIAL FINE STRUCTURE OF MANGANESE ACTIVATION AT DIFFERENT HEIGHTS IN CELL [CORE 3]

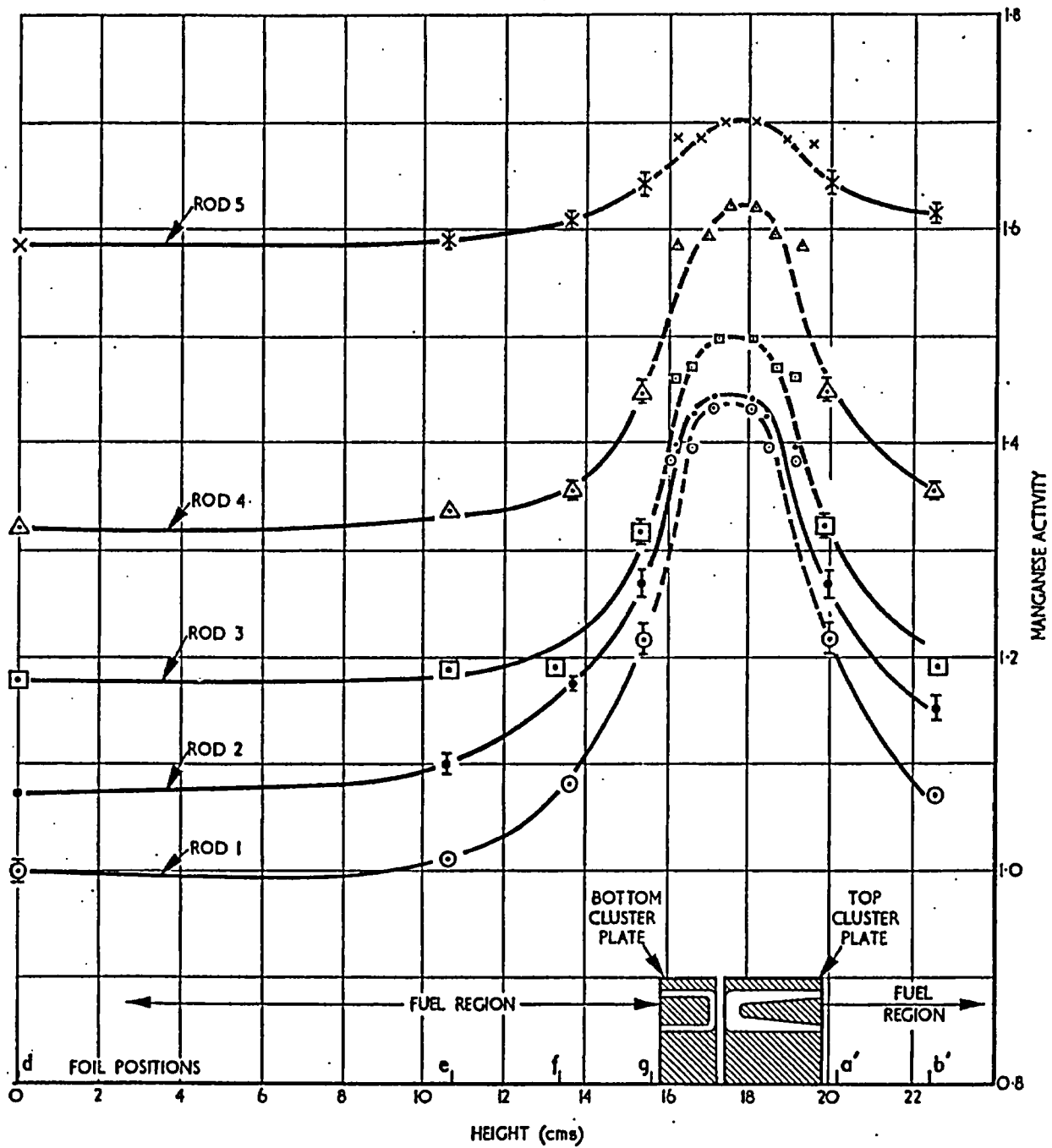


FIG. 10 AXIAL FINE STRUCTURE OF MANGANESE ACTIVATION AT DIFFERENT RADII IN CELL (CORE 3)

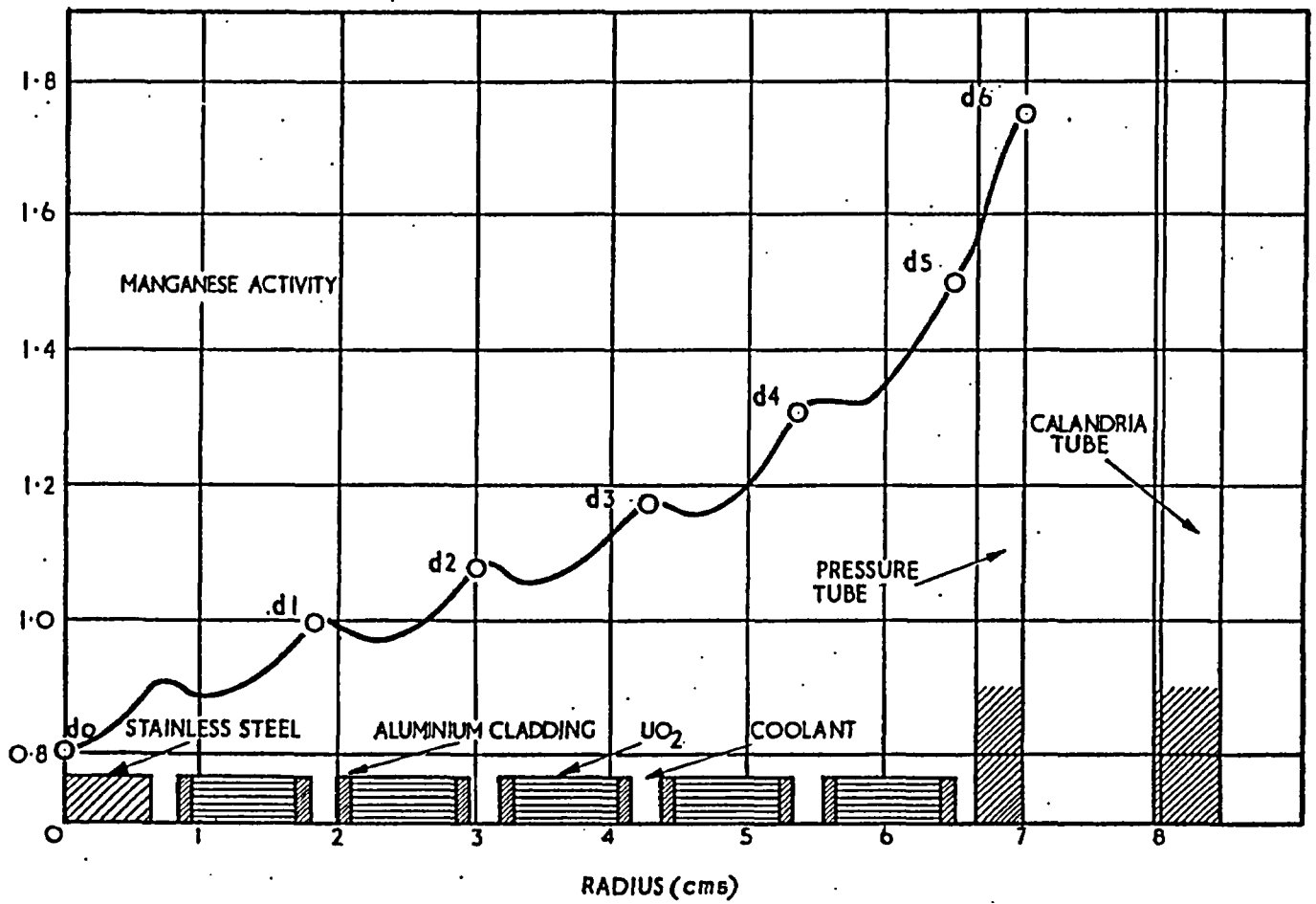
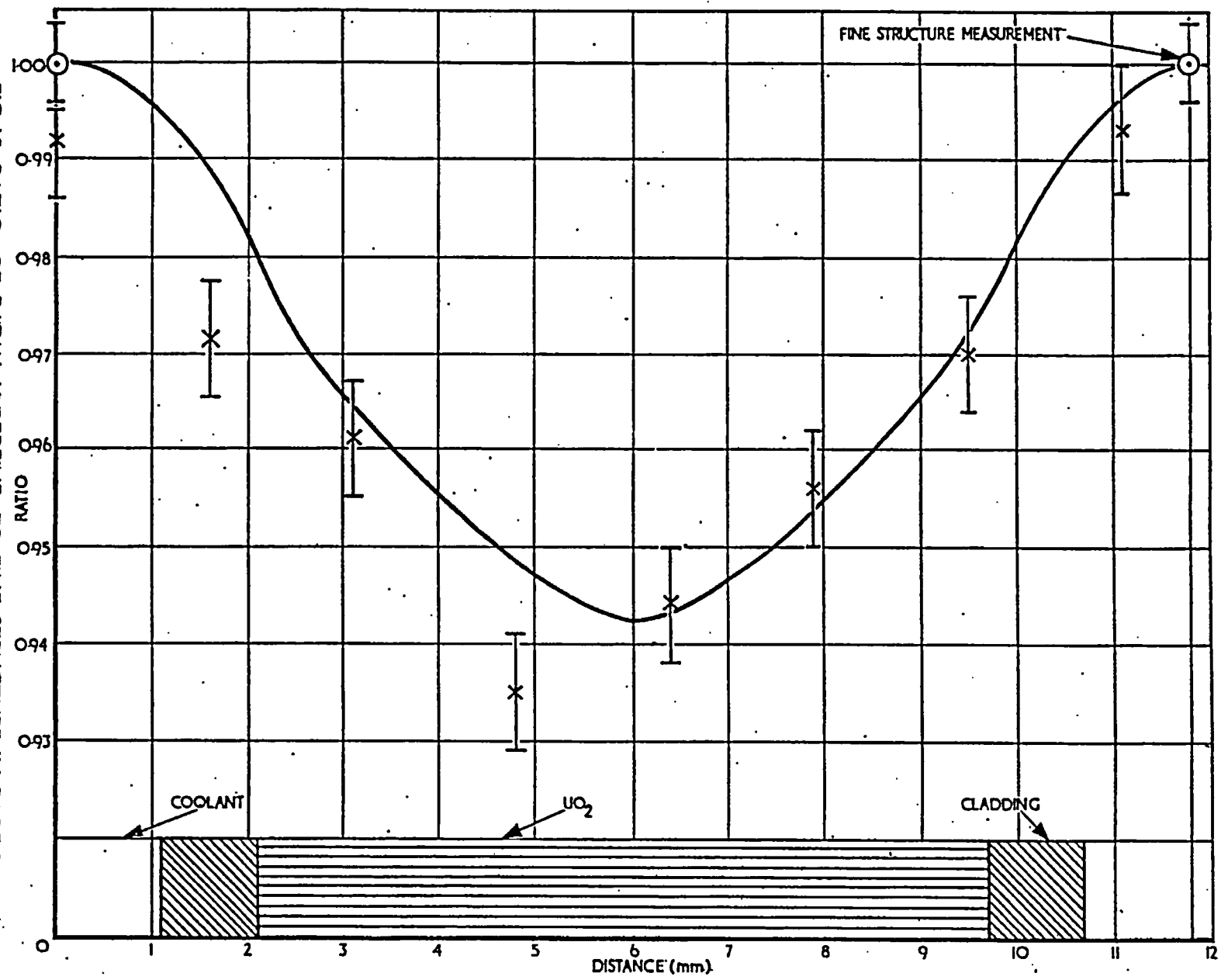


FIG.II. RADIAL HYPERFINE STRUCTURE OF MANGANESE ACTIVATION IN CORE 3.

FIG.12 RATIO OF RADIAL HYPERFINE TO FINE STRUCTURE IN CORE 3



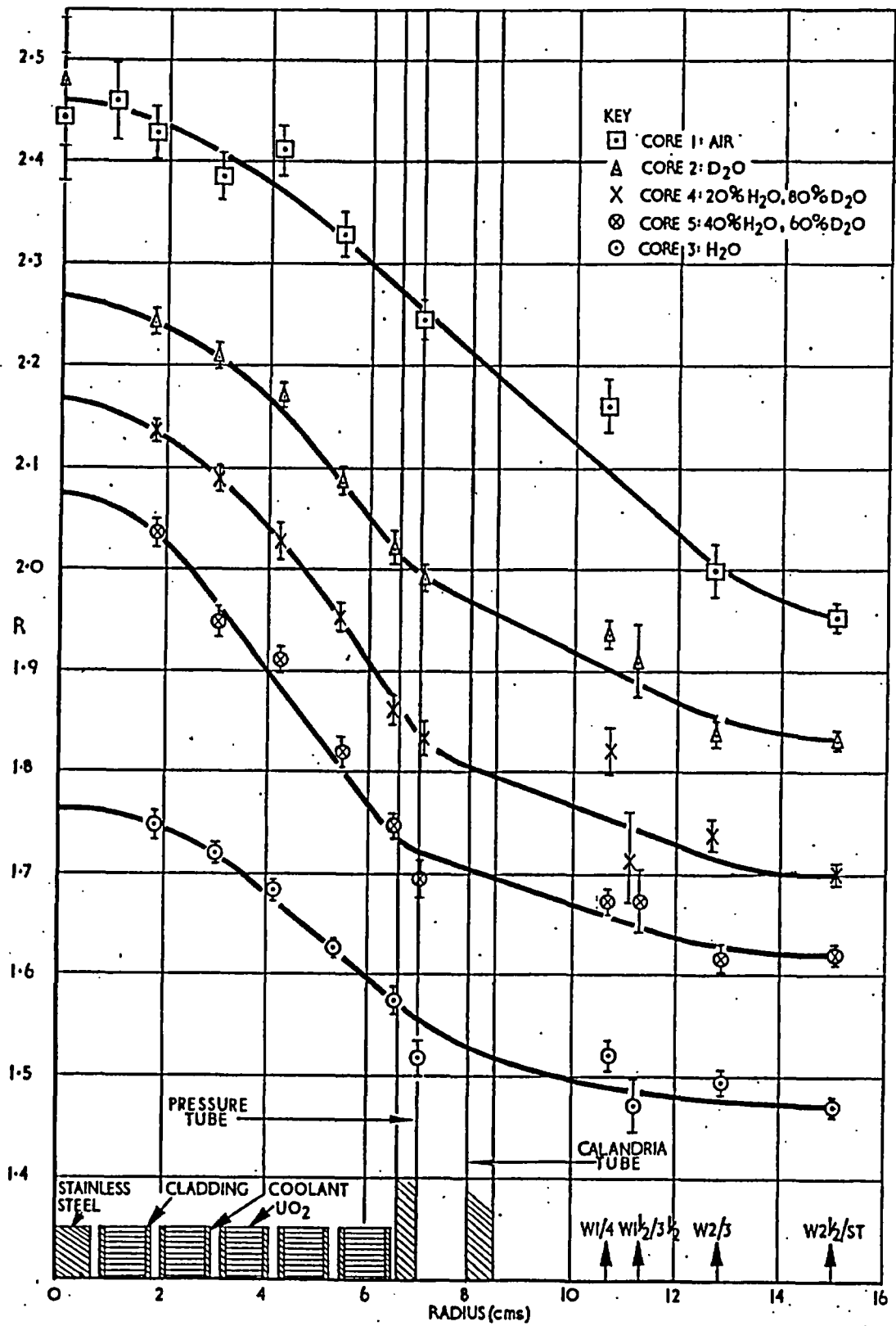


FIG.13. RADIAL FINE STRUCTURE OF GOLD MANGANESE RATIO IN CORES 1-5

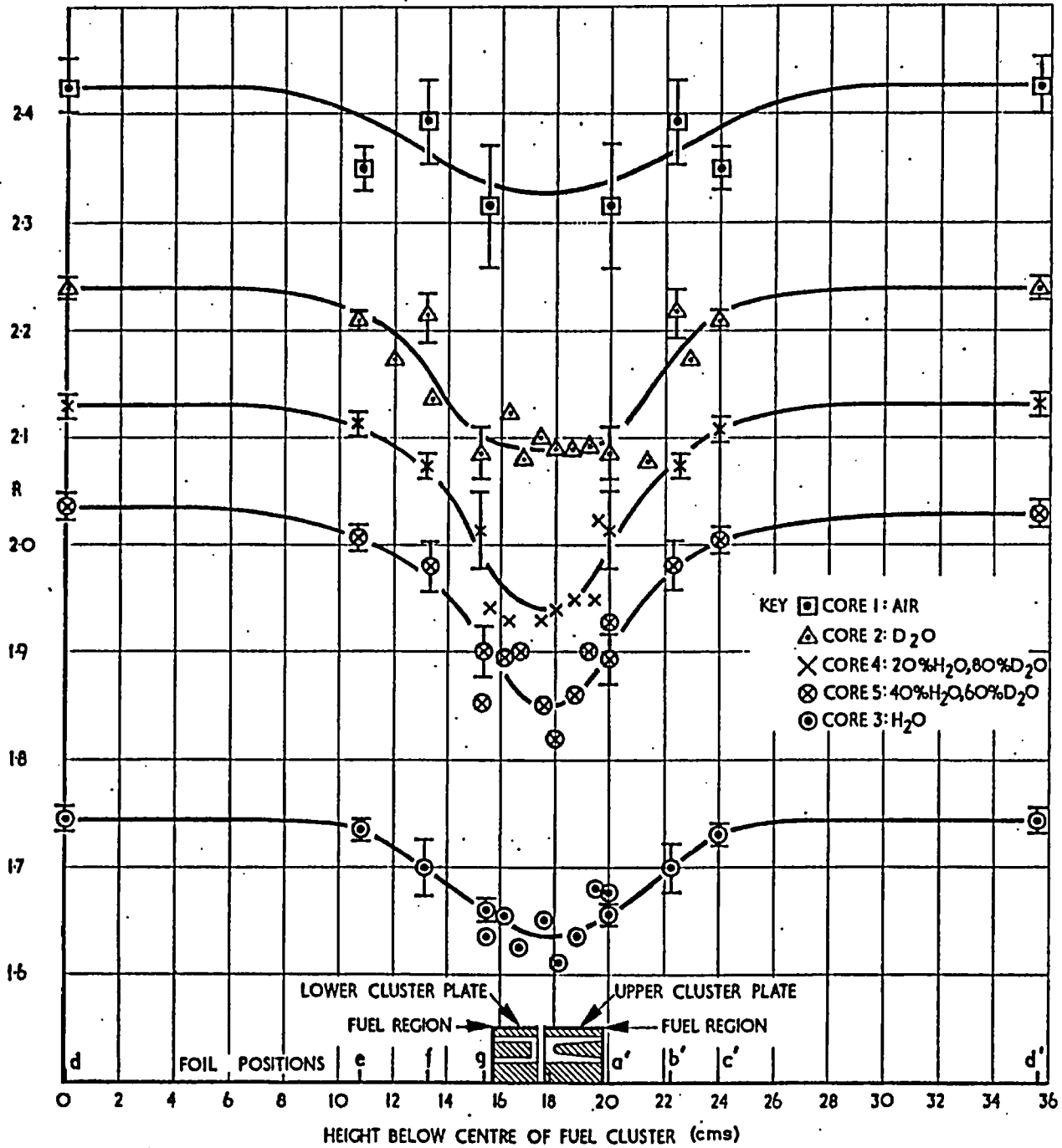


FIG. 14 AXIAL FINE STRUCTURE OF GOLD/MANGANESE RATIO IN CORES 15
 (MEASUREMENTS IN RADIAL FOIL POSITION I)

KEY:

- CORE 1: AIR
- ▲ CORE 2: D₂O
- X CORE 4: 20% H₂O, 80% D₂O
- ⊗ CORE 5: 40% H₂O, 60% D₂O
- CORE 3: H₂O

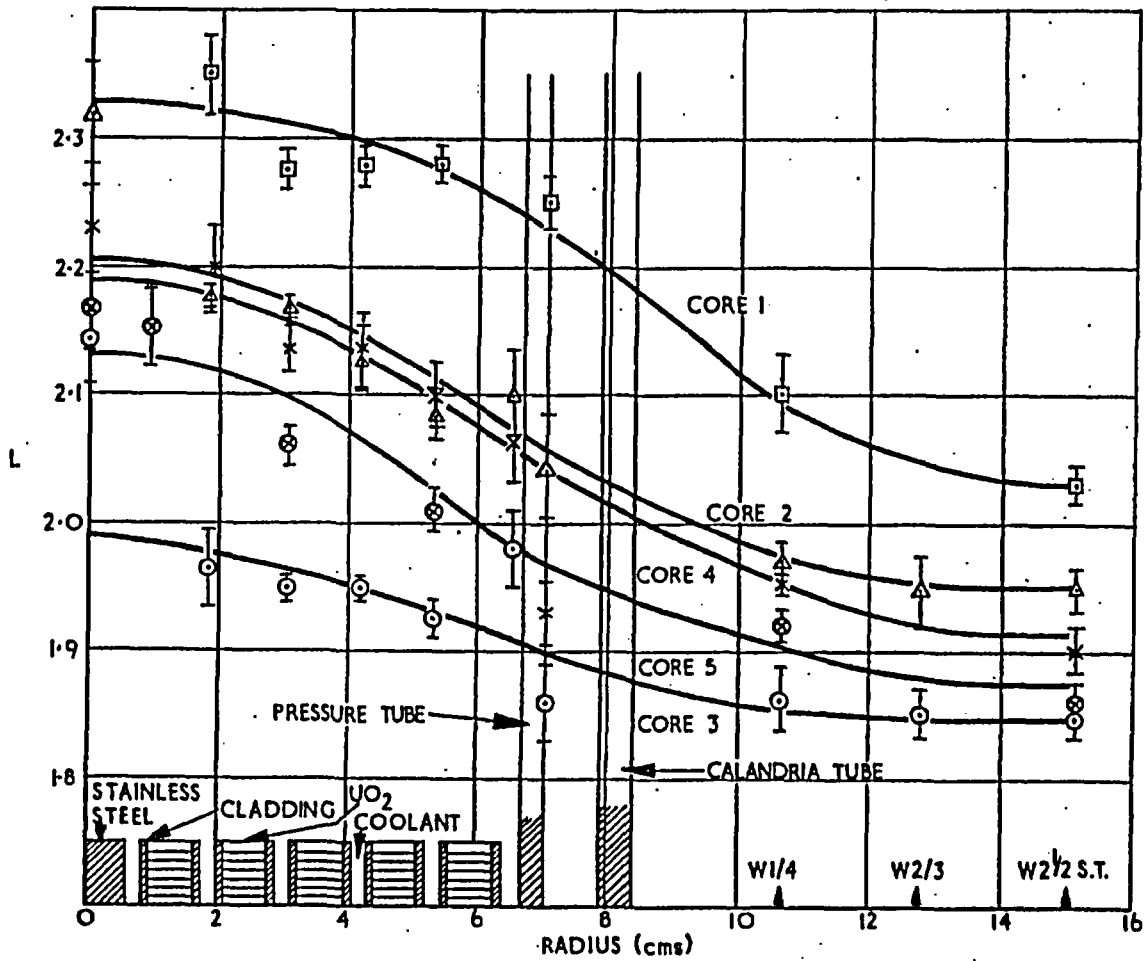


FIG.15 RADIAL FINE STRUCTURE OF LUTECIUM/MANGANESE RATIO IN CORES 1-5

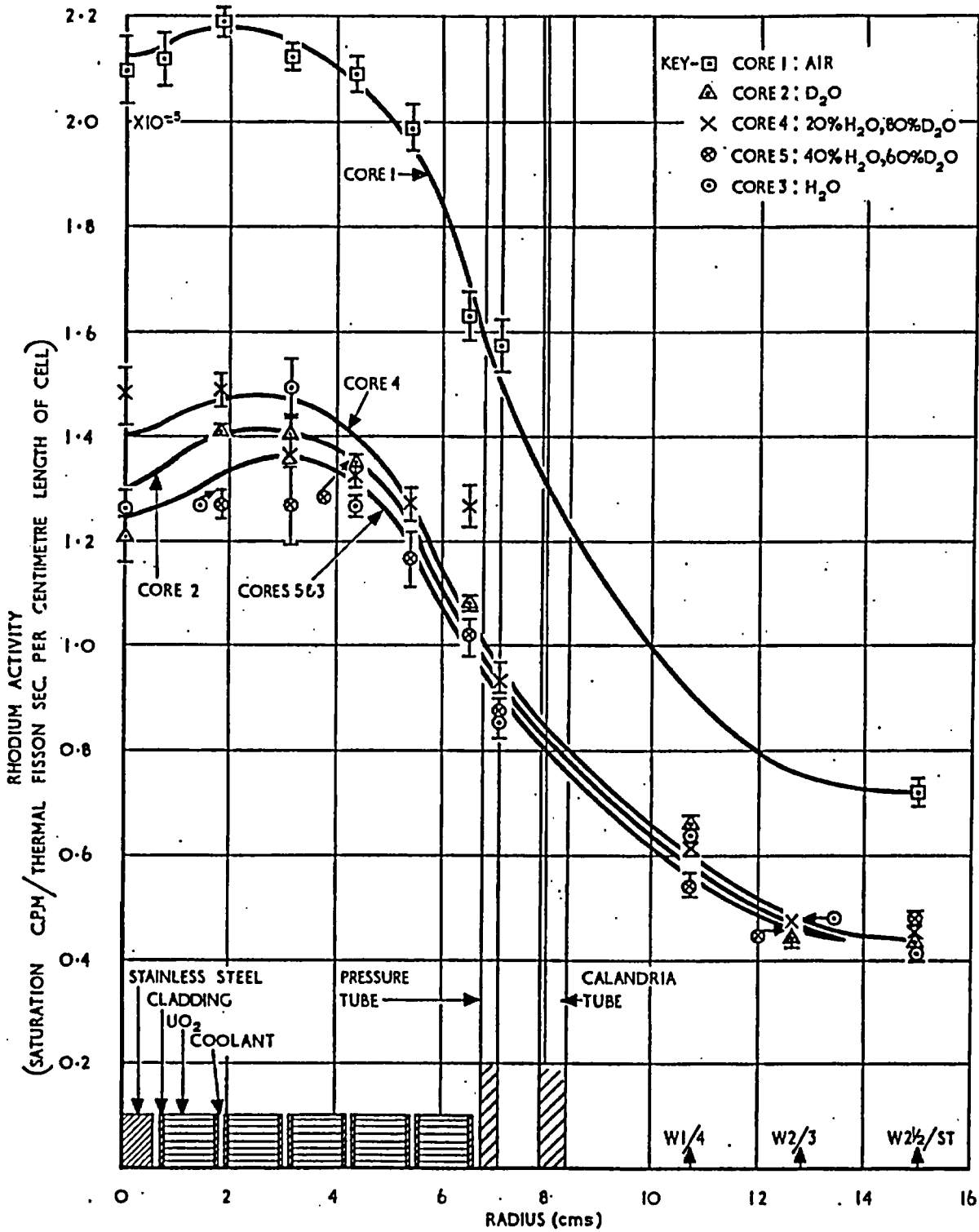


FIG.16. RADIAL FINE STRUCTURE OF RHODIUM ACTIVATION IN CORES 1-5

FIG.17 SPECTRUM PARAMETERS IN THE FUEL IN CORES
I-5 MEASURED IN D3 POSITION

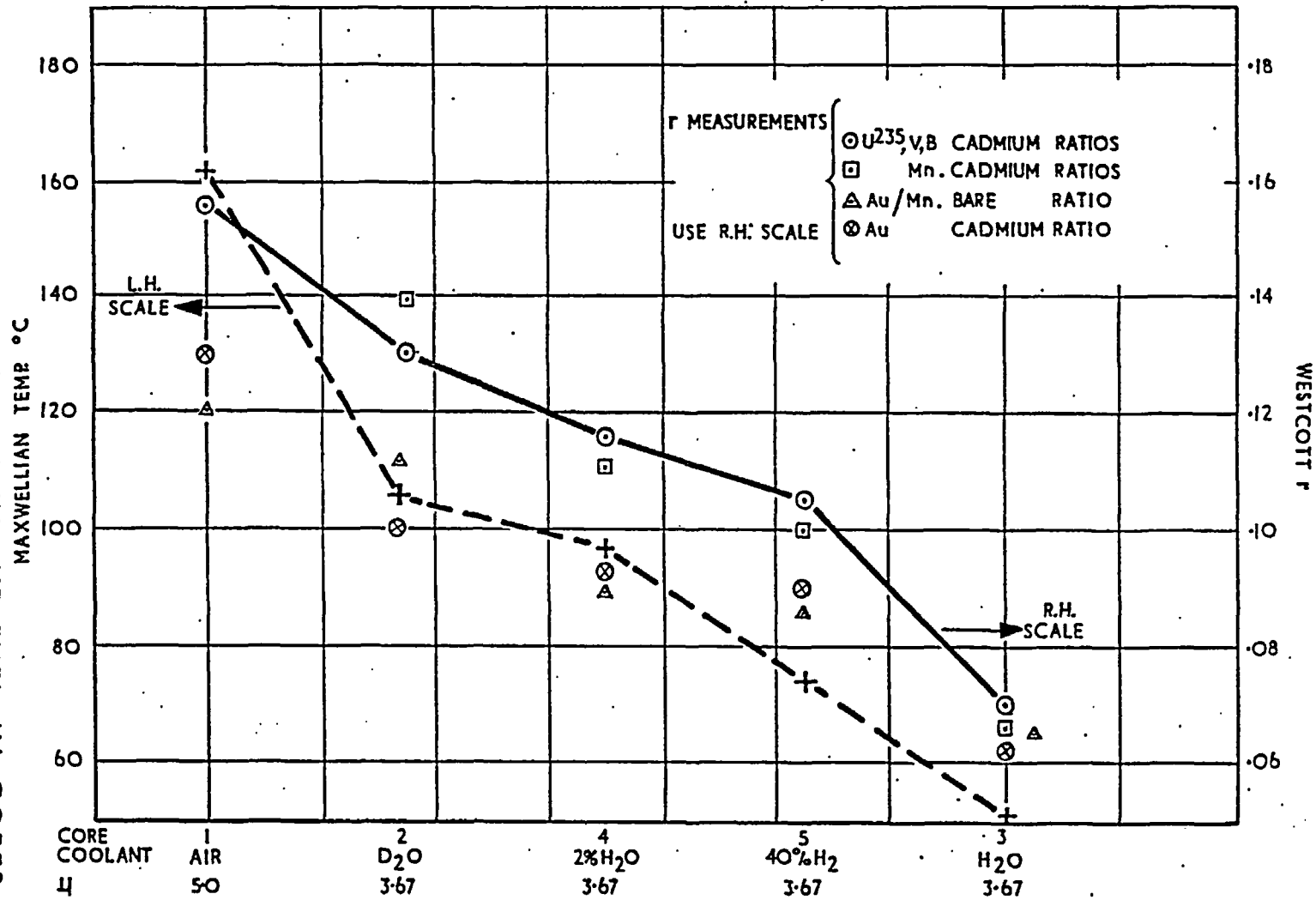
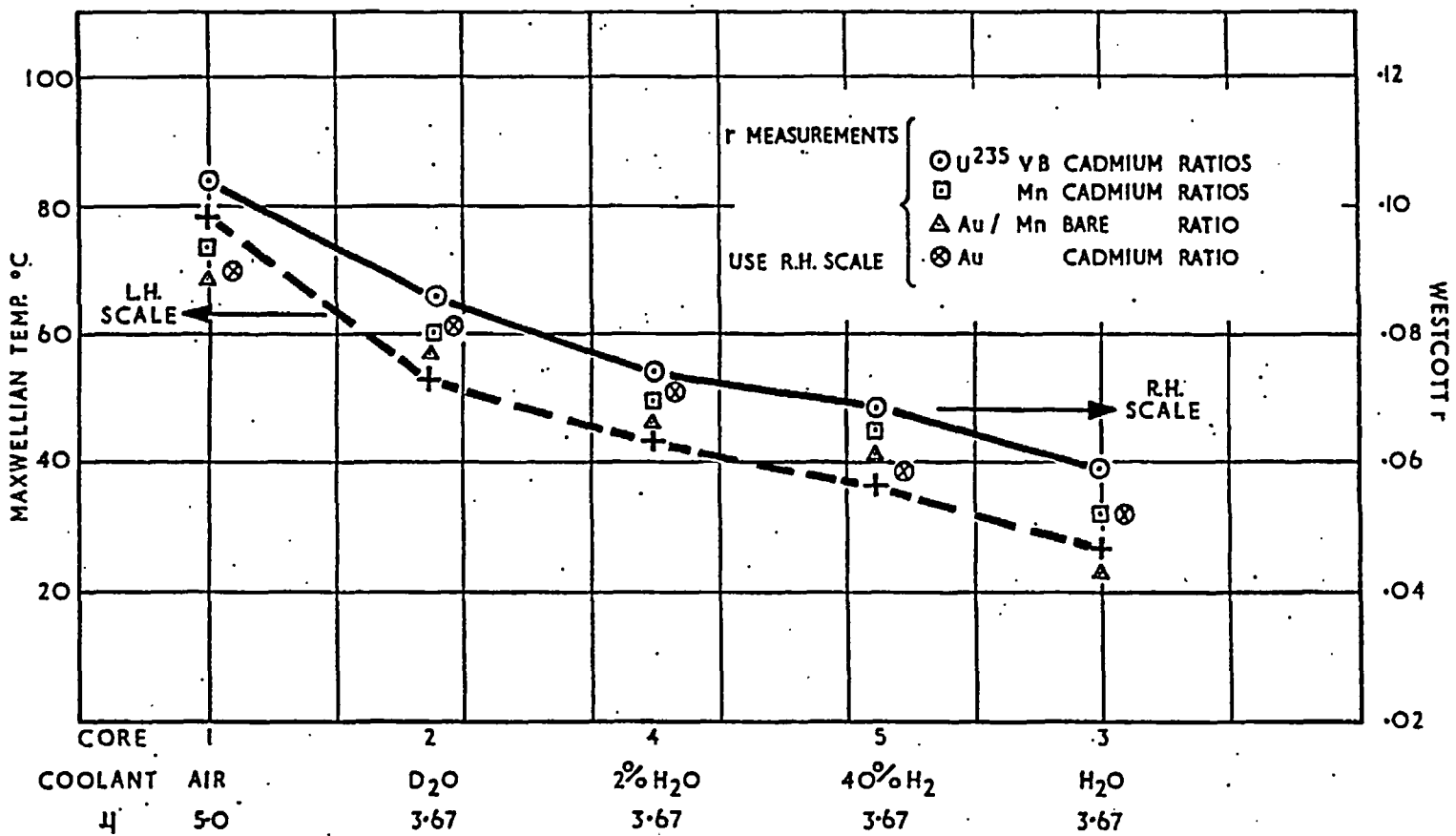


FIG.18. SPECTRUM PARAMETERS IN THE MODERATOR
IN CORES 1-5 MEASURED IN A SEARCH TUBE



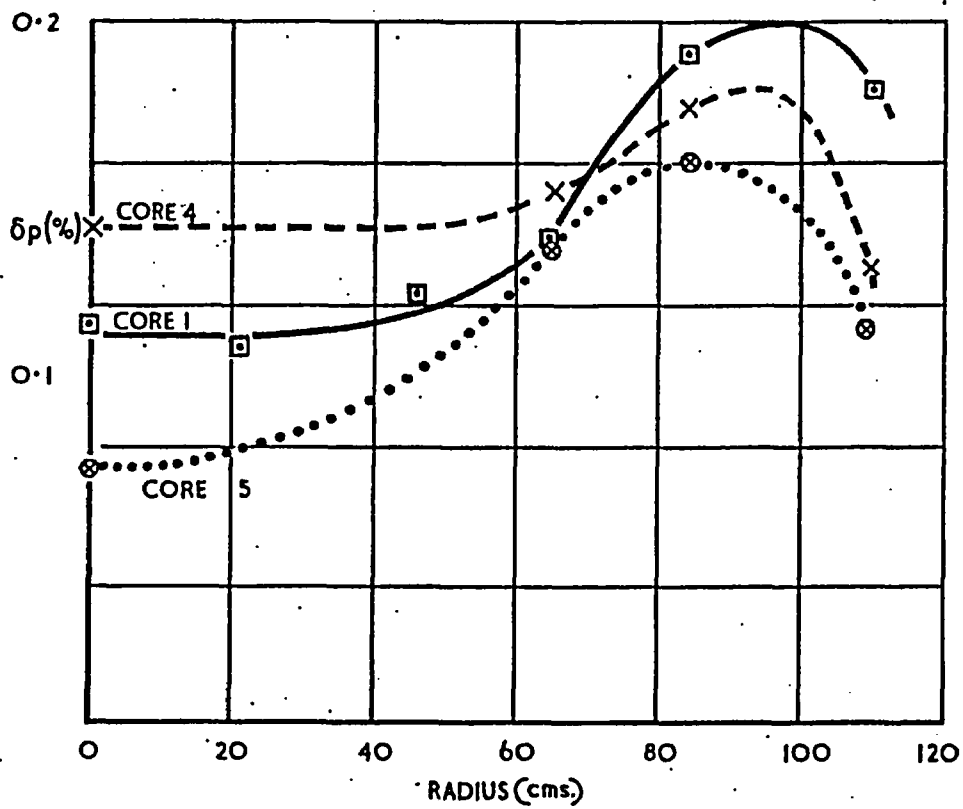


FIG.19. REACTIVITY WORTH OF CADMIUM ABSORBER AT DIFFERENT RADII

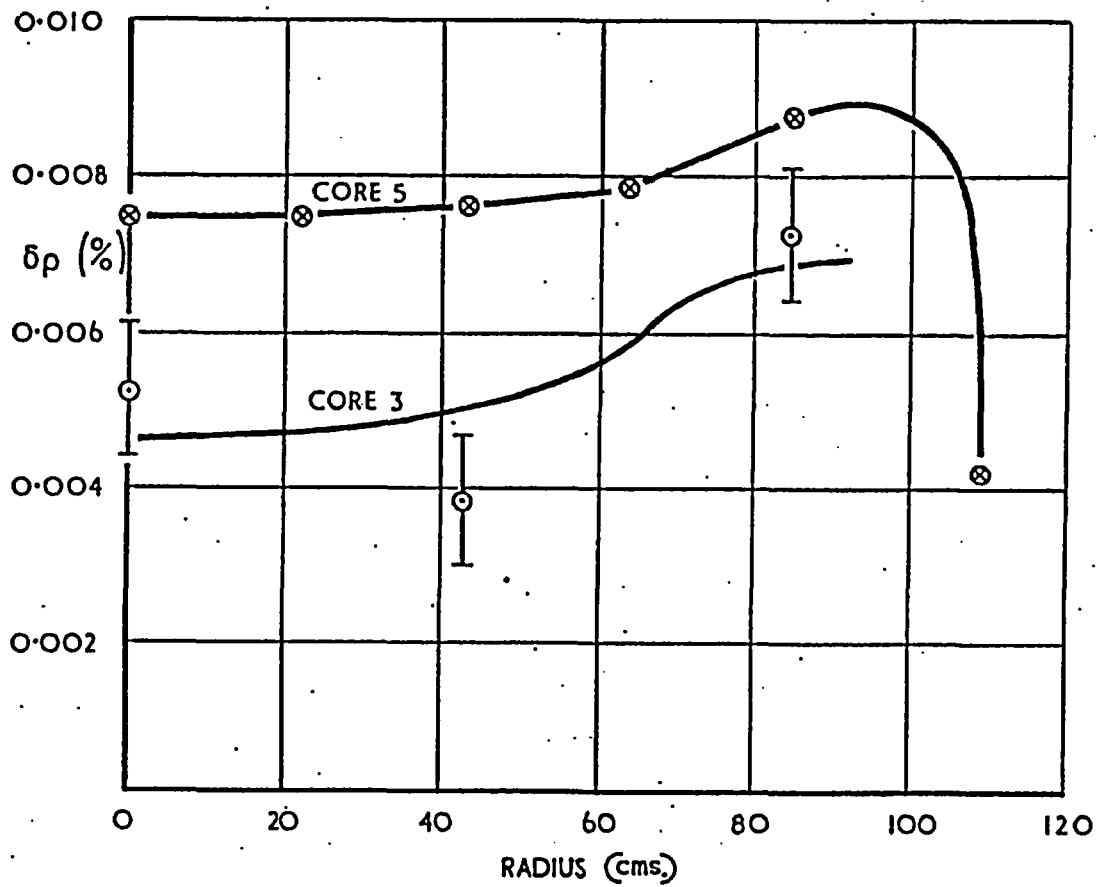


FIG.20. REACTIVITY WORTH OF AN AIR VOID AT DIFFERENT RADII

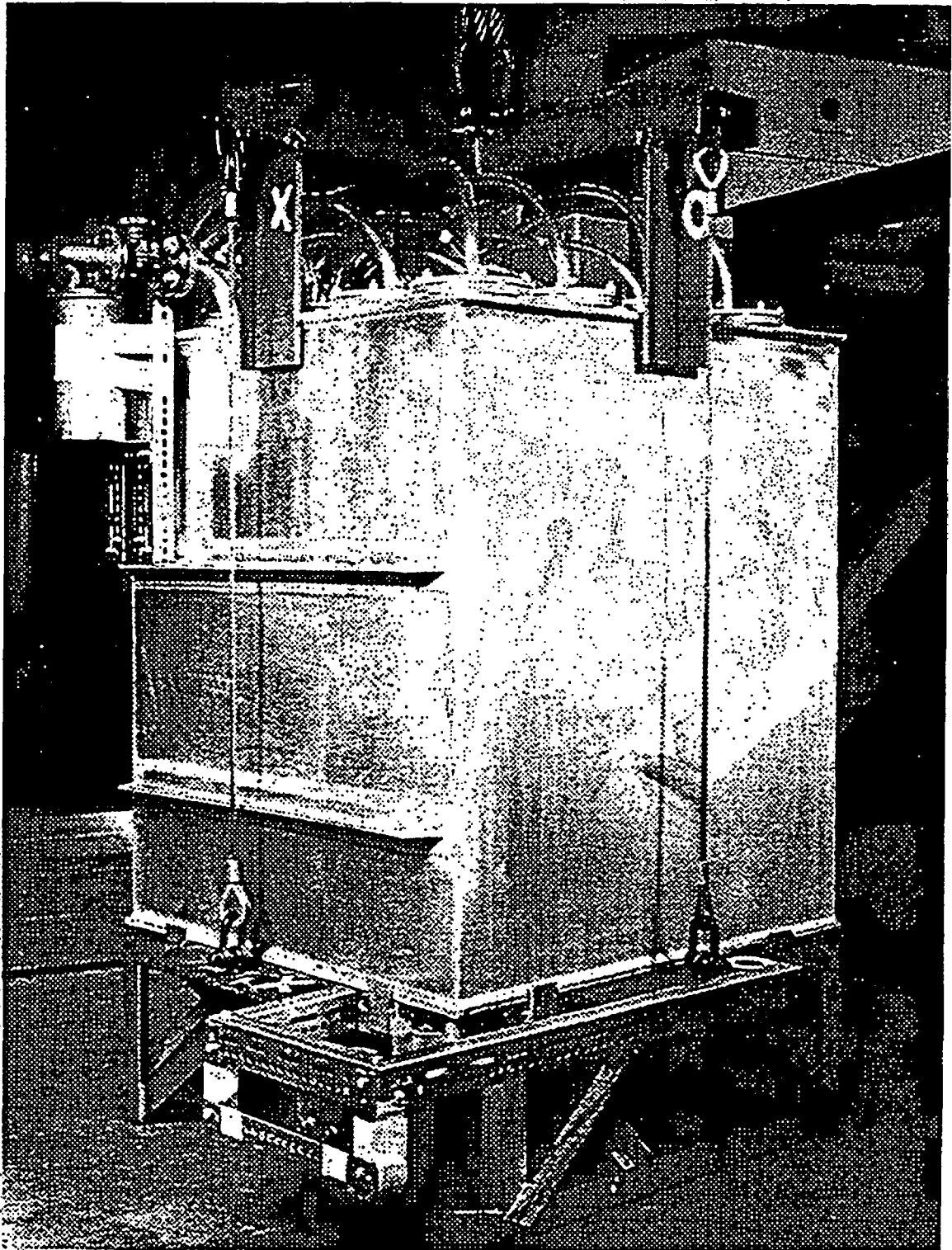


FIG. 21 FINE STRUCTURE STACK AND LIFTING GEAR

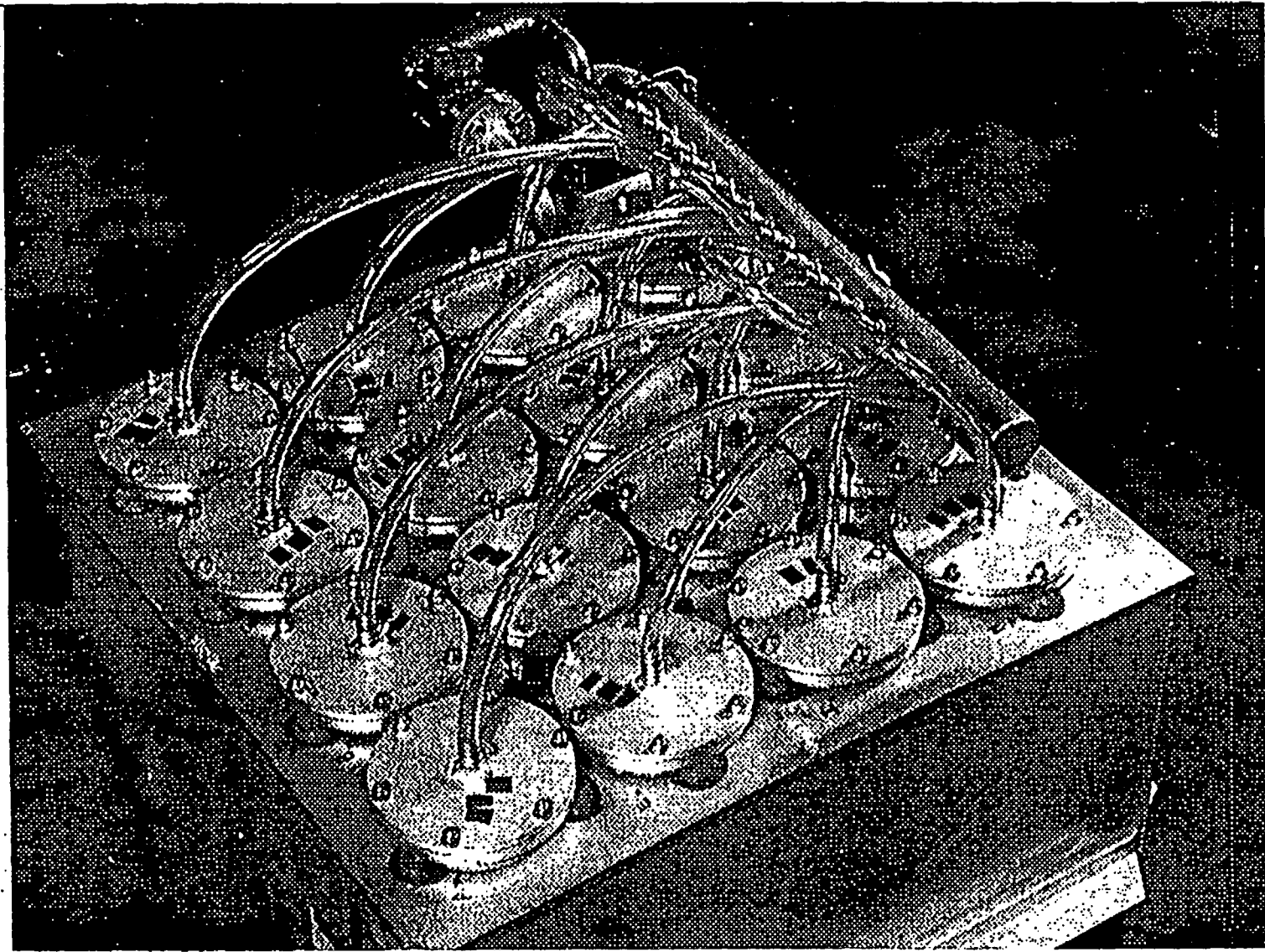


FIG. 22 FINE STRUCTURE STACK SHOWING TOP HEADER

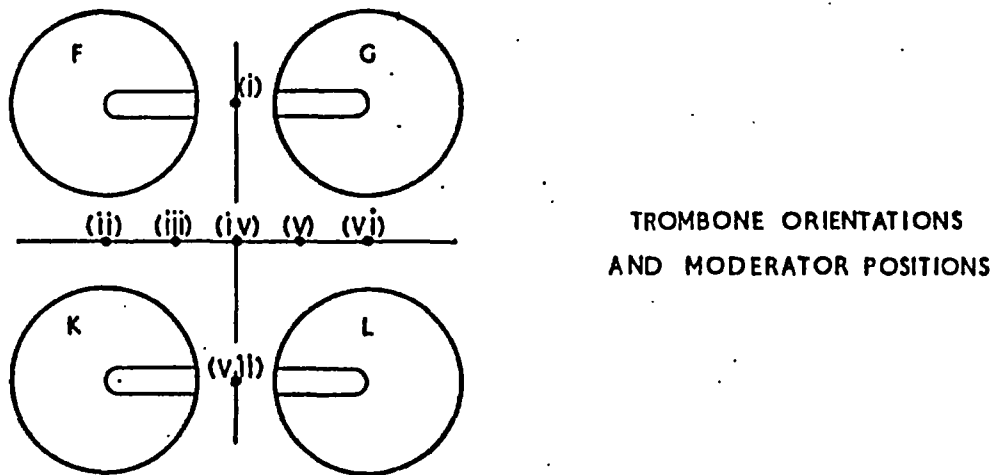
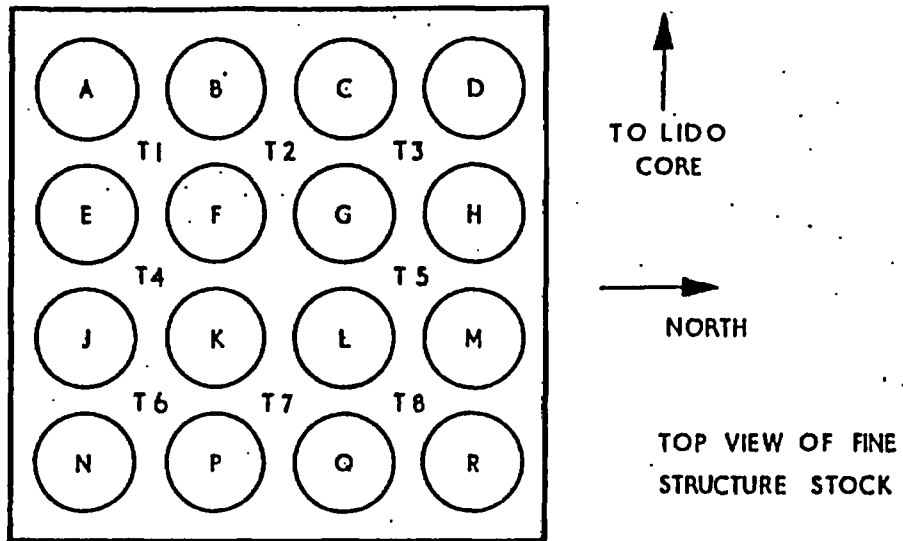


FIG 23. FOIL POSITIONS IN FINE STRUCTURE STACK.

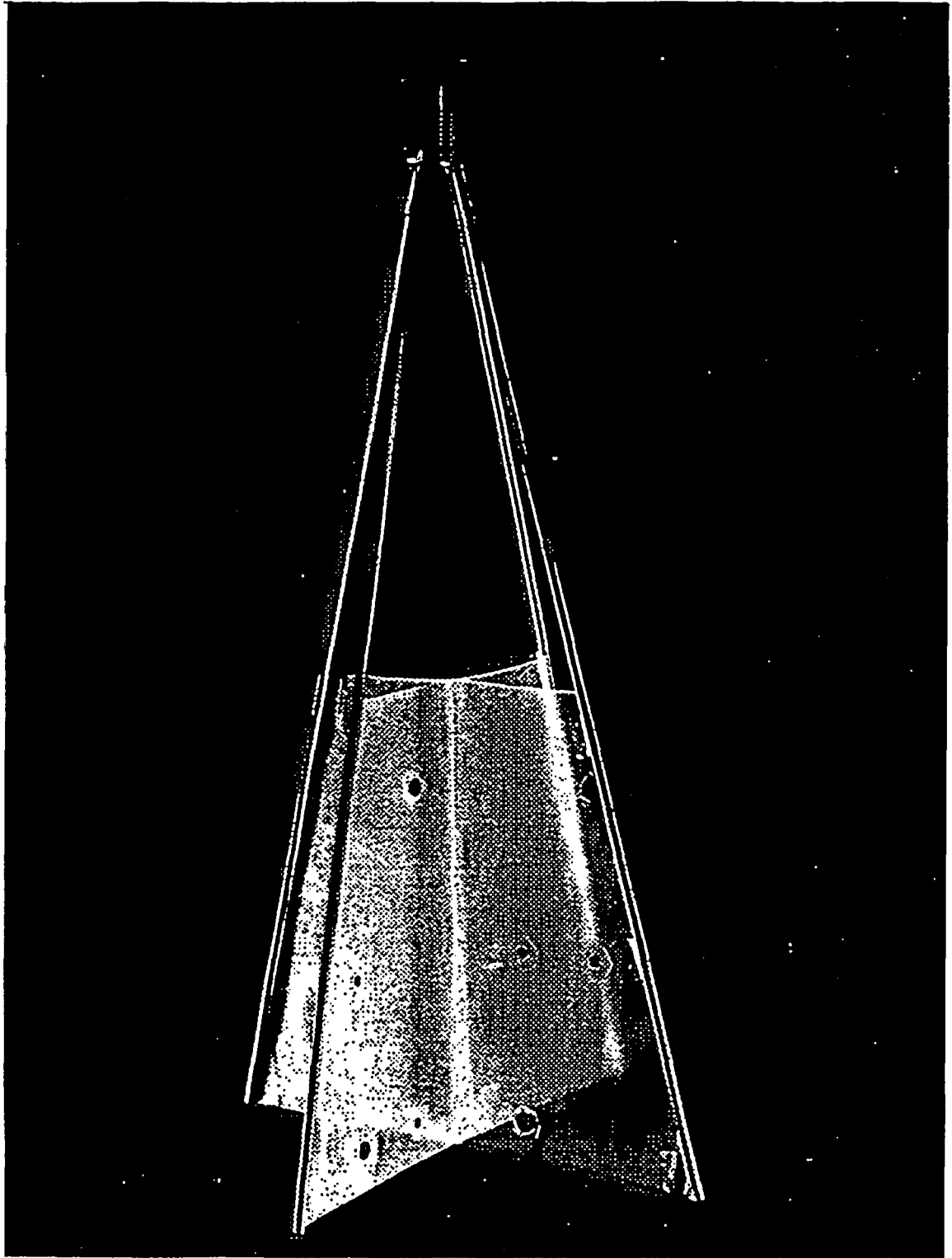


FIG. 24 UMBRELLA FOIL HOLDER

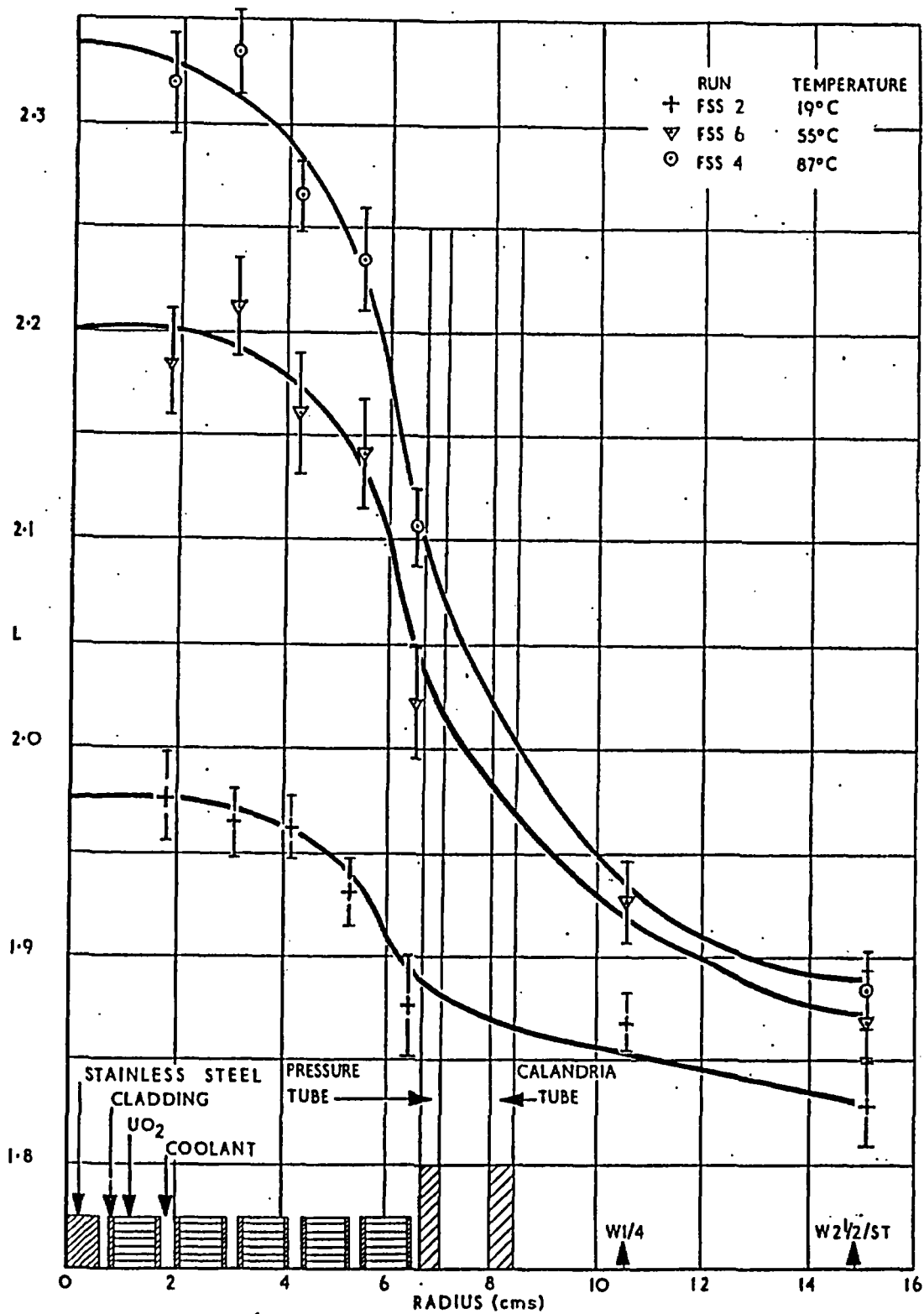


FIG. 25. LUTECIUM/MANGANESE RATIOS IN THE FINE STRUCTURE STACK.

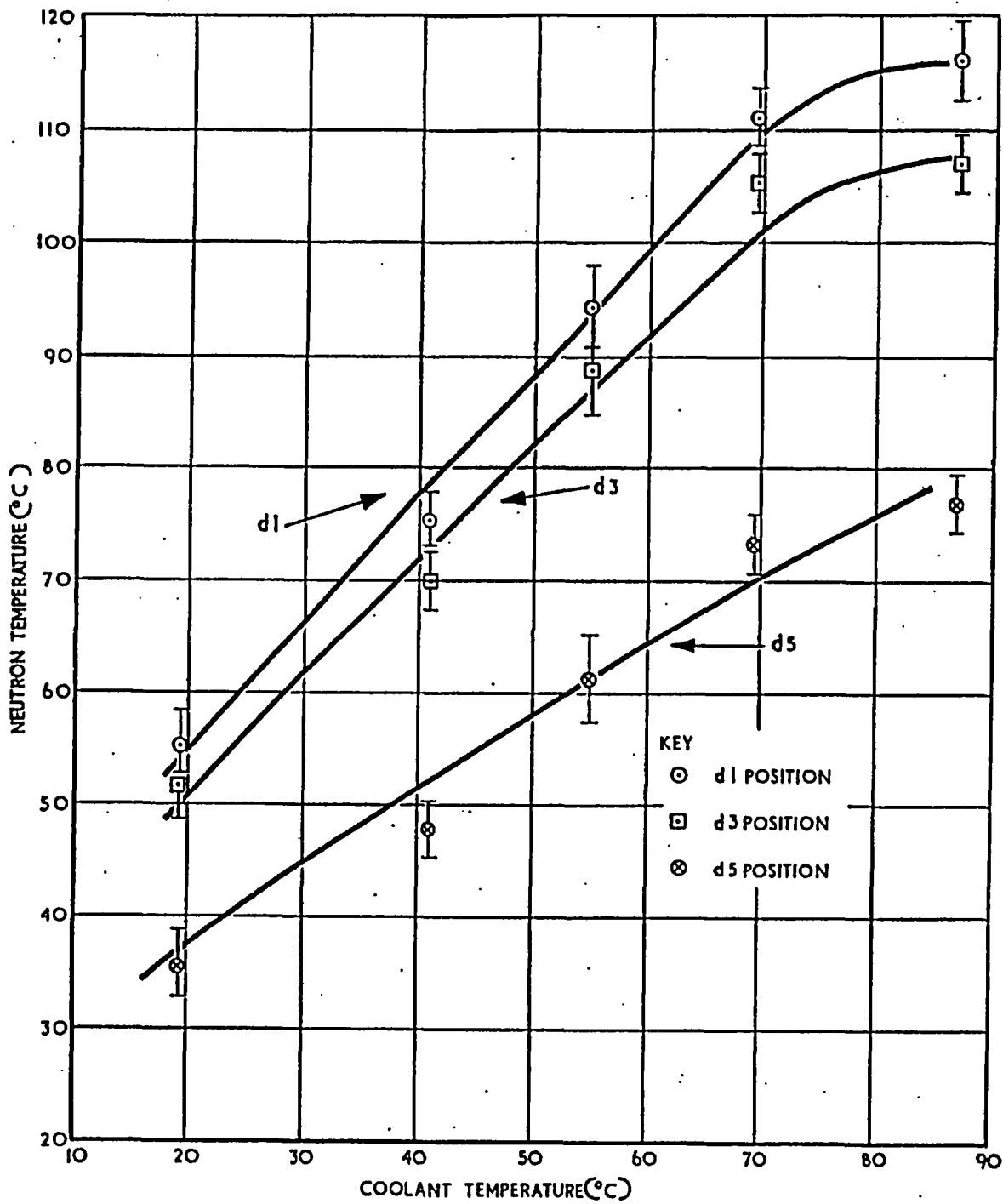
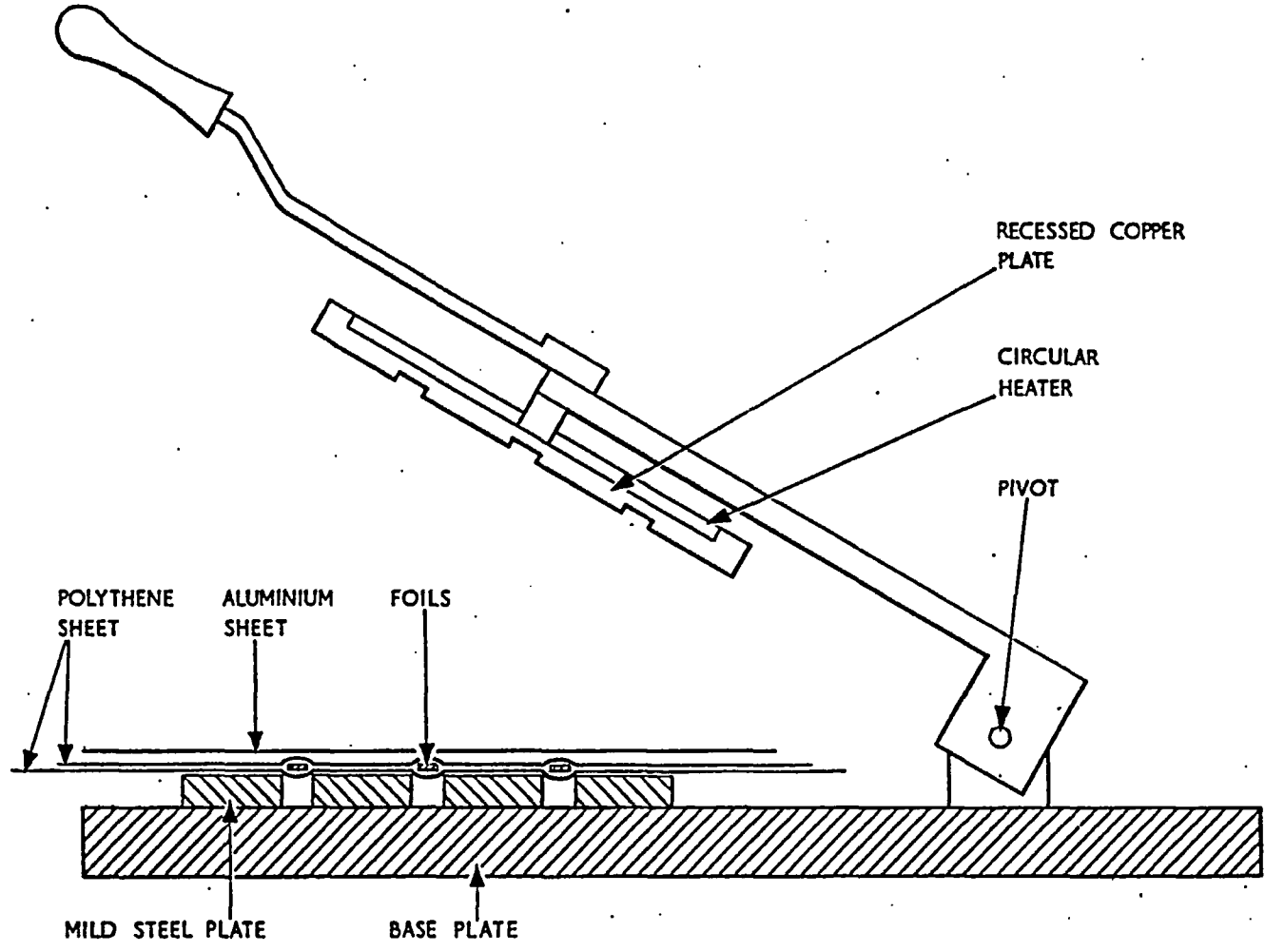


FIG. 26 VARIATION OF NEUTRON TEMPERATURE WITH COOLANT TEMPERATURE IN FINE STRUCTURE STACK

FIG.27. FOIL ENCAPSULATOR



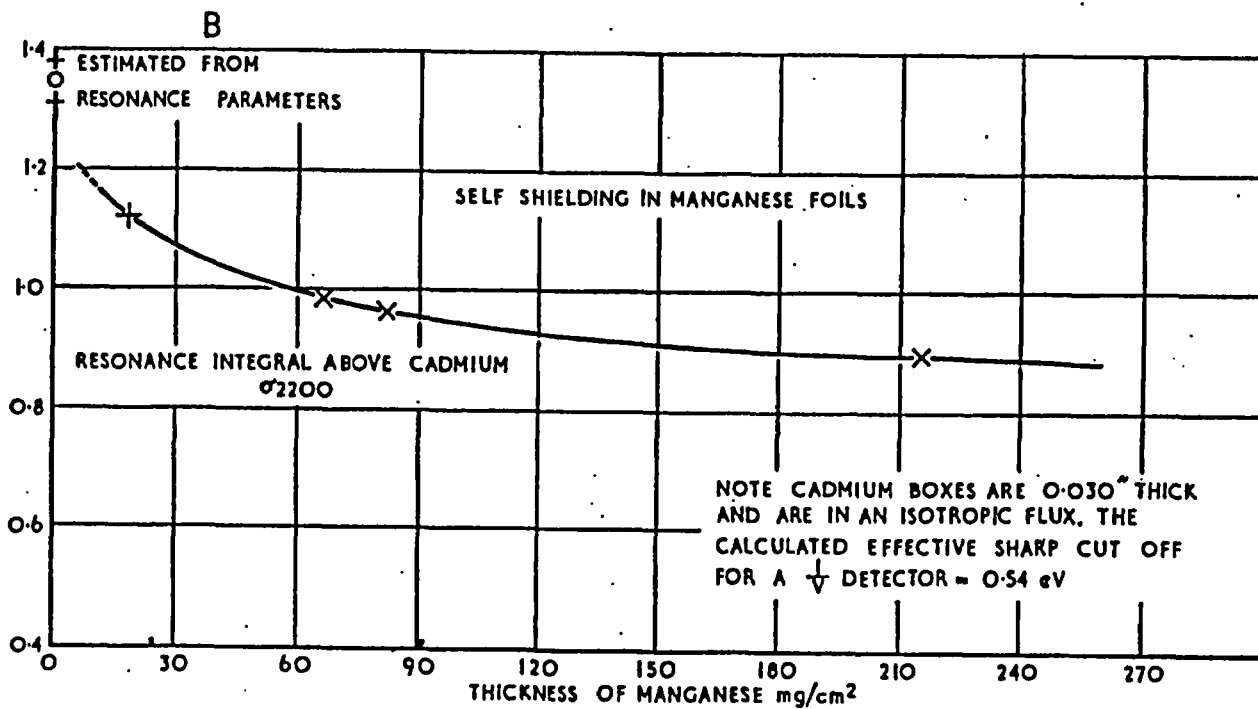
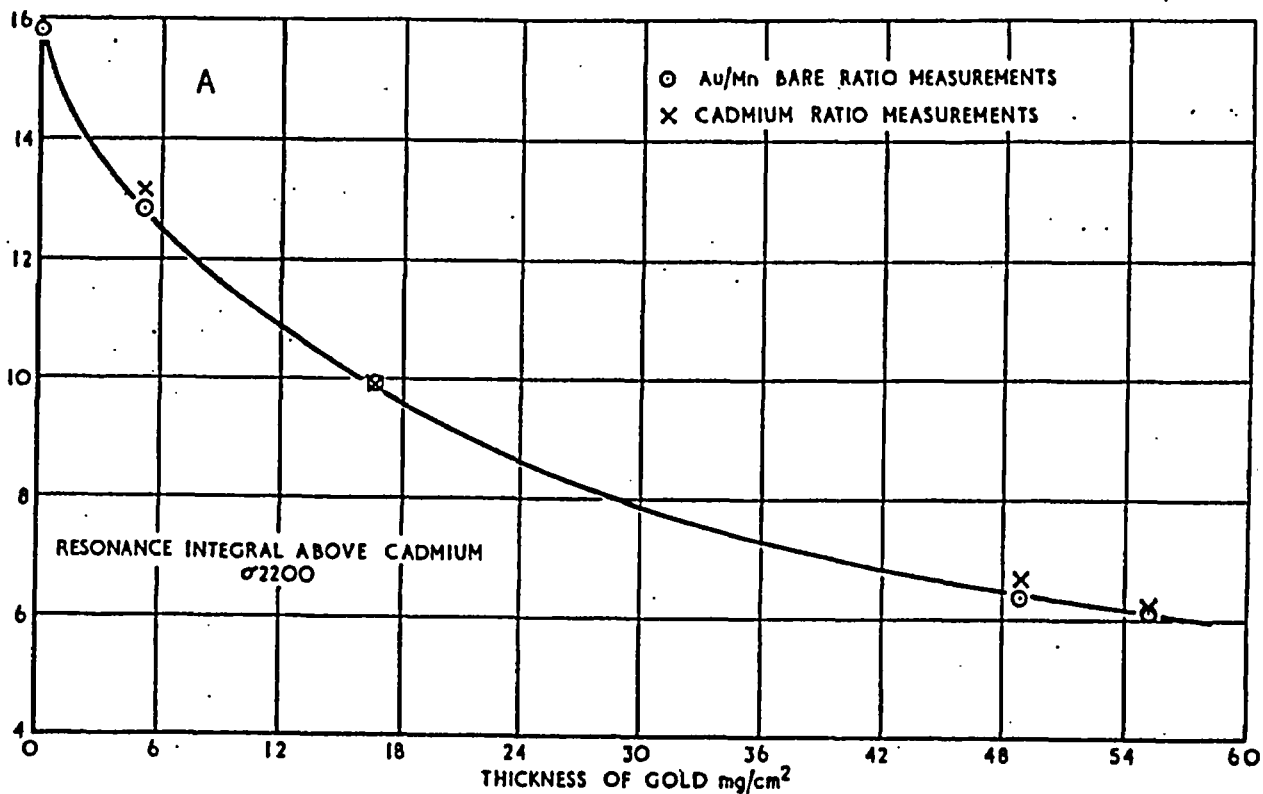


FIG. 28 SELF SHIELDING FACTORS FOR THE GOLD AND MANGANESE RESONANCES

DISTRIBUTION:

Sir William Penney
Sir William Cook

London Office

Mr. D. W. Fry
Dr. J. V. Dunworth
Dr. C. G. Campbell
Dr. J. E. R. Holmes
Dr. D. C. Leslie
Mr. J. Fell
Dr. D. Hicks
Mr. R. Alpiar
Mr. I. Johnstone (3 copies)
Mr. J. Smith
Mr. P. W. Mummery
Mr. W. Eastwood
Mr. G. Paravicini
Dr. W. N. Fox
Dr. J. E. Sanders
Mr. C. T. Chudley
Mr. M. J. Terry
Dr. R. Richmond
Mr. D. B. McCulloch
Dr. D. Jakeman
Dr. R. D. Smith
Mr. M. F. Smith
Mr. E. J. Maunders
Mr. H. A. Roberts
Mr. D. A. Newmarch
Mr. G. W. Watson
Mr. G. R. J. Wilkinson
Mr. D. R. Dickie

A.E.E., Winfrith

Dr. F. A. Vick
Mr. L. Grainger
Mr. W. F. Wood
Mr. J. F. Hill
Dr. V. S. Crocker
Mr. H. R. McK. Hyder (20 copies)
Mr. C. J. Kenward
Mr. D. H. Day
Mr. E. D. Jones
Mr. P. G. F. Moore
Mr. S. K. Pattenden
Dr. C. Carter
Mr. D. W. Holbrough
Mr. A. W. Batten
Mr. A. M. Mills
Mr. S. Dunk

A.E.R.E., Harwell

A.E.E. Winfrith
A.E.E. Winfrith

Dr. W. B. Lewis
Dr. A. G. Ward
Dr. J. W. Hilborn (3 copies)
Dr. R. G. Jarvis (3 copies)
Mr. G. L. Brookes

AECL Chalk River, Ontario, Canada) via Mr. N. Geary
Chalk River

Mr. B. H. Jones London Office

Mr. R. V. Moore
Mr. S. Fawcett
Mr. J. Tatlock
Dr. M. D. Jepson
Mr. B. Cutts
Mr. V. Walker
Dr. T. Marsham
Mr. A. Green
Mr. H. Burstall
Mr. N. Bradley
Mr. J. F. Pearson
Dr. J. D. McCullen
Mr. R. J. Haslam
Mr. F. W. Fenning
Mr. R. Anscomb
Mr. C. R. Bennett
Mr. P. M. Boocock
Mr. C. E. Iliffe
Mr. R. P. Kinsey
Dr. H. Kronberger
Mr. V. H. B. Macklen
Mr. R. C. R. Nickolson
Mr. R. C. Orford
Mr. D. R. Poulter

Risley

Mr. J. N. Wanklyn
Mr. J. G. Collier
Mr. G. F. Aitchison
Dr. J. K. Dawson

A.E.R.E.

Dr. A. J. M. Hitchcock (3 copies) R.D.B. Windscale Works

Mr. K. Saddington Windscale